September 1965

Technical Summary Report for Period
27 June 1964 to 27 June 1965

SOLAR-RADIATION-INDUCED DAMAGE TO OPTICAL PROPERTIES OF ZnO-TYPE PIGMENTS

NAS 8-11266

LOCKHEED MISSILES & SPACE COMPANY
A GROUP DIVISION OF LOCKHEED AIRCRAFT CORPORATION
SUNNYVALE, CALIFORNIA

FOREWORD

This report was prepared by the Research Laboratories of Lockheed Missiles & Space Company, for the George C. Marshall Space Flight Center of the National Aeronautics and Space Administration. The work was performed under contract NAS 8-11266. The contract was administered by the Research Projects Laboratory of Marshall Space Flight Center, with Mr. W. C. Snoddy as Contract Officer.

This Technical Summary Report describes work performed from 27 June 1964 to 27 June 1965.

ACKNOWLEDGMENT

The authors gratefully acknowledge the advice, assistance, encouragement, and continued interest of Mr. W. C. Snoddy, Mr. E. R. Miller, Mr. G. M. Arnett, and Mr. G. Heller of the Research Projects Laboratory, Marshall Space Flight Center.

PERSONNEL

The following personnel are responsible for the work described in this report.

J. S. Blakemore	L. A. McKellar
K. F. Cuff	A. F. Sklensky
S. A. Greenberg	W. E. Spicer
C. D. Kuglin	E. R. Washwell
H. F. MacMillan	L. R. Williams

The program was carried out under the direction of L. A. McKellar. Critical review of the literature was performed primarily by J. S. Blakemore. The theoretical and experimental studies of bulk properties were carried out by K. F. Cuff, J. S. Blakemore, E. R. Washwell, and L. R. Williams. Preparation and characterization of particulate samples were performed by S. A. Greenberg. Design and construction of the bidirectional reflectance apparatus and the in situ measurements were performed by H. F. MacMillan and A. F. Sklensky, assisted by consultation with R. E. Rolling and D. J. Ballegeer; R. A. Breuch initially conceived the apparatus.

The band structure calculations were carried out by C. D. Kuglin. General advice on band structure calculations were provided by F. Herman. Review, evaluation, and intercomparison of data and information obtained from the studies of particulate and single crystal samples was performed primarily by K. F. Cuff, S. A. Greenberg, W. E. Spicer, and E. R. Washwell. General consultation on all aspects of the program was provided by W. E. Spicer.

CONTENTS

ILLUSTRATIONS

TABLES

Section 1
INTRODUCTION

Successful operation of space vehicles demands that components be maintained within their designed temperature limits. Control of temperatures on an operational spacecraft is based on the exchange of radiant energy with the vehicle's environment, and therefore with the optical properties of the exterior surfaces. Design requirements often dictate the use of a surface with a low ratio of solar absorptance, α_s, to emittance ϵ. These surfaces are generally susceptible to damage by natural or induced radiation in space, resulting in an increase in α_s. Emittance is generally unaffected.

Of all sources of radiation encountered in space, both natural and induced, the ultraviolet portion (0.2 to 0.4 μ) of the solar spectrum is the most important source of damage to low α_s/ϵ surfaces. For most low α_s/ϵ surfaces, ultraviolet induced damage is at least as great as that due to other forms of radiation. In addition, all space vehicles are exposed to high fluxes of solar radiation. In contrast, all vehicles do not experience high doses of Van Allen, nuclear, or other forms of high-energy radiation. Since 96.90% of solar radiation is between the wavelengths of 0.2 and 2.6 μ, the α_s of a material is essentially determined by its optical properties in this wavelength range. Furthermore, high-intensity ultraviolet sources and optical equipment for wavelengths from 0.2 to 2.6 μ are readily available.

Investigation of the effects of ultraviolet irradiation on the optical properties from 0.2 to 2.6 μ therefore constitutes a logical starting point for study of the mechanisms of radiation-induced damage to thermal control surfaces.

Over the past five years a large body of data on the effects of simulated solar ultraviolet radiation in vacuum on low α_s/ϵ thermal control surfaces has been generated

by various agencies concerned with spacecraft (Refs. 1 through 12). Time requirements necessitated concentration on the achievement of relatively crude engineering design data. Available information on solar-radiation-induced damage to thermal control surfaces is virtually entirely empirical. Since complete environmental simulation is never achieved in the laboratory, precise prediction of behavior in space from the existing laboratory testing data is not possible. This problem is demonstrated by the comparison of laboratory and spacecraft data shown in Ref. 13.

The type of low α_s/ϵ surface usually employed on spacecraft is a white coating made up of a pigment dispersed in a binder. A definitive understanding of the changes in the spectra of such systems is impossible unless the behavior of each component alone is first understood. A detailed study has been undertaken to better understand the behavior of the pigment itself. If this study is to produce positive results, it must concentrate on one pigmenting material. The ideal material would possess the following attributes:

- Simple, well-defined chemical and electronic structure
- Data available on optical, electrical, and related physical properties
- Representative of a class of stable white pigments
- In use in promising thermal control coatings

Zinc oxide possesses each of the above characteristics to a greater degree than does any other single material. ZnO is the most widely quoted example of a metal excess (n-type) semiconductor, and a great deal of work has been done with sintered material as well as single crystals. Considerable progress has been made in characterizing the electrical and optical properties of ZnO, although it is by no means completely understood. Furthermore, its properties are similar to those of titanium dioxode, zinc sulfide, and stannic oxide; ZnO, TiO_2, ZnS, and SnO_2 are all in use as pigments in promising white thermal control surfaces. Study of ZnO, then, provides a logical starting point for investigation of the mechanisms involved in solar-radiation-induced damage to low α_s/ϵ surfaces.

The study has been directed toward identification of the primary mechanisms involved in solar-radiation-induced damage to the optical properties of ZnO-type semiconductor pigments, as exemplified by ZnO itself. Knowledge of the damage mechanisms would greatly simplify the problem by providing a rational basis both for the design of environmental tests and for interpretation of the resulting data. Ultimately, such knowledge would guide materials specialists in the development of optimum materials.

Central to the investigation has been an experimental study of the optical behavior of particulate samples of zinc oxide; particle size is essentially that of the pigment in a low α_s white paint. Carefully prepared particulate samples were exposed to radiation of wavelengths between 0.2 and 2.6 μ. Parameters varied in both initial exposures and studies of damage reversibility are the flux density, spectrum, time of exposure, sample temperature, and gaseous environment. Selected exposures were performed in which the bidirectional spectral reflectance of the sample was monitored during exposure (in situ). The in situ measurements provide the key to comprehensive detailed knowledge of optical damage to particulate samples. Static ultraviolet tests with before- and after-exposure measurements have been carried out to supplement the slower, more thorough tests with in situ measurements. In addition, single crystals of zinc oxide have been irradiated, in an attempt to ascertain the relative importance of surface and bulk damage processes.

A parallel theoretical and experimental program to describe the pertinent bulk and surface properties of zinc oxide has been carried out; the goal of these parallel efforts has been a comprehensive explanation of phenomena observed in the particulate samples. The extensive and often contradictory literature on zinc oxide was critically evaluated and related to the observed optical damage. Selected measurements of optical and transport properties of zinc oxide single crystals were performed, when required, to formulate a coherent picture of zinc oxide optical behavior, or to resolve contradictions and fill voids in the open literature. Electronic energy band structure calculations for the ideal crystal have been performed as a point of departure for the understanding of electronic behavior in real crystals.

This report documents the activities and results of an investigation into the mechanisms of solar-radiation-induced damage to the optical properties of zinc oxide.

Section 2
ZINC OXIDE PROPERTIES AFFECTING OPTICAL BEHAVIOR

ZnO is a II-VI compound semiconductor which crystallizes in the hexagonal wurtzite structure (B4-type). The binding is largely polar, but there is also significant covalent binding; ZnO stands somewhat between the polar alkali halides and the covalent-bonded Group IV semiconductors.

The energy gap of ZnO is 3.2 eV (0.38 μ) at 300° K and appears to be a direct gap located at the center of the Brillouin zone. The optical absorption coefficient has the characteristic steep rise at this energy and reaches a value greater than 2×10^5 cm^{-1} at photon energies greater than the band gap. The ultraviolet reflection spectra (Ref. 14) is just beginning to receive serious attention and will play a strong role in elucidating the overall band structure of ZnO (see Sec. 5). Infrared studies on single crystals have revealed the characteristic lattice absorption spectra of ZnO, and also distinct free carrier absorption effects. Electron paramagnetic resonance, visible and infrared absorption, photoconductivity, and luminescence studies have provided some information on the details of the impurity levels in ZnO.

ZnO is an n-type semiconductor; hole conductivity has not been observed to date. The conduction band has an effective mass of 0.27 m_o (where m_o is the rest mass of the free electron) and an electron mobility of 60 $cm^2/V\text{-sec}$ at 300° K (Ref. 15). The resistivity of ZnO crystals can be varied over a wide range by doping; from about 10^{-2} Ω-cm to greater than 10^{11} Ω-cm at 300° K. Extensive transport studies have been carried out on ZnO and many of its basic semiconducting properties have been characterized.

Because ZnO has been rather thoroughly studied there is a relatively large amount of information concerning its transport, optical, photoconductive and catalytic properties. In Secs. 2.1 through 2.4, some of these properties of ZnO which have a direct bearing

on the formulation of the ultraviolet damage mechanism are discussed in detail. Finally, a working degradation model is formulated in Sec. 2.5.

2.1 SURFACE PHENOMENA

Before discussing photoconduction and degradation effects in ZnO, it is important to point out some of the pertinent phenomena which occur at semiconductor surfaces. For simplicity, we will consider an n-type semiconductor as is the case for ZnO. In Fig. 1 we have indicated a semiconductor surface with a net negative charge and in Fig. 2,a surface with a net positive charge.

A negative surface charge will, of course, repel electrons near the surface creating a depletion region (depleted of electrons) with a net positive charge near the surface due to ionized donors. The potential barrier height V_s is produced at the surface, bending both the conduction and valence bands upward (with respect to the bands in the volume of the crystal). It should be noted that in this case holes in the depletion region are strongly attracted to the surface.

A positive surface charge on the other hand, will attract electrons toward the surface causing an accumulation layer of electrons adjacent to the surface. In this instance the bands bend downward at the surface with respect to the bulk; holes in the valence band are repelled from the surface.

Without developing the relationship between the donor density, barrier heights, surface charge and space charge dimension ℓ, it is important simply to point out the magnitudes of these quantities expected in ZnO crystals and pigments; for a full treatment see G. Heiland (Ref. 16). The maximum surface charge density, as would exist in an atmosphere of air, will be $\sim 10^{12}$ to 10^{13} charges/cm^2. In vacuum the surface charge density will in general be much less than this. At this maximum surface charge density and with donor concentrations in the range of 10^{16} to 10^{18} charges/cm^3, the barrier height V_s will be in the range of 0.1 to 1.0 eV and the depletion region depth

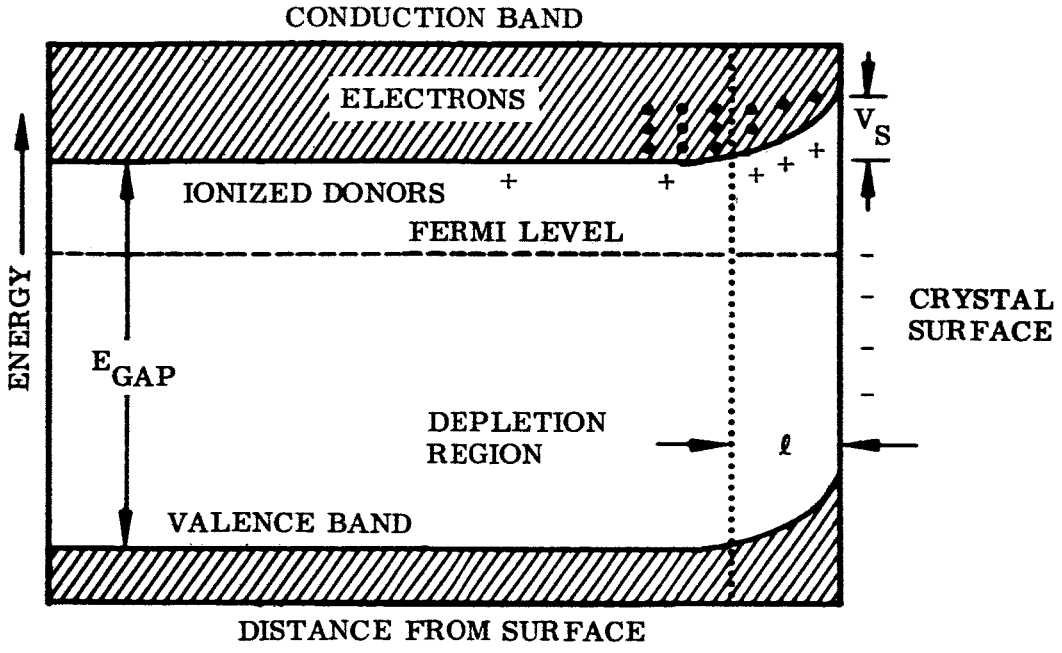

Fig. 1 Surface Band Bending in Depletion Region

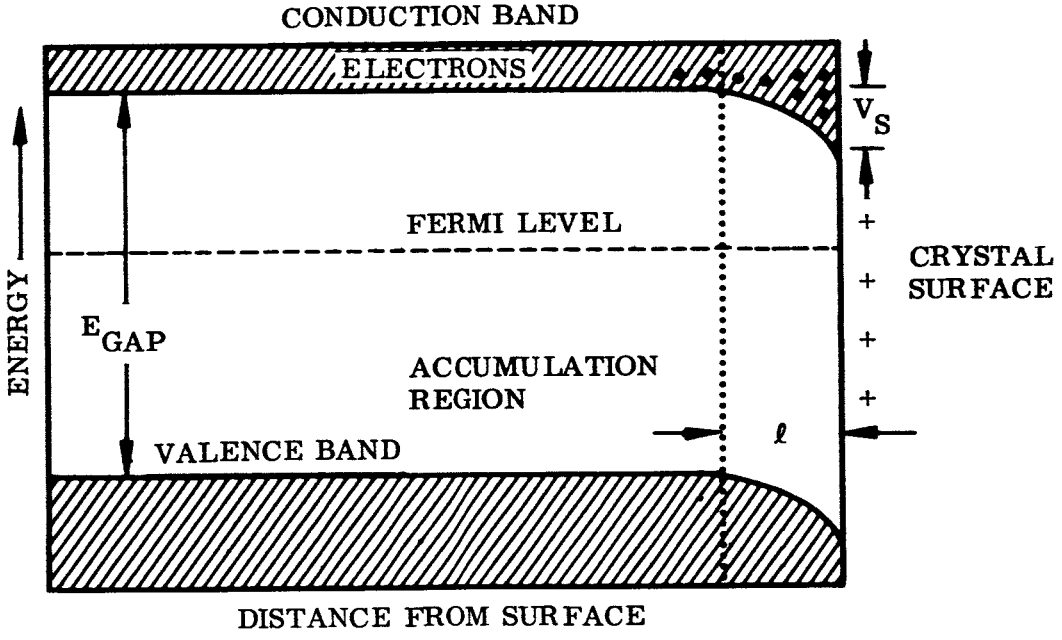

Fig. 2 Surface Band Bending in Accumulation Region

will be of the order of 100 to 1000 Å. These are the magnitude of the effects to be expected in the pigments under investigation in this contract.

The phenomenon of surface conduction in a ZnO crystal occurs, for example, when the surface has been reduced; say with hydrogen or excess zinc. This will produce the band bending shown in Fig. 2 where the electron conduction now occurs predominately in the accumulation region near the crystal surface. The enhanced conductivity which is observed when surface conduction occurs is the result of donors diffusing inward to provide additional free carriers. The diffusion distance does not have to be any greater than the accumulation layer depth which is relatively small (~ 100 to 1000 Å).

Another important feature to bear in mind is the relationship between the Fermi level in the crystal and the location of the surface states in energy in determining the type and degree of band bending at the surface. First let us consider a negative surface-charge state with a sufficiently small density ($\ll 10^{12}$ charges/cm^2) such that the Fermi level is not pinned at the surface state. Then if the Fermi level is above the energy level of the surface state, that surface state will contain electrons and provide a negative surface charge. If the Fermi level is below the surface state, it must be depleted of electrons, and no negative surface charge will exist. This model is shown in Fig. 3 for the two cases, where it will be noted that the usual depletion region and upward band bending occurs in the first case and no band bending occurs in the second case. By appropriate doping of the ZnO crystal, the Fermi level in the bulk can be lowered; e.g., down to approximately midway between conduction and valence bands by Li substitutional impurities. It is then possible to control the band bending at the surface by changing the volume characteristics of the crystallites. If the surface charge density is sufficiently large, however, then the Fermi level at the surface will be anchored at the surface impurity level, regardless of the position of the Fermi level in the bulk of the crystal. Therefore, it can be seen that modification of the position of the Fermi level in the bulk of the crystallites can produce marked changes in its surface properties such as its photoadsorption-desorption characteristics.

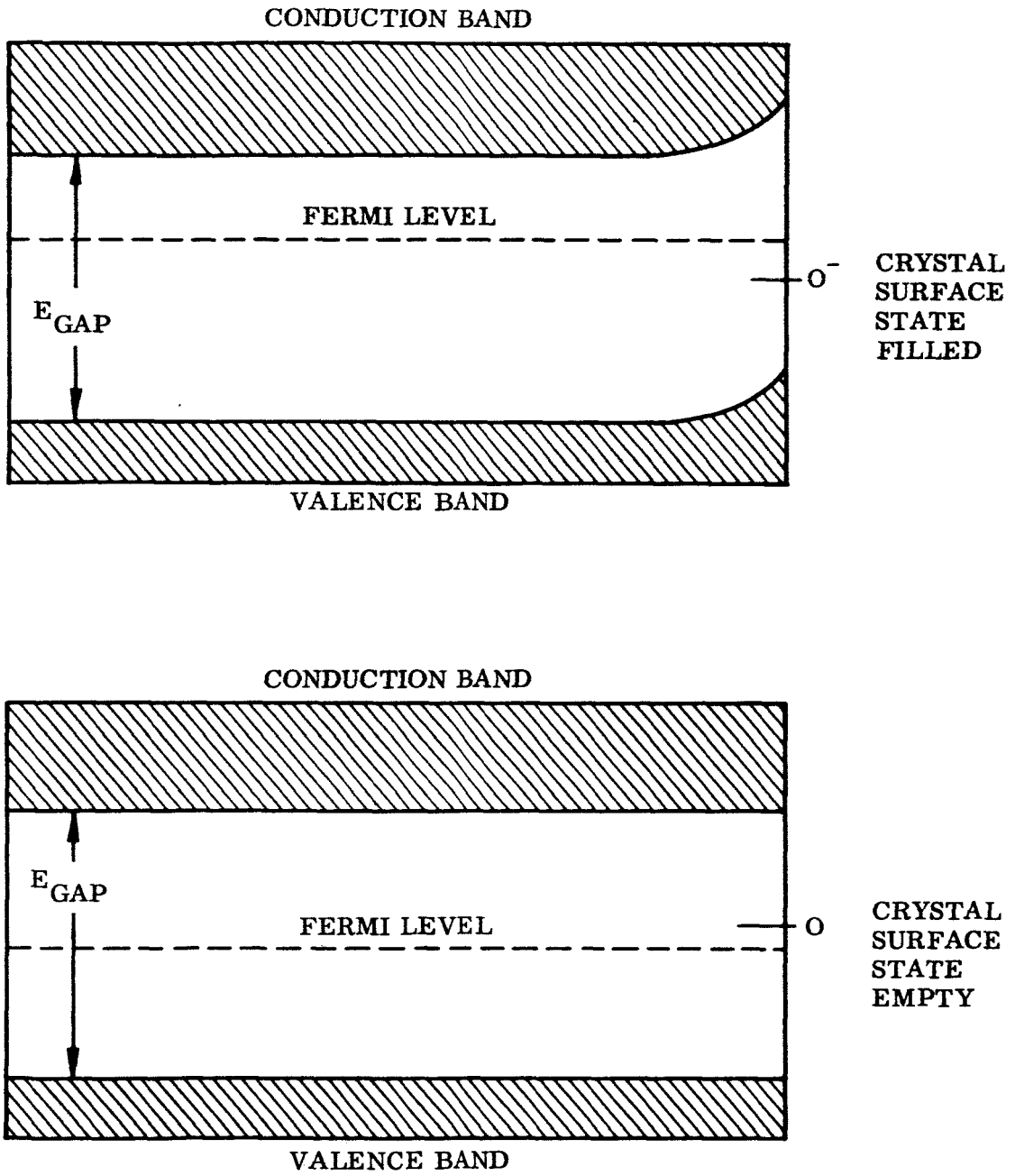

Fig. 3 Effect of Fermi Level on Surface State Occupancy

2.2 BULK IMPURITY STATES

Donors. The known donor states are interstitial Zn and interstitial Li and Cu when added as impurities. Also, Group III elements such as Ga and In when incorporated substitutionally act as donors. These levels, which are singly ionized, exist ~ 0.05 eV below the conduction band and appear to take the form of simple hydrogen-like impurity levels. It should be noted that an electron in a hydrogen-like impurity state near a band edge will have a binding energy of

$$E = \frac{13.6\ m^*}{K^2}\ eV$$

where m^* is the effective mass of an electron in the band in question and K is the static dielectric constant ($K = 8.5$ for ZnO). As an example, for an electron in or "near" the conduction band of ZnO we have $m^* = 0.27\ m_o$ (Ref. 15) and therefore

$$E = \frac{(1.36)(0.27)}{72} \approx 0.05\ eV$$

in reasonable agreement with the singly ionized states observed. Oxygen vacancies can also exist; the singly ionized vacancy having the binding energy of approximately that of the singly ionized interstitial donors and the doubly ionized vacancy being approximately 0.8 eV below the conduction band edge. The doubly ionized state has definitely been observed in electron paramagnetic resonance work (Ref. 17) and being doubly ionized can act as an electron trap. In fact, the 2.4 eV luminescence of ZnO has been ascribed to the radiative transition between this level and the valence band.

Acceptors. Monovalent Cu and Li act as acceptors in ZnO, when they substitute for Zn in the lattice. The level of the Cu acceptor from the valence band is somewhat uncertain; however the Li acceptor level appears to exist ~ 0.85 eV above the valence band. These acceptor centers have a net negative charge in the lattice when ionized, which is generally the case; i.e., the acceptor levels lie beneath the Fermi level.

The impurity levels are summarized in Fig. 4.

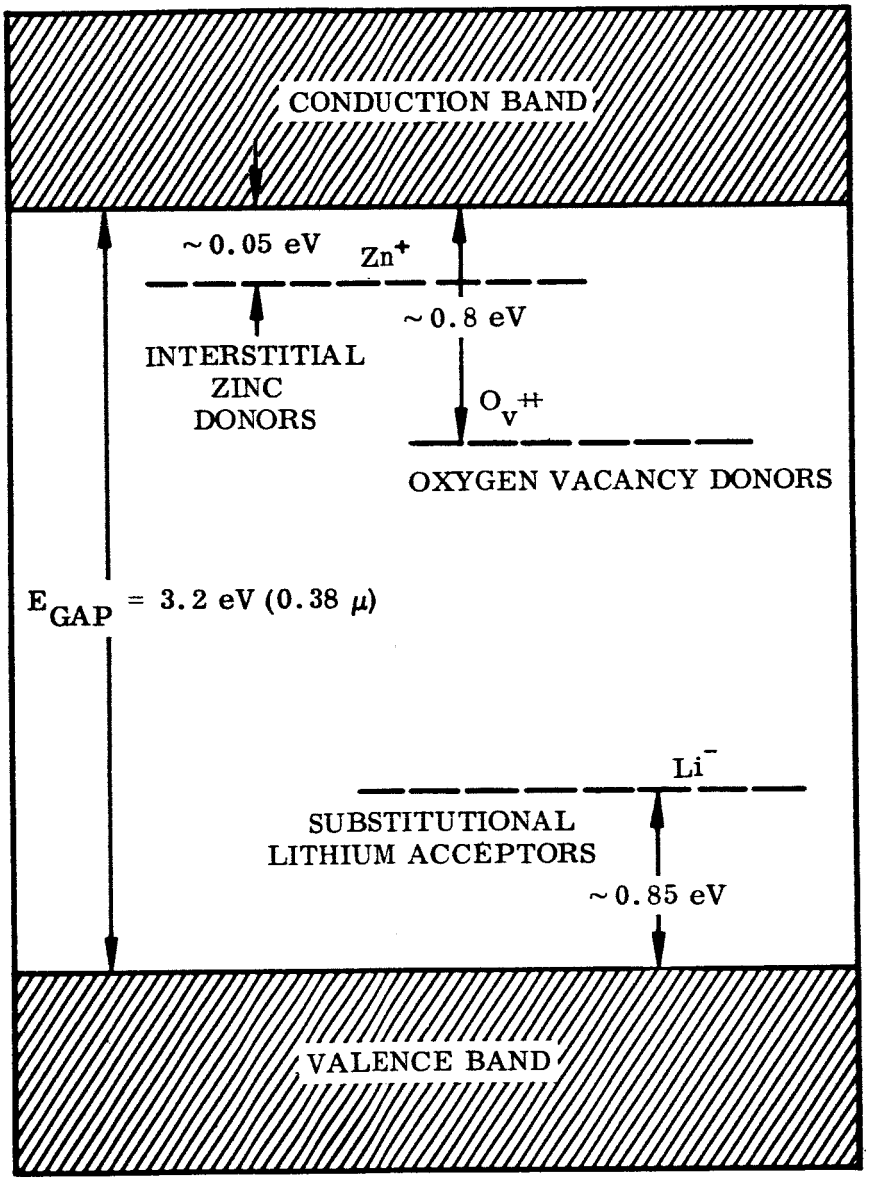

Fig. 4 Bulk Impurity States

2.3 FAST PHOTOCONDUCTIVITY AND TRAPPING

The most comprehensive investigation of the nature and energy spectrum of the carrier trapping states in ZnO was made by Hieland (Ref. 18). In this work he investigated both field effect and photoconductivity in the surface conduction region of single crystals. Basically, the field effect will determine the effective mobility of the electrons in the space charge region which is determined by the density of states distribution for the electron traps, and the photoconductivity determines the density of states for the hole traps. The essential results of these studies can be summarized as follows:

- The trapping of excess holes or electrons is not determined by the dark surface conductivity, that is by the density of surface charges.
- The electron mobility increases and the photoconductivity decreases with increasing intensity of radiation with energy greater than or equal to the band gap. This says that electron trapping (from field effect) and hole trapping (from photoconductivity) decreases with increasing illumination.
- Both of the above results would occur if the quasi-Fermi levels for the electron and holes (each quasi-Fermi level approaches the corresponding band edge with increasing illumination) are moving through a continuum of trapping states. A quasi-Fermi level is used to describe electron and hole distributions under steady state nonthermal-equilibrium conditions. In the case of photoconductivity the quasi-Fermi levels describe the separate distribution functions of the electron and hole densities produced by illumination.
- The density of states of trapping levels for electrons and holes obtained in Heiland's work is shown in Fig. 5. The important point to note here is the preponderance of trapping levels found near the conduction and valence band edges. It is difficult to interpret from his results alone what the actual spectrum of trapping states is because of the complexities of the situation at the crystal surface. In fact, the spectrum he finds can be reasonably accounted

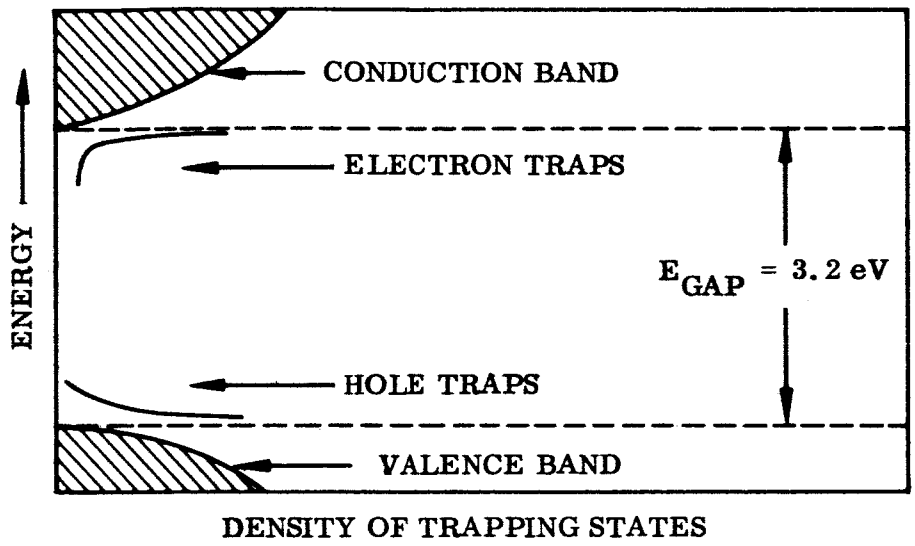

Fig. 5 Density of Hole and Electron Trapping States

for simply by assuming that the quasi-Fermi level passes through a single trapping level in the region near the surface where the bands are bent. It should be mentioned that this observed density of states could also be the result of a single level which crosses the Fermi level inside the space charge layer because of band bending.

- The electron traps are located at the surface or in the space charge region and they are not effective in recombination. Also the traps for electrons must be located near the traps for holes with regard to the distribution of charge; a spatial separation of the two levels of traps would result in bending of the bands and great changes in the surface conductivity which is not observed.
- The hole trapping effects indicate that the holes are protected against recombination with electrons. This can only occur if, in the trapped state, the trap still has a negative charge. Therefore, the hole traps must have a double negative charge when empty of holes. Oxygen ions, $O^{=}$, at the surface can satisfy this requirement, but the hole trap density has been shown to be independent of the coverage of the surface with adsorbed oxygen (over four orders of magnitude). Therefore the oxygen bound in the lattice may provide hole traps at the surface or additionally in the bulk.

2.4 SLOW PHOTOCONDUCTIVITY

In addition to the fast photoconductive process which is electronic in origin, there is a slow photoconductive process which is related to the adsorption and desorption of oxygen from the surface. This process is characterized by a sluggish rise (minutes to days) of the conductance during irradiation and a similar decay upon cessation of the irradiation. The general characteristics of this photoconductivity, such as its time-dependence and saturation level, depend on the experimental conditions such as light intensity, temperature, and ambient pressure. The general features of the experimental results can be understood in terms of the photoadsorption-desorption mechanism discussed below.

This slow process is irreversible in a vacuum to the extent that although there is a slow decay of the conductivity after the irradiation is stopped, the initial conductivity is not regained. However, admission of air accelerates the decay and, eventually, the initial conductivity is regained. It has been noted that there is an attendant pressure rise in the system when the ZnO is irradiated and a corresponding decrease in the pressure when the irradiation is stopped. The kinetics of this photodesorptive and photoadsorptive process have been extensively investigated. The results clearly show that the kinetics of the slow photoconductance behavior are determined by the kinetics of the photoadsorption-desorption process. Studies of the photocatalytic behavior and surface potential measurements of ZnO give a further clue to the processes involved. In particular, it has been shown that oxygen is adsorbed both physically and chemically, the chemisorbed form resulting in a negative surface charge. The exact species involved have not been conclusively determined, but the most likely chemisorbed forms are O^- and $O^=$. Their activation energies lie in the range 0.5 to 1.5 eV; the physically adsorbed species about 0.05 eV. Reduced ZnO, on the other hand, has been shown to have a positive surface charge. As an example, heating ZnO in an atmosphere of H_2 at elevated temperatures results in a positive surface charge. Also, changes in the surface charge of ZnO have been brought about by variations in the Fermi level as a result of bulk doping of the crystal. Doping with Li, for instance (which is an acceptor when incorporated substitutionally) lowers the surface charge by emptying the negatively charged surface states as a result of the lower Fermi level.

With this background information we are in a position to discuss a mechanism which best relates these observations. The negatively charged surface resulting from the adsorption of oxygen on ZnO is considered to consist of negative oxygen ions which have been formed by the transfer of conduction electrons to the adsorbed species. If adsorbed at low temperatures O^- is considered to be the predominant species and if adsorbed at high temperatures (above 200° C) $O^=$ is more likely. In addition to these chemisorbed species, physically adsorbed oxygen is also present. The adsorption of oxygen on the surface thus gives rise to a decrease in conductivity by removing electrons from the conduction band. This electron transfer creates a compensating space charge layer of ionized donors and a Schottky barrier is formed, i.e., the negative charge on the surface gives rise to an upward band-bending at the surface. This is the normal configuration of a ZnO surface in air as in Fig. 1.

The adsorbed ions can be desorbed by illuminating the surface with band-gap light in the following way. When band-gap light is incident on an oxidized ZnO surface, i.e., one that has a negatively charged oxygen surface layer, an electron-hole pair is created and the holes will be accelerated by the field to the surface where they neutralize a negative charge on the oxygen. The oxygen is now only physically adsorbed. The electron created by the action of the light is weakly attracted to this physically adsorbed oxygen and is available for conduction only after the oxygen is desorbed. Thus the rate of increase in photoconductivity is determined by the rate of desorption of the physically adsorbed oxygen. Therefore, it can be seen that the photoconductive response will increase at a rate which is initially relatively independent of the ambient oxygen pressure. However, the saturation value of the photoconductivity will depend on the ambient oxygen pressure such that in a vacuum the photoconductivity will show a gradual increase which will ultimately saturate at much higher levels than the corresponding level in an oxygen atmosphere.

When the irradiation is stopped, the decay time of the photoconductivity is essentially determined by the rate at which electrons can overcome the surface barrier to create chemisorbed oxygen from the physically adsorbed oxygen. When oxygen is admitted to this system, the rate of decay is increased because there are more physically adsorbed oxygen sites to accommodate the electrons.

In general, these processes appear to dominate the slow photoconductive effects. However, the situation is in fact much more complicated. As an example, during the slow process diffusion of such species as oxygen vacancies and excess zinc may occur. This diffusion not only would modify the rate of the observed effects but through electron trapping can modify the electron mobility in the space charge region and consequently the magnitude of the photoconductive effects.

2.5 WORKING DEGRADATION MODEL

Obviously, the degradation of the optical properties of ZnO by ultraviolet radiation is a complicated phenomenon. However, in this section, we would like to outline a degradation model in a general sense and then point out those features which are uncertain at the present time. For this outline, we will first start with a ZnO particle in an oxygen atmosphere. The surface (shown in Fig. 1) should take on a net negative charge due to electrons bound to the oxygen atoms at the surface. The potential barrier produced at the surface is such that electrons will be repelled and holes will be attracted to the surface within the space charge layer. The volume near the surface will therefore be a depletion region because ZnO is an n-type semiconductor.

When ultraviolet radiation of energy greater than the intrinsic energy gap (3.2 eV) is incident on the sample, electron-hole pairs are created within the bulk of the crystal or particle; the absorption depth for the radiation is 0.1 μ or less. The electrons have difficulty in getting to the surface but the holes will be accelerated to the surface by the action of the strong electric field in the space charge region. The holes recombine with the O^- at the surface and change the oxygen from the chemisorbed to the physically adsorbed form which then can leave the surface with relative ease. The activation energy for physical adsorption is roughly 0.05 eV. This process results in oxygen leaving the surface which becomes Zn rich. Furthermore, this Zn rich surface layer gives a positive contribution to surface charge, thus decreasing the band bending and potential barrier at the surface. As the degradation proceeds the surface charge will tend to change to a net positive charge and the bands at the surface will begin to bend down (Fig. 2). Under this condition the holes have a retarding potential at the surface

to overcome and the rate of charge neutralization slows down severely. Thus the degradation process (loss of oxygen) proceeds initially at a rate largely determined by the rate of evolution of adsorbed oxygen and eventually at a rate limited by the arrival of holes through the retarding potential of the positive surface charge.

With this general trend outlined, the next step is to ascertain what changes produced by this oxygen loss manifest themselves as the permanent damage observed in various spectral regions by the reflectivity from pigments. Two general consequences are expected to result from the oxygen loss. Changes in the band-bending can be expected to modify the availability for optical absorption of the defect states already present in the ZnO crystallites because of changes in the relative positions of the defect states and the Fermi level. Diffusion of defects and impurities is also expected to occur and would give rise to additional absorption.

There is insufficient information at this time to specify the exact nature of the defect states giving rise to the optical absorption observed in the damaged ZnO pigments. We can, however, make some comments as to the defects to be expected. With the loss of oxygen from the surface both interstitial Zn and oxygen vacancies can be expected to diffuse into the material. It should be pointed out that the problem of predicting diffusion rates in the pigments is very difficult. Even if the diffusion rates of the defects were well-known in single crystals – and there is much contradiction in this area – the complexities of the interactions near the surface of the crystallites prevents realistic estimates of these diffusion rates in the pigments with our present information. However, assuming interstitial Zn and oxygen vacancies as the defects we can indicate some of the consequences. Interstitial Zn provides rather shallow (~ 0.05 eV) donor states and oxygen vacancies provide donor states ~ 0.8 eV below the conduction band. At the densities of defects expected in the degraded material these levels are expected to be considerably broadened; thus if these levels were present, significant absorption should be observed in the material for photon energies from ~ 2.1 to 3.2 eV; that is, over the wavelength interval of 0.38 to $0.6\ \mu$.

In the infrared two types of absorption can occur as a result of the degradation. First, the existence of levels with energies up to 1 eV below the conduction band can provide

absorption for wavelengths longer than 1 μ. Also, since Zn interstitial and oxygen vacancies are donors, the electron density in the bulk of the crystal can be increased, which would result in increased free carrier scattering absorption. It should again be emphasized that the data presently available do not allow an unambiguous assignment of the levels giving rise to the optical absorption observed in the degraded material.

There is one consequence of the degradation model which should be pointed out. The model would predict that the photodesorption rate of oxygen from the surface should be significantly retarded if the Fermi level in the bulk of the crystallites can be lowered sufficiently. This should occur regardless of whether the Fermi level is pinned at the surface state energy or not. If it is not pinned and the Fermi level can be lowered beneath the surface state energy the surface charges will be depleted of electrons (see Sec. 2.1) and the photodesorption rate should be decreased. If the Fermi level is pinned at the surface (which will occur at large surface coverage) a lower Fermi level in the bulk of the crystallites will decrease the band bending. It can even cause the bands to turn down at the surface depending upon the relative level of the bulk Fermi level and the surface state energy. This decreased band bending will also tend to decrease the photodesorption rate.

The lowering of the Fermi level in the bulk of the crystallites can be accomplished by Cu or Li substitutional doping. However, doping the pigments with Cu or Li will tend to give added optical absorption in the energy region just below the band gap, such that the overall visible reflectivity may be slightly lower than that for an undoped pigment. Thus, with doping, the pigment might start out slightly degraded but subsequent ultraviolet degradation may be greatly reduced if not eliminated.

The specific application of this model to the experimental results of the degradation effects observed in ZnO pigments will be discussed in Sec. 6.

Section 3
STUDIES ON SINGLE CRYSTALS

The experiments carried out on single crystals in the present contract were designed to demonstrate the applicability of single crystal studies to the understanding of the mechanisms of solar irradiation induced damage to thermal control pigments. We feel that studies on single crystals are important for the following reasons:

- Surface and bulk effects can be unambiguously differentiated.
- Important parameters such as the Fermi-level and defect distributions are more clearly determined than in particles so that defect production may be delineated from the redistribution of carriers in existing defects.
- Defects and surface state properties can be characterized more accurately in single crystals by more definitive techniques.

3.1 ULTRAVIOLET DEGRADATION STUDIES OF SINGLE CRYSTALS

These studies were undertaken to determine whether the optical properties of ZnO single crystals could be degraded by UV irradiation in a vacuum. Several single crystals were irradiated for 2020 sun-hr (A-H6 lamp) in a vacuum of $\sim 2 \times 10^{-7}$ Torr on a water-cooled substrate. The spectral content of the irradiating light was varied by employing (1) no filter, (2) a yellow filter and (3) a Pyrex filter, respectively, over each of three pairs of single crystals which consisted on an undoped (low resistivity) and a Li-doped (high resistivity) crystal. For spectral curves of these filters see Fig. 41. The yellow filter removes wavelengths shorter than the band gap, and the Pyrex filter removes only that band gap radiation with $\lambda < 0.32\,\mu$. The undoped single single crystals were cut from the same ingot, ground to size, lapped, and polished. The Li-doped crystals were obtained in the form of discs which were ground to the same size, lapped, and polished. The transmission of an undoped single crystal and two Li-doped single crystals was determined both before and after the UV irradiation. The measurements covered the range from 0.35 to 0.57 μ and from 2 to 8 μ.

The spectral transmission data were obtained by focusing the radiation from a Perkin-Elmer monochromator onto the ZnO sample mounted over a slot and comparing the intensity transmitted to that transmitted by a matched slot. A tungsten lamp and either a 1P28 photomultiplier or a PbS detector were used with a fused silica prism to cover the region 0.35 to 2.7 μ; a globar and a Au-doped Ge detector were used with a NaCl prism to cover the region 2 to 8 μ. The undoped crystal showed the characteristic absorption edge and the expected maximum of approximately 80% (based on the refractive index of ZnO).

The Li-doped crystals, however, were of poor optical quality as evidenced by their transmission in the visible, viz., the transmission did not show the characteristic band edge of ZnO but a transmission from the visible to about 2.5 μ which is characteristic of scattering. Therefore, the visible data on these crystals are discounted and not discussed further. The original Li-doped crystals were of excellent optical quality and were employed in the photoconductivity experiments.

The results obtained on the undoped crystals before and after the irradiation under the different filtering conditions are shown in Fig. 6. The results indicate that only the crystal exposed to the A-H6 irradiation with no filtering shows evidence of degradation in the visible. That the observed effect was not due to surface contamination was conclusively shown by the fact that the same value of transmission was obtained in this region after etching the crystal in HCl and repolishing. This process was repeated several times with the same results. The samples exposed to Pyrex and yellow filtered A-H6 irradiation showed no apparent change in the visible. The data in the infrared indicate an apparent degradation in all three samples. The transmission of the three undoped single crystals stored in air at room temperature was redetermined after approximately 2 months and are shown in Fig. 7. The Pyrex and yellow filtered samples show essentially the same transmission throughout the entire region covered (0.35 to 8 μ) and corresponds to an unexposed undoped crystal. The unfiltered crystals show evidence of recovery in the infrared and partial recovery in the visible.

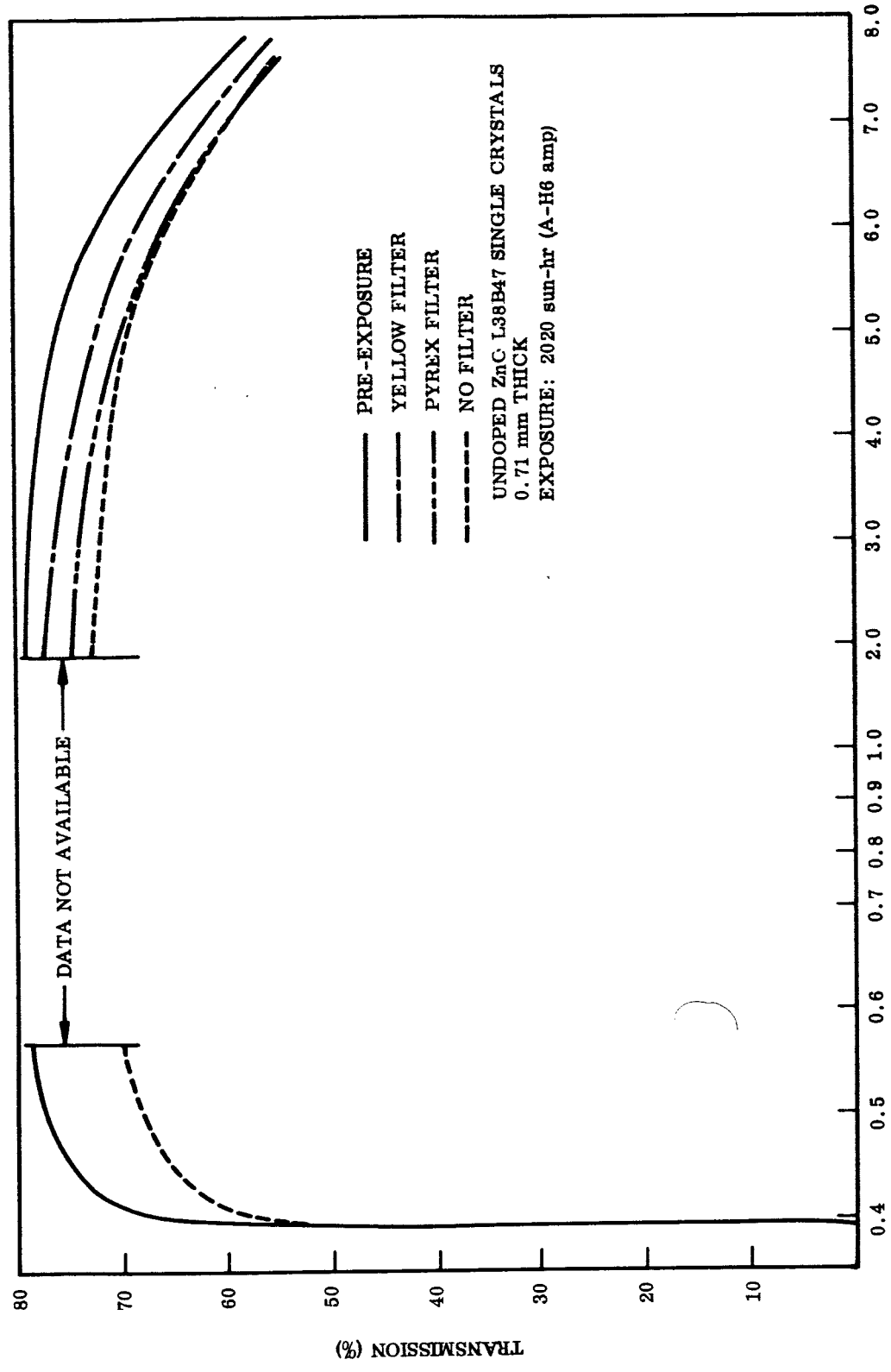

Fig. 6 Spectral Transmission of Undoped ZnO Single Crystals Before and After UV Irradiation in Vacuum

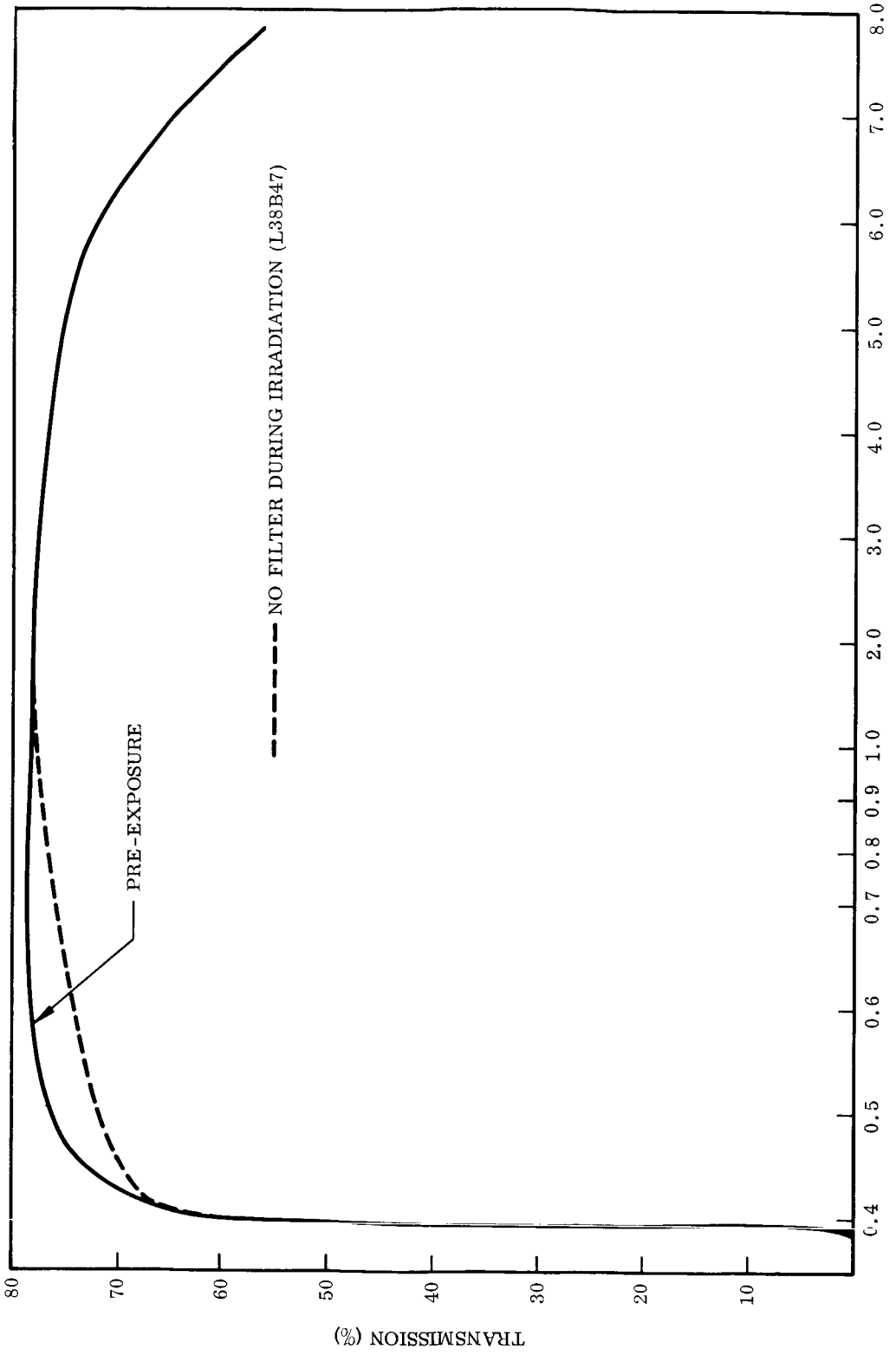

Fig. 7 Spectral Transmission of Undoped ZnO Single Crystals Stored in Air for 2 Months After 2020 sun-hr UV Exposure

The results with the Li-doped crystals in the infrared are shown in Fig. 8. The results show considerable infrared damage for the unfiltered crystal, a smaller effect for the Pyrex filtered crystal and essentially no effect for the yellow filtered crystal. The decreasing transmission at the shorter wavelengths is due to a surface scattering effect and no significance should be attached to it. The transmission of the same samples after storage in air at room temperature for 2 months is shown in Fig. 9. A considerable annealing effect is to be noted in the unfiltered and Pyrex filtered samples.

As a check on the initially observed apparent damage in the undoped crystals, a second irradiation test was carried out. Six undoped ZnO crystals were cut from the same ingot, ground to two different thicknesses (0.25 and 0.52 mm), lapped, and polished (doped crystals were no longer available). The spectral transmission was determined for each crystal and two crystals were kept as control samples. The irradiation was for 710 sun-hr the last of which was in a vacuum of 10^{-5} Torr, the sample temperature being 550° F. The exposure test encountered various difficulties which are given in detail on p. 64 in connection with Fig. 30. These experiments were run together. The item of greatest concern here is the relatively poor vacuum conditions that were experienced. The post-exposure spectral transmission measurements were identical to the pre-exposure measurements to within experimental error over the spectral range covered (0.35 to 8 μ). This is also the case for two samples not exposed to the irradiation but held at 550° F during the test. The results are shown in Fig. 10. The lack of degradation may be attributed not only to the poor vacuum but to the fact that the sample temperature was relatively high in the poor vacuum for a long period (several hours) after the lamp was turned off.

The two degradation runs described above were carried out under different experimental conditions. The fact that significantly different results were obtained does not allow us, at this time, either to make a critical analysis of the data or to draw a firm correlation between the effects observed in the single crystals and the pigments. However, if we assume that the effects observed in the first run are characteristic of ultraviolet damaged single crystals we can draw some tentative conclusions as to the origin of the damage in the single crystals in various spectral regions.

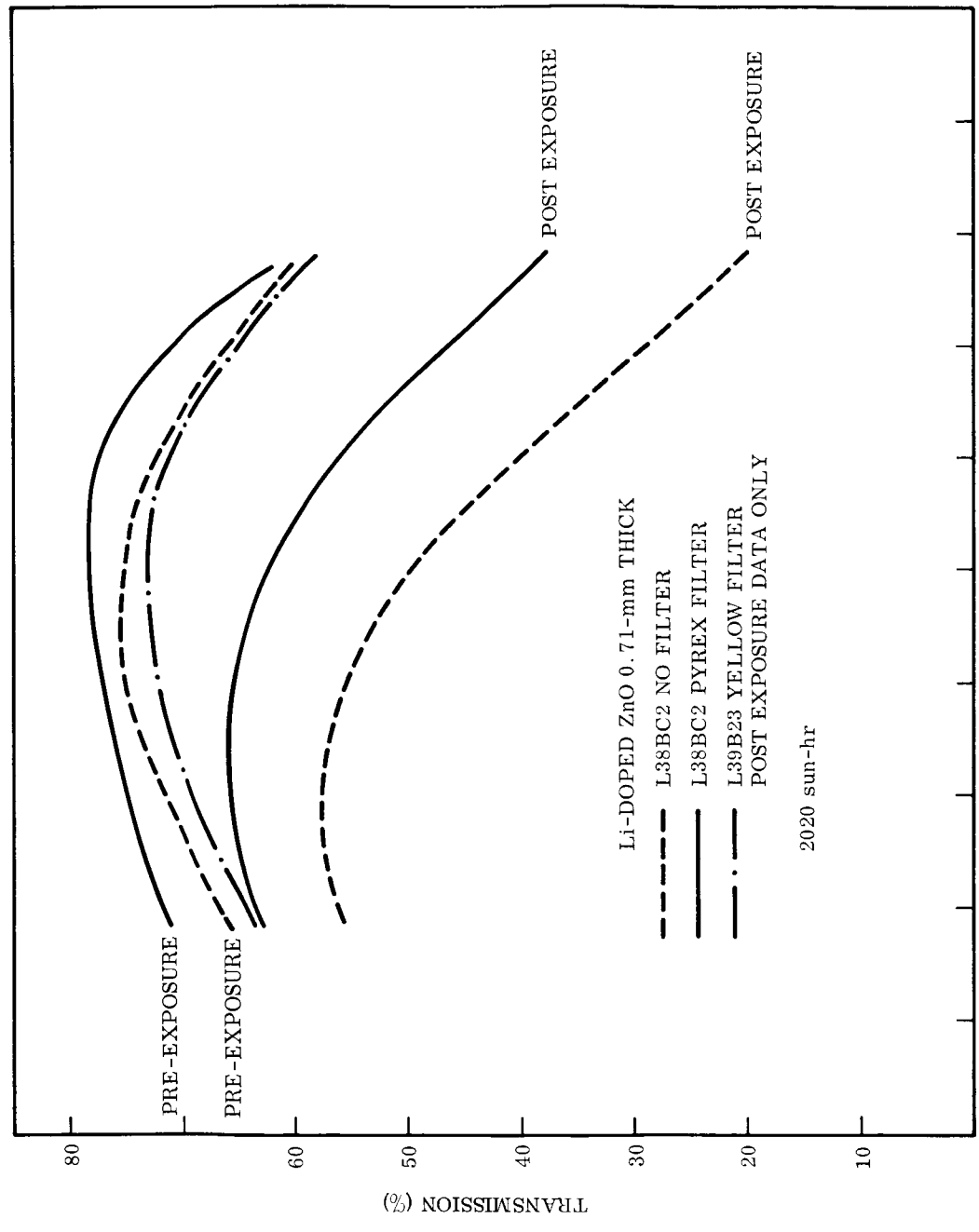

Fig. 8 Spectral Transmission of Li-doped ZnO Single Crystals Before and After UV Irradiation in Vacuum

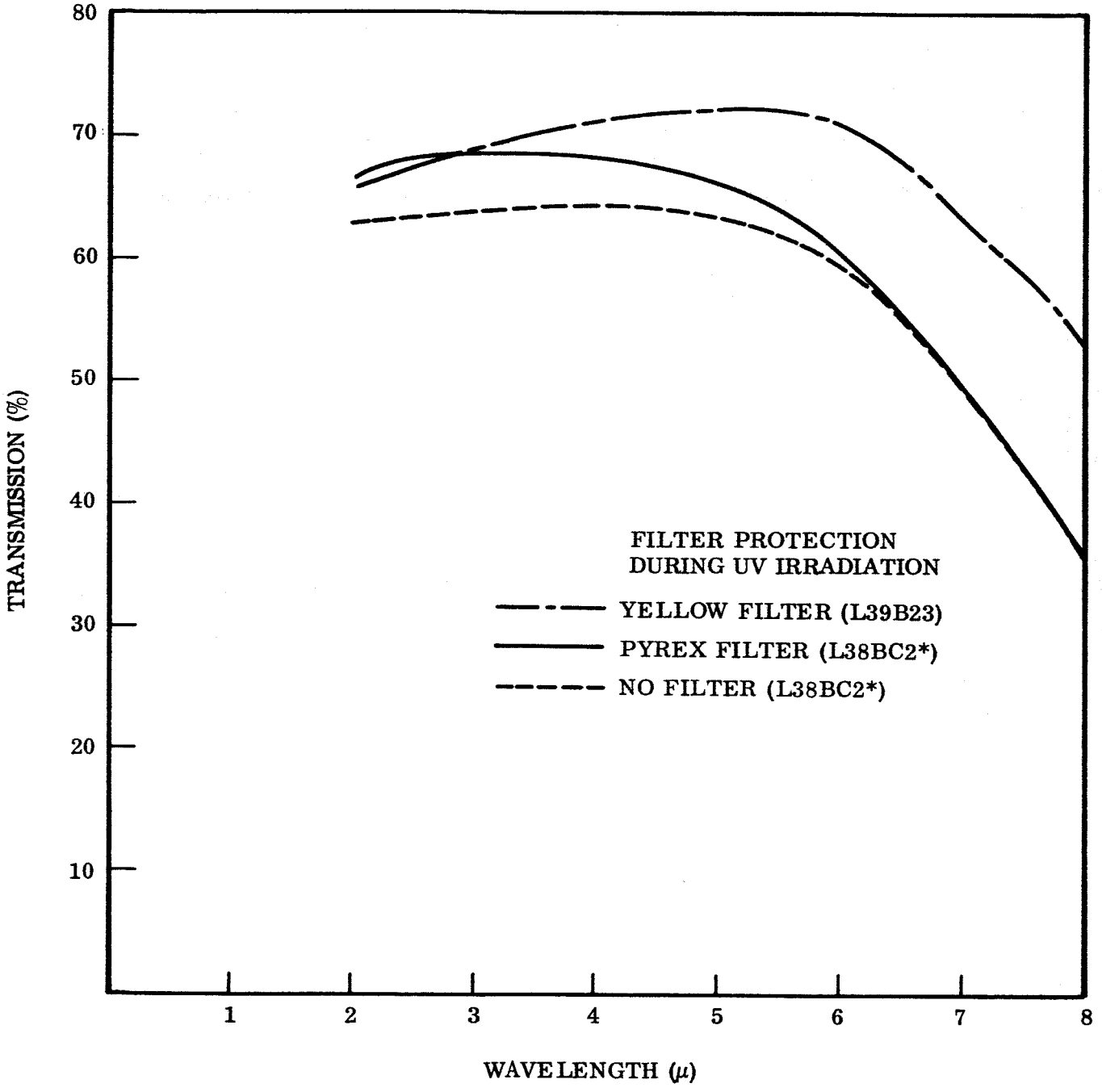

Fig. 9 Spectral Transmission of Li-doped ZnO Single Crystals Stored in Air for 2 Months After 2020 sun-hr UV Exposure

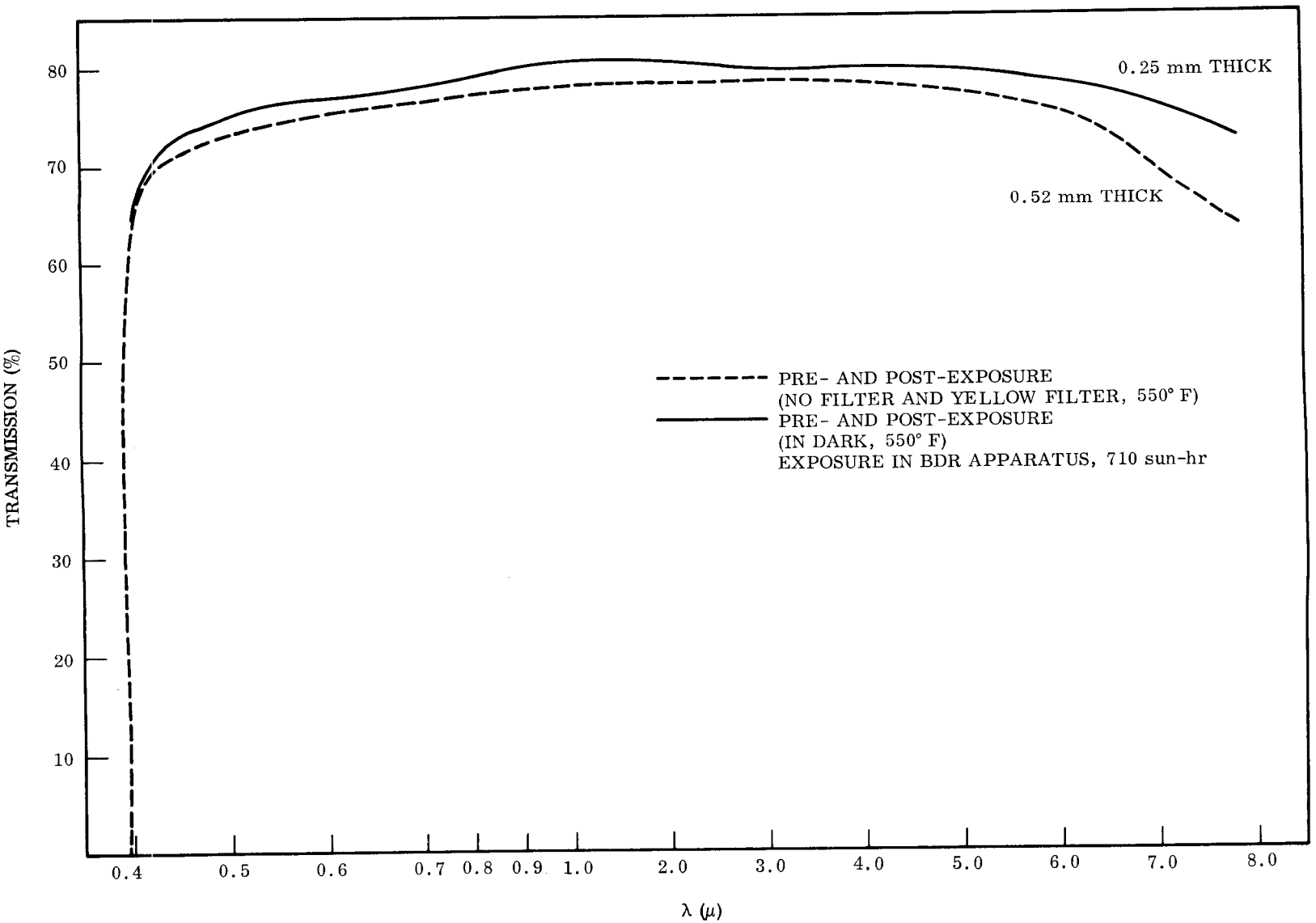

Fig. 10 Spectral Transmission of Undoped ZnO Single Crystals Before and After UV Irradiation in Vacuum

The first point to note concerning the damage observed in the visible spectral region on the undoped single crystal is that this damage requires greater than band-gap radiation and is, therefore, generated near the surface of the crystal. However, subsequent polishing and etching did not remove the damage which implies that the damage resides deeper in the crystals. The unfiltered crystal presumably is at a higher temperature during irradiation than the other samples. This higher temperature would enhance diffusion, thus allowing damage to diffuse deeper into the material. The Fermi level in the crystal as determined from its carrier concentration both before and after the irradiation was approximately 0.1 eV below the conduction band. The visible damage extends for photon energies at least 1 eV less than the energy gap. Therefore, the defects giving rise to the visible damage cannot be donor type states near the conduction band, but rather acceptor type states residing up to at least 1 eV above the valence band.

We are now in a position to discuss the damage observed in the infrared. Based on the results of Fig. 6, we note that comparable IR damage was obtained under all filtering conditions indicating that less than band gap, i.e., penetrating, radiation was principally responsible for the observed damage.

The fact that the Fermi level did not change indicates that the additional IR absorption is due to defects created by the penetrating radiation rather than to a redistribution of carriers in existing defect levels. Further, because the Fermi level is close to the conduction band the defects introduced must be donor states within perhaps 1 eV of the conduction band edge. The added absorption in the IR cannot be due to free carrier absorption since the carrier concentration did not change and the shape of the transmission curves at the longest wavelengths before and after irradiation are consistent with no change in free carrier absorption.

The data for the doped crystals are insufficient to relate the magnitude of the IR damage observed in the doped single crystals to that in the undoped crystals. However, it does not appear that the difference in the Fermi-levels alone in these two crystals (doped and undoped) is sufficient to account for the differences observed.

It is important to note that the above results on the single crystals bear a marked similarity to the effects observed with the particulate samples. In particular, the visible damage appears to be temperature sensitive and requires greater than band-gap irradiation; the infrared damage appears to result from less than band-gap (penetrating) irradiation; and similar annealing effects are observed.

The preceding interpretation, being based on the results of only a single degradation run does not permit a high confidence level in the data. The important point is that the type of data obtained above can yield significant information leading to an understanding of the basic mechanisms of the degradation process, and also indicating the types of experiments which would prove useful for a more complete understanding of the degradation phenomena.

3.2 TRANSIENT PHOTOCONDUCTIVITY

Measurements carried out on transient photoconductive effects in ZnO single crystals are discussed in this section. These studies were specifically concerned with the fast photoconductive process and particularly, the spectral photoconductivity and the decay rate of the photoconductivity. The studies were made to obtain information on the recombination and trapping states which bear directly on the degradation mechanism and to lay the groundwork for the use of the photoconductivity technique in investigating defects produced in degraded single crystals.

The optical absorption data on an undoped ZnO crystal (excess Zn) and a Li-doped crystal were taken on a double-beam grating spectrometer from 0.35 to 2.8 μ. Samples are described in Table 1. The results are shown in Fig. 11. The first point to note is the apparent shift of the fundamental absorption edge to lower energy (a shift of ~ 0.04 eV) with the Li addition. This shift is either the result of a high density of

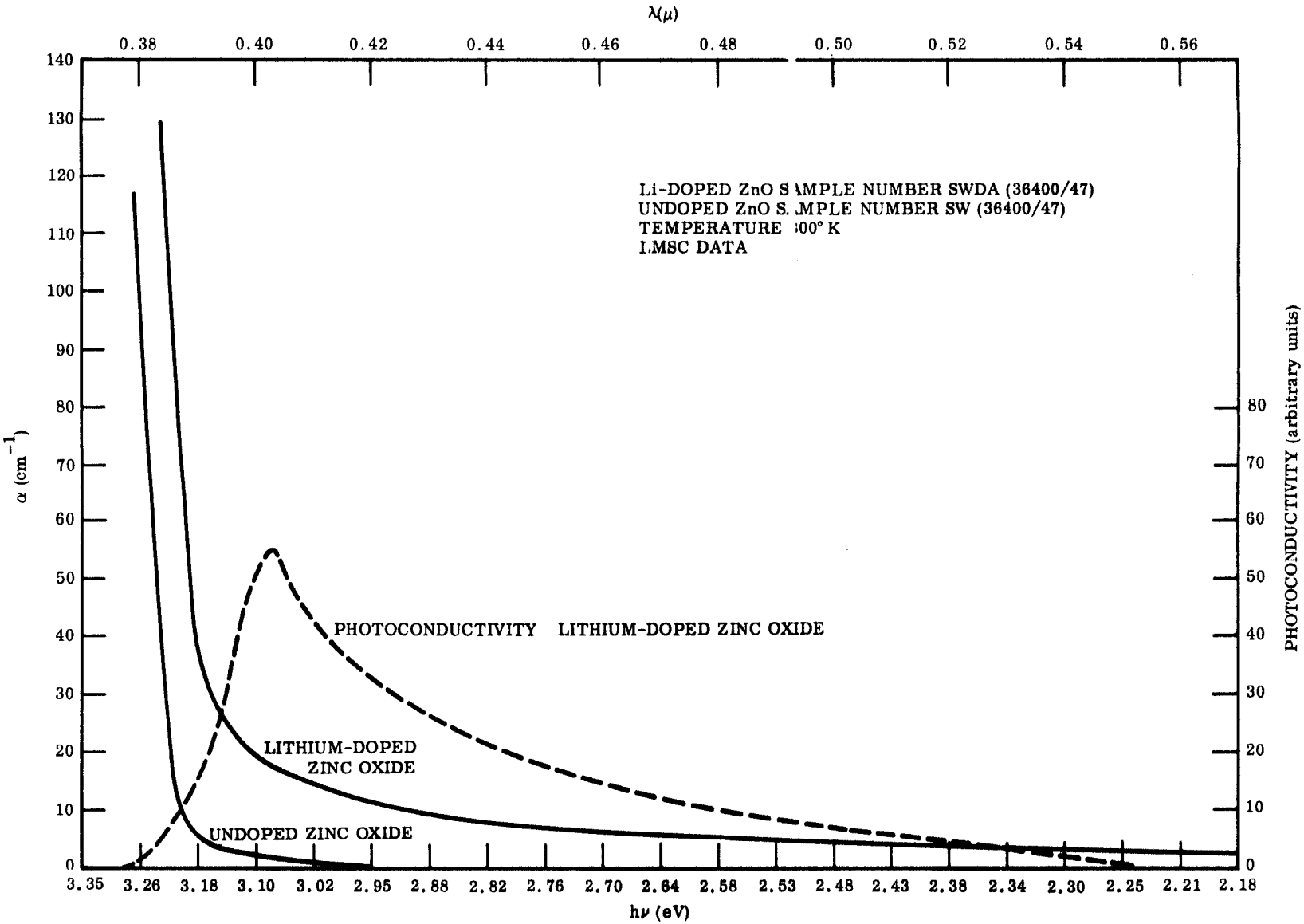

Fig. 11 Spectral Dependence of Optical Absorption and Photoconductivity

Table 1

SINGLE CRYSTAL SAMPLES

Sample Number	Dopant	Resistivity at 300° K (Ω-cm)	Carrier Concentration (cm^{-3})	Thickness (mm)	Length and Width (mm)	Electrode Material[a]
SW (36400/47)	Excess Zn (as grown)	4	2.5×10^{16}	1	5	In or Ag Paste
SWDA (36400/47)	Li	$\sim 10^{10}$	10^{7}	1	5	In or Ag Paste
SWDB (36400/47)	Li	2×10^{3}	5×10^{13}	0.7	5	In or Ag Paste

(a) Supplier: Minnesota Mining and Manufacturing Co.

shallow acceptor states or a deformation of the lattice itself due to the high impurity concentration. Our absorption data do not go to high enough values of the absorption coefficient to resolve this point.

The measurements of the spectral dependence of the photoconductivity were carried out at room temperature in air on the Li-doped crystals. Radiation from a xenon compact arc source was passed through a Perkin Elmer-112 monochromator and then brought to a focus on the sample. The chopping frequency of 1 kc was chosen to insure that only the fast photoconductive process was being observed. This point was verified by obtaining the spectral dependence of the photoconductivity from the amplitude using the transient d-c apparatus described in Appendix D. The results were the same in both cases and the observed photoconductive signal is shown in Fig. 11 as a function of wavelength. The measurements were carried out to 6 μ but no other photoconductive signals were detected. The photoconductive response and the absorption edge data on the Li-doped sample are compared in Fig. 11. The essential feature is that the photoconductivity which we are observing is a bulk as opposed to a surface phenomenon. The following argument supports this statement. It is to be noted that the photoconductive signal decreases as the absorption coefficient increases sharply due to the

band-to-band absorption (the fundamental band edge). The sample surface was purposely not etched, thus providing a surface with a high recombination rate. Therefore, in these experiments radiation which is absorbed very close to the surface (high absorption coefficient) does not give rise to a photoconductive signal. The next feature to note is that the signal peaks at that wavelength for which the absorption coefficient corresponds approximately to the reciprocal of the sample thickness (~ 0.04 cm). At longer wavelengths an increasing amount of the incident energy is transmitted through the sample, due to the decreasing absorption coefficient. The photoconductive response decreases proportionately. Consequently, it is clear that the observed photoconductive effect is a bulk phenomenon. The optical absorption and spectral dependence of the photoconductivity of a lower resistivity Li-doped crystal (SWDB) gave similar results again indicating that the photoconductivity is a bulk phenomenon.

Since ZnO shows only n-type conduction, the photoconductive spectral response must be associated with the excitation of electrons from acceptor levels to the conduction band. The photoconductive response turns on at 2.25 eV, thus indicating that the acceptor levels involved are located about 0.95 eV above the valence band. This is in good agreement with previous assignments of the Li acceptor level (~ 0.85 eV).

The transient behavior of the photoconductivity in the Li-doped single crystals was investigated with the apparatus described in Appendix D. When either a short light pulse (0.5 μsec) or a chopped d-c light source irradiates the sample, there is an immediate rapid rise and then an immediate rapid decay of the photoconductivity. This is followed by a relatively longer decay process (milliseconds) which can provide information on the trapping processes in the crystal.

The decay characteristics of the photoconductivity experiments have been carried out over a range of temperature and as a function of background illumination. The first point to note is that the photoconductivity observed is the fast photoconductive effect which is determined by the carrier recombination processes in the crystal and is not determined by adsorption or desorption of oxygen at the surface. The second point to

note is that the response observed in the transient behavior is a bulk and not a surface effect. This can be established as follows. The transient behavior is completely independent of the surrounding atmosphere whether it be vacuum, oxygen,or hydrogen. Furthermore, when an undoped ZnO filter was placed between the light source and the ZnO photoconductor, no essential change was detected in either the magnitude of the photoconductivity or its decay time. Therefore, the fact that the filter did not alter the photoconductive characteristics indicate that photon energies less than the band gap gives rise to this photoconductive response. The spectral dependence of the absorption constant and the photoconductive response previously mentioned indicate that the transient photoconductivity observed is indeed a bulk effect.

Since the photoconductive current is carried by electrons the photoconductive decay will be determined by the length of time the electron is free in the conduction band once it has been excited. The electron will remain free as long as the accompanying hole remains trapped; once the hole becomes untrapped, electron-hole recombination occurs very rapidly. Thus the rate of photoconductive decay is determined by the occupancy of the hole trapping states as determined by the hole quasi Fermi level under steady-state illumination.

Typical photoconductive decay responses observed for the Li-doped single crystals are shown in Fig. 12. Essentially the same response is obtained for the higher and lower resistivity crystals. As indicated in Fig. 12 a decrease in the decay rate with both increasing intensity of background illumination and temperature is evident. In Figs. 13 and 14, the temperature dependence of the decay rate in the higher and lower resistivity samples, are shown. We note that the decay rate is exponential in all cases and although a slightly different dependence of the decay rate is observed for the two samples, the important point to note is the relatively weak dependence of the decay rate.

The effect of background illumination on the decay curves is shown in Fig. 15 for the lower resistivity sample. The only observable effect on the decay time was obtained

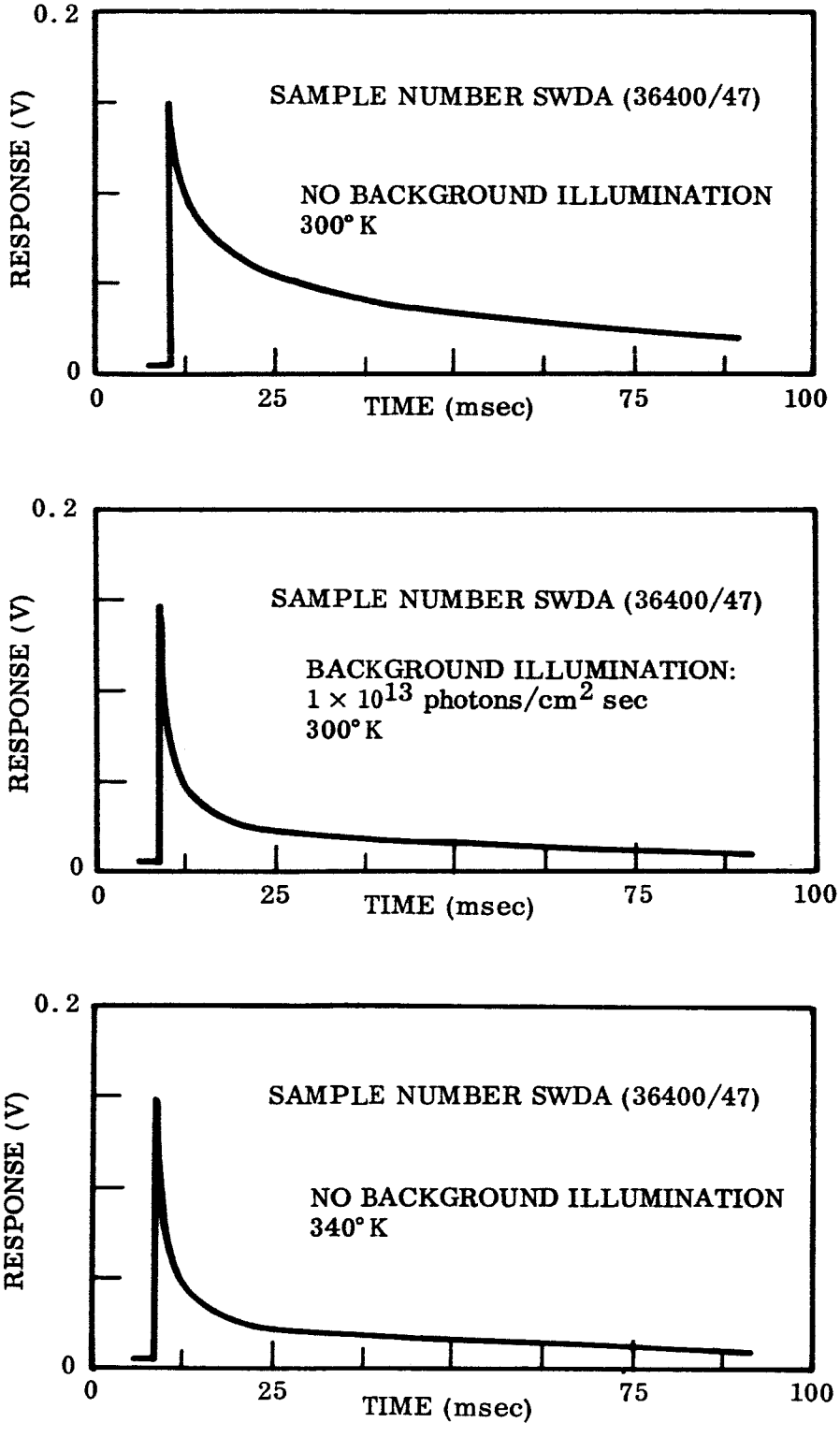

Fig. 12 Photoconductive Response of Li-Doped ZnO

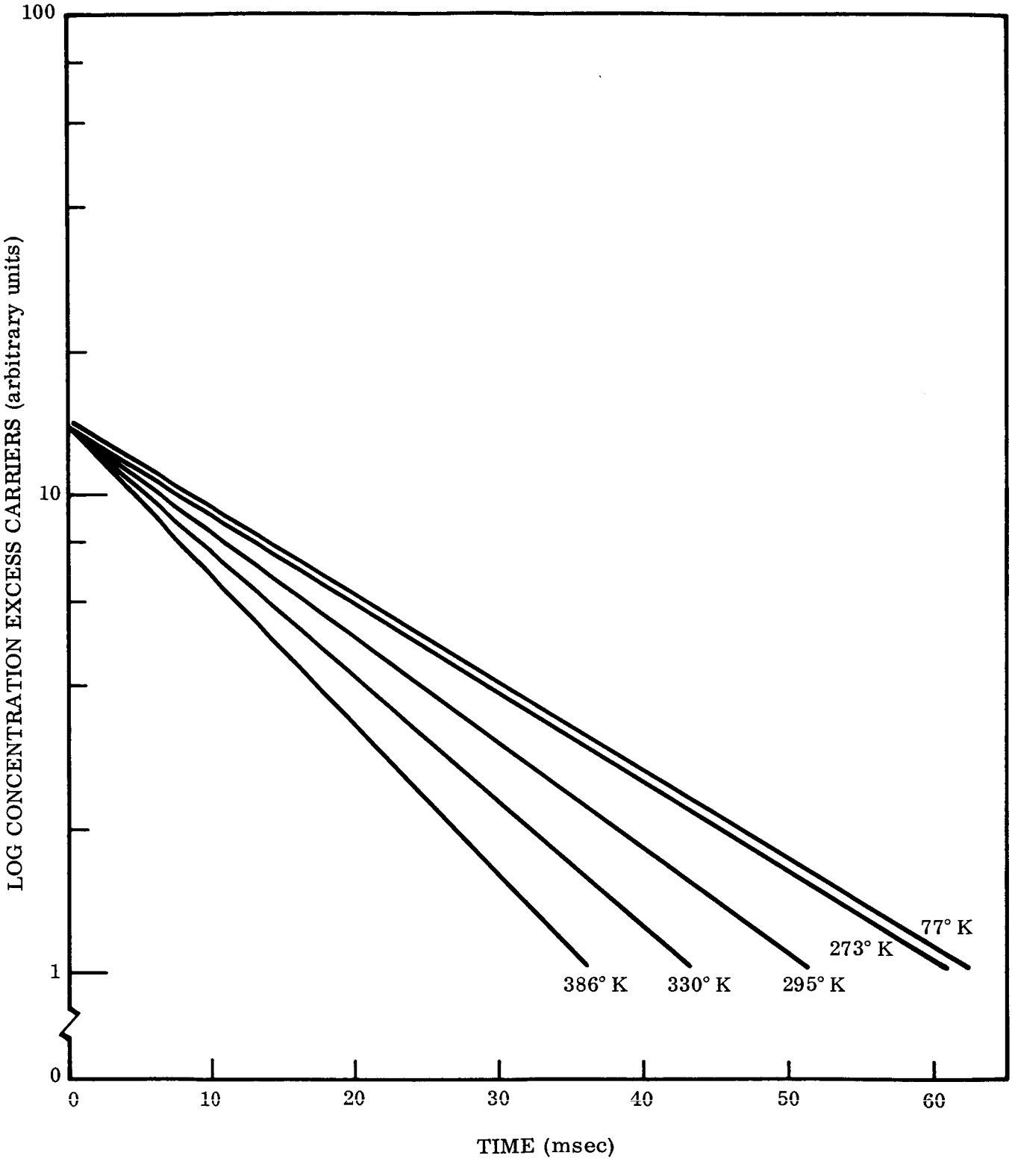

Fig. 13 Photoconductive Decay of Li-Doped ZnO at Different Temperatures

when the background radiation had the same spectral content as that which gave rise to the photoconductivity. Therefore, the effect of the background illumination on the decay rate is the movement of the hole quasi Fermi level through the hole trapping state distribution. In addition the effect of the background illumination on the d-c level of the photoconductivity was obtained. From these results it was determined that for the range of background illumination intensity employed in the experiments shown in Fig. 15, the hole quasi Fermi level varied from 0.4 eV above the valence band.

These results imply a monotonic distribution of hole trapping states, in this energy interval, which increases in density as the valence band edge is approached. The existence of a distribution of hole trapping states is consistent with the observed weak dependence of the decay rate. The exact nature of the hole trapping states has not been determined, however, it must be a doubly negative charged site such as a Zn vacancy or $O^{=}$ in the lattice.

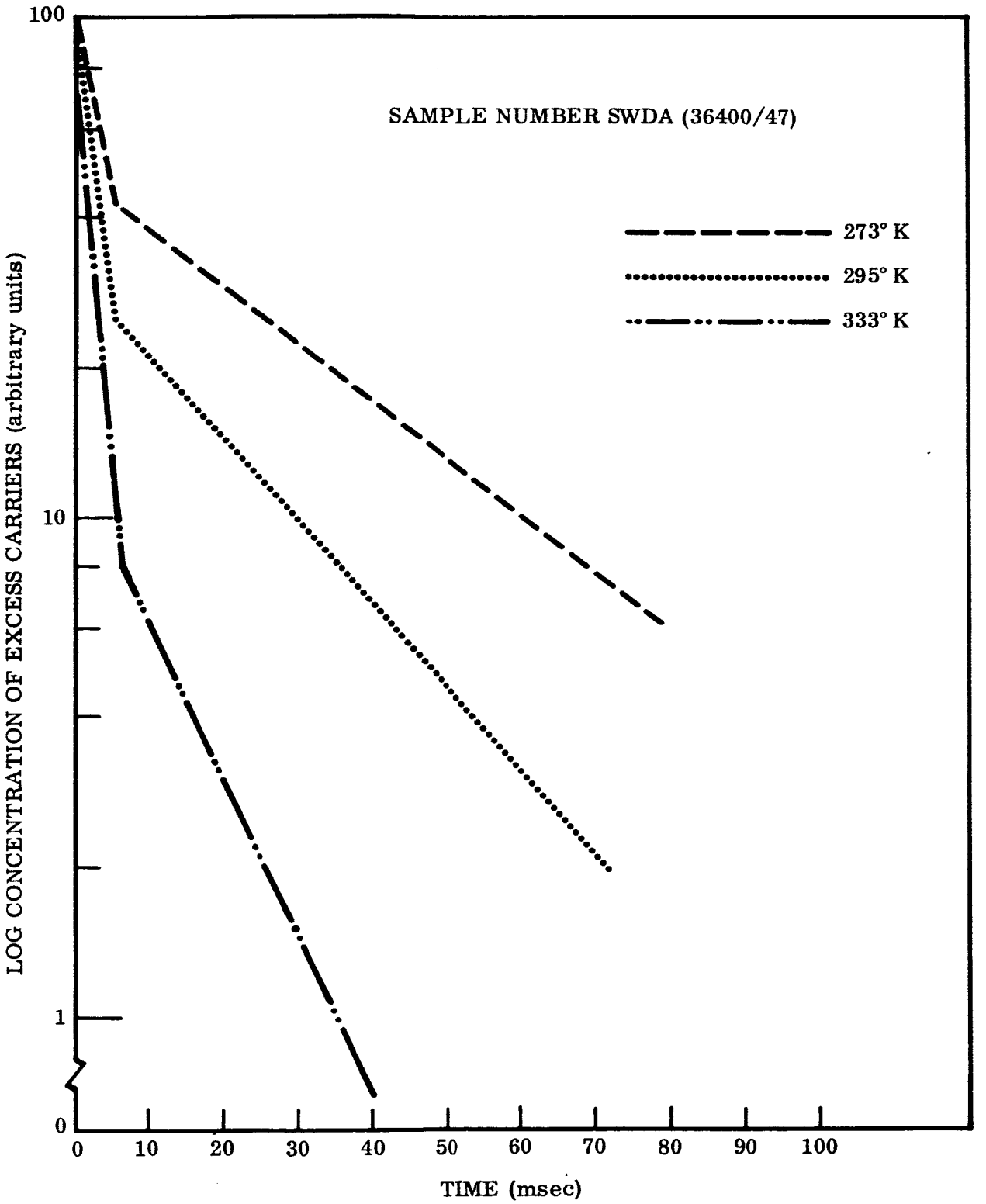

Fig. 14 Photoconductive Decay of Li-Doped ZnO as a Function of Temperature

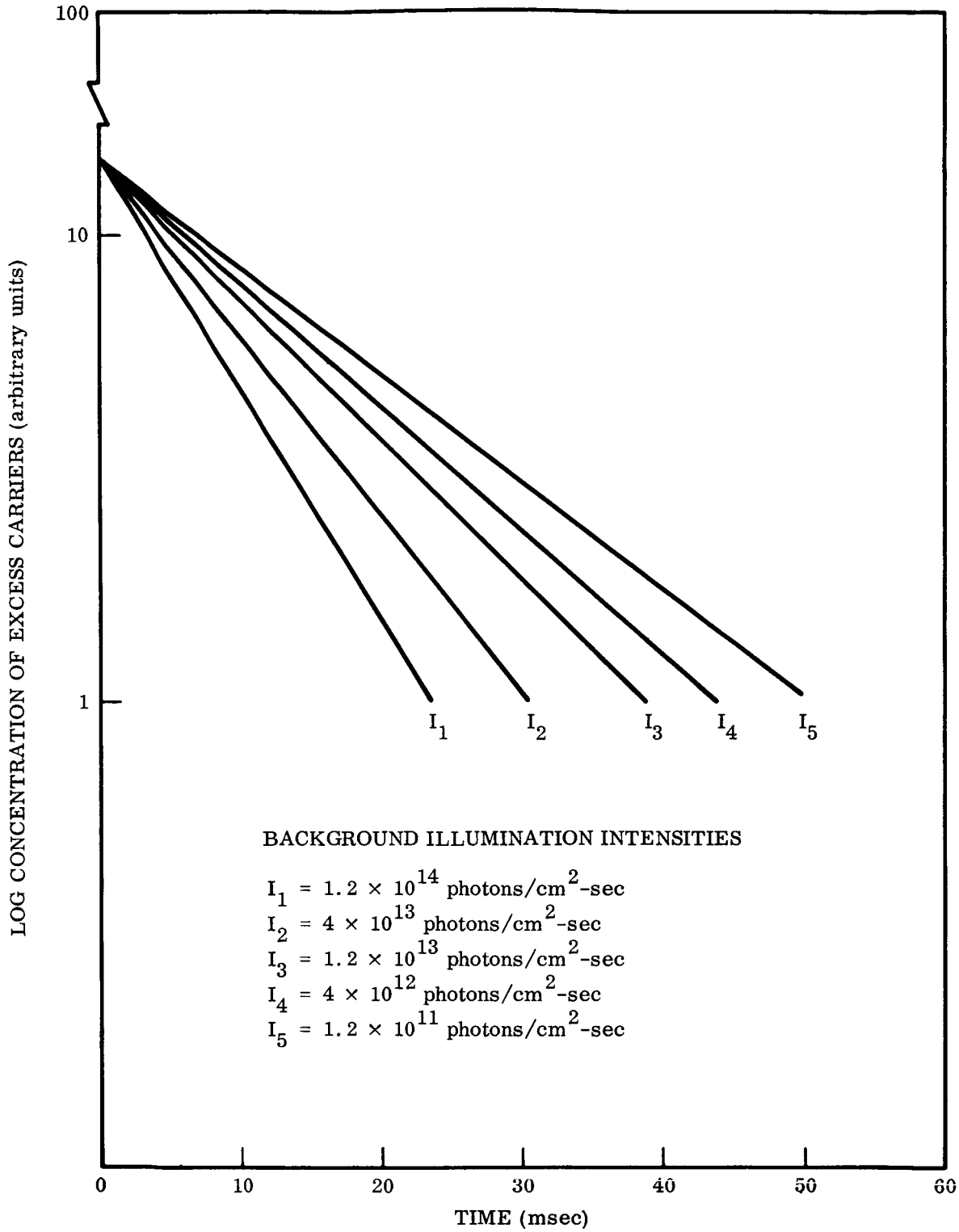

Fig. 15 Effect of Different Background Illumination on the Photoconductive Decay of Lower Resistivity Li-Doped ZnO Samples

Section 4
STUDIES ON PARTICLES

The major portion of the experimental program has been concerned with studies of particulate samples of zinc oxide. The emphasis on this type of sample is especially appropriate in view of the particulate nature of the pigments incorporated into thermal control paints. Since this program is concerned with the effects of solar radiation on the optical properties of the pigment exclusively, it has been necessary to devise methods of sample preparation which preserve the integrity of the zinc oxide particles without significantly altering the original properties of the pigment. Samples prepared by controlled pressing and sintering of zinc oxide powder have been found to adequately meet these requirements as discussed in Sec. 4.1 and 4.2.

Studies of the effects of solar radiation on particulate samples have been performed in two modes: static ultraviolet exposures and in situ measurements. The details of these experiments are discussed in Secs. 4.3 and 4.4. The static experiments are useful for collecting a relatively large amount of data in a routine manner. The in situ method permits detailed investigation of such factors as recovery and the influence of temperature and pressure, while maintaining the samples under the irradiation conditions. Both types of data are necessary for the formulation of a coherent model of the damage processes.

In all of the studies involving particulate samples, the primary index of damage was taken to be changes in the reflection spectra. The initial reflectance spectra of all samples were measured using a Cary Model 14 double-beam spectrophotometer with an integrating sphere attachment. In some cases, where data extending out to 2.5 μ were desired, a Beckman DK-2 spectrophotometer equipped with an integrating sphere was employed. The spectra obtained from the two instruments were found to be substantially the same.

4.1 SAMPLE PREPARATION

All particulate samples (except those specifically indicated) were prepared from the same material: zinc oxide powder, supplied by Merck & Co., Batch No. 52319. An analysis of the material, indicating the maximum impurities, is shown below:

Arsenic	0.0002%
Calcium and Magnesium	0.010
Iron	0.001
Lead	0.005
Manganese	0.0005
Insoluble in H_2SO_4	0.01
Chloride	0.001
Nitrate	0.003
Phosphate	0.001
Sulfur Compounds	0.01
Maximum total impurities	0.0417%

On the basis of this analysis, the zinc oxide utilized throughout this program has a purity of better than 99.9%. In addition, samples were prepared from New Jersey Zinc Co. SP 500, which has a nominal stated purity of 99.90%. In respect to initial optical properties and behavior under static ultraviolet exposure, the samples prepared from the two materials were identical within the limits of the measurements, as shown in Sec. 4.4.

The parameters involved in the preparation of the pressed particulate samples include forming pressure, sintering temperature and sintering atmosphere. The precise regulation of these parameters has been shown to be of considerable importance for the preparation of samples with reproducible optical properties. The method used for the preparation of zinc oxide samples throughout the course of this program is as follows: 3-gm aliquots of the ZnO powder are weighed out, deposited in a 1-in. diameter stainless steel pellet die, pressed at the requisite forming pressure, removed from the die, sintered under appropriate conditions, cooled, and stored.

The major conceptual problem involved in the sample preparation procedure is the production of reproducible, mechanically stable samples, composed of ZnO particles. It is felt that the zinc oxide in the composed samples should be identical to the original powder material from which they are formed. Unfortunately, loose powder samples are not amenable to handling and have no structural integrity. In this regard, pressed and sintered samples provide an adequate compromise. Under mild forming conditions the particles contained in the sintered samples have been shown to retain their original geometry to a large extent.

The effect of forming pressure has been investigated in an effort to ascertain the minimum pressure necessary for adequate compaction, as well as to examine the effect of mechanical damage on the zinc oxide samples. Experimentally, it was found that a minimum pressure of 10,000 lb/in.^{2} was required for the formation of stable pellets, in the absence of any binding additives. This forming pressure was used for the majority of the samples. At higher pressures, a pronounced yellowing of the zinc oxide throughout the bulk of the samples was found to occur. Figures 45 and 46 show the effect of forming pressure on the reflectance spectrum of zinc oxide pellets, before and after irradiation, respectively. It can be seen that the reflectance changes in an approximately linear fashion with forming pressure. It is of particular interest that the changes in reflectance induced by mechanical damage (pressure) bear a marked resemblance to the ultraviolet induced spectral changes, indicating that the damage processes may be intimately related.

The forming pressure also has a pronounced affect on the specularity of the samples. Sample pressed at 10,000 lb/in.^{2} appear highly diffuse, while those formed at higher pressures assume a more specular appearance.

As the program progressed, it became of interest to study particulate samples doped with copper. Zinc oxide doped with a nominal 0.1% copper was prepared by coprecipitation as the mixed carbonate:

$$0.999\ Zn(NO_3)_2 + 0.001\ CuCl_2 + Na_2CO_3 \rightarrow Zn_{0.999}Cu_{0.001}CO_3\ (\text{solid}) + 1.998\ NaNO_3 + 0.002\ NaCl$$

The precipitate was washed three times with distilled water to free it of dissolved salts, and heated at 400° C for 6 hr to decompose the carbonate:

$$Zn(Cu)CO_3 \xrightarrow{400^\circ C} Zn(Cu)O + CO_2$$

In order to study the effects of the copper doping on the zinc oxide powder, material was prepared in a similar manner without the added copper.

All particulate samples investigated are described in Table 2.

4.2 SINTERING STUDIES

Although the pressing operation performed on the zinc oxide powder forms the material into pellets, they do not have appreciable mechanical stability unless they are sintered. The effects of sintering temperature, time, and atmosphere have been investigated in an attempt to determine the mildest conditions compatible with adequate sample integrity. The criterion by which the extent of sintering was determined was surface area, as measured by nitrogen adsorption using the standard Brunauer-Emmett-Teller (BET) technique. The surface area of the unsintered zinc oxide was found to be 3.54 m^2/gm, corresponding to an average particle diameter of 0.3 μ.

The effect of sintering temperature was determined by measuring the final surface areas of samples sintered in air at various temperatures in the range 500 to 1000° C, for times varying between 5 min and 2 hr. Sintering at the higher temperatures resulted in a yellow discoloration of the material, and pronounced distortion of the initial sample geometry. The minimum temperature at which sintering could be detected was found to be 600° C. Sintering of the pressed samples at 600° C for 15 min was found to be the optimum combination of conditions. Surface area measurements on six samples prepared in this manner indicated that the material had a specific surface area of 3.2 ± 0.1 m^2/gm. This corresponds to a reduction of 10% in the surface area. These results indicate that in terms of geometry, the material in

Table 2

PARTICULATE SAMPLES

Thermophysics Sample Number		Figure Number	Preparation [a]			Optical Measurement Wavelength Range (μ)	Ultraviolet Exposure Conditions				Other Remarks	Difference between reflectance spectrum before and after irradiation
			Forming Pressure (1000 psi)	Sintering Atmosphere	Other Remarks		Pressure (Torr)	Total Exposure [b] (sun-hr)	Irradiation Time (hr)	Nominal Sample Temperature (°F)		
14218			20	air		0.3 to 1.8	3×10^{-6} to 6×10^{-7}	730	49	100 – 125		Visible and infrared lowered
14507	A		12	air		0.3 to 2.6	6×10^{-6} to 4×10^{-7}	950	61.5	100 – 125		Visible and infrared lowered
	AA	40	12	air		0.3 to 2.6	6×10^{-6} to 4×10^{-7}	950	61.5	100 – 125		Visible and infrared lowered
	AB	40	12	air		0.3 to 2.6	4×10^{-6} to 2×10^{-7}	860	100	100 – 125		Visible and infrared lowered
	AC		12	air		0.3 to 2.4	atmospheric	950	60	100 – 125	BDR [c]	No change
14671	A		101.6	air		0.3 to 2.6	4×10^{-6} to 2×10^{-7}	860	100	100 – 125		
	AA	45,46	101.6	air		0.3 to 2.6	4×10^{-6} to 2×10^{-7}	860	100	100 – 125		
	AB	45,46	76.2	air		0.3 to 2.6	4×10^{-6} to 2×10^{-7}	860	100	100 – 125		
	AC		76.2	air		0.3 to 2.6	4×10^{-6} to 2×10^{-7}	860	100	100 – 125		
	AD		76.2	air		0.3 to 2.6	4×10^{-6} to 2×10^{-7}	860	100	100 – 125		
	AE	45,46	50.8	air		0.3 to 2.6	4×10^{-6} to 2×10^{-7}	860	100	100 – 125		
	AF		50.8	air		0.3 to 2.6	4×10^{-6} to 2×10^{-7}	860	100	100 – 125		
	AG		50.8	air		0.3 to 2.6	4×10^{-6} to 2×10^{-7}	860	100	100 – 125		
	AH		25.4	air		0.3 to 2.6	4×10^{-6} to 2×10^{-7}	860	100	100 – 125		
	AI	45,46	25.4	air		0.3 to 2.6	4×10^{-6} to 2×10^{-7}	860	100	100 – 125		
	B		25.4	air		0.3 to 2.6	4×10^{-6} to 2×10^{-7}	860	100	100 – 125		Higher forming pressure gave lower reflectance in the visible and infrared; ultraviolet exposure produced additional decrease in visible and infrared reflectance
14690	A		12	air	Stored in	0.3 to 2.6	4×10^{-6} to 2×10^{-7}	860	100	100 – 125		
	AA		12	air	water 18 hr	0.3 to 2.6	4×10^{-6} to 2×10^{-7}	860	100	100 – 125		Different initial spectrum due to adsorbed water; same post-exposure reflectance as irradiated standard sample
14691	A		10	air		0.3 to 2.6	4×10^{-6} to 2×10^{-7}	860	100	100 – 125		Visible and infrared lowered
	AA	45	10	air		0.3 to 2.6	4×10^{-6} to 2×10^{-7}	860	100	100 – 125		
14701	A		10	air		0.3 to 2.0						
14804	A		10	nitrogen		0.3 to 1.8						
	AA		10	nitrogen		0.3 to 1.8						
	AB		10	10 μ pressure		0.3 to 1.8						
	AC		10	10 μ pressure		0.3 to 1.8						
14805	A	26	10	air		0.3 to 2.4	10^{-5} to 10^{-6}				BDR	
	AB		10	air		0.3 to 2.4	10^{-5} to 10^{-6}				BDR	
14852			10	air		0.3 to 2.4	10^{-5} to 10^{-6}				BDR	
14858			10	air	SP500	0.3 to 1.8	atmospheric	1070	88	100 – 125		No change
14859	A		10	air		0.3 to 1.8	atmospheric	1070	88	100 – 125	No filter	No change
	AA		10	air		0.3 to 1.8	atmospheric	1070	88	100 – 125		
	AB		10	air		0.3 to 1.8	atmospheric	0	88	100 – 125	0.4 cutoff filter	No change
	AC		10	air		0.3 to 1.8	atmospheric	0	88	100 – 125		
	AD		10	air		0.3 to 1.8	atmospheric	535	88	100 – 125	0.3 cutoff filter	No change
	AE		10	air		0.3 to 1.8	atmospheric	535	88	100 – 125		

(a) All samples are formed in air and sintered at 600° C for 15 min. Further sample preparation information is given in Sec. 4.1.
(b) One sun-hr is defined as the total irradiation in the wavelength range 2000 to 4000 Å incident during 1 hr on a unit surface area normal to the solar vector at 1 AU from the sun.
(c) BDR signifies in situ bidirectional reflectance measurements.

Table 2 (cont'd)

Thermophysical Sample Number	Figure Number	Preparation[a]			Optical Measurement Wavelength Range (μ)	Ultraviolet Exposure Conditions				Other Remarks	Difference between reflectance spectrum before and after irradiation
		Forming Pressure (1000 psi)	Sintering Atmosphere	Other Remarks		Pressure (Torr)	Total Exposure[b] (sun-hr)	Irradiation Time (hr)	Nominal Sample Temperature (° F)		
14860 A	47	10	10 μ pressure		0.3 to 1.8	atmospheric	1070	88	100 – 125		Increase large in visible, less in infrared
↓ AA		10			0.3 to 1.8	atmospheric	1070	88	100 – 125		
14861	28, 29	10	air		0.3 to 2.4	10^{-5} to 2×10^{-7}	1130	54	490	BDR[c]	Visible and infrared lowered
14863 A	39	10	air	0.050 in. thick, vapor deposited gold backed	0.2 to 19.0						
↓ AA	39	10		0.020 in. thick, applied as slurry to aluminum substrate	0.2 to 19.0						
14872 AB	42	10	air		0.3 to 1.8	10^{-4} to 2×10^{-7}	860	67	100 – 125	No filter	Lowered in visible and infrared
AE		10	air		0.3 to 1.8	10^{-4} to 2×10^{-7}	860	67	100 – 125		
A	42	10	air		0.3 to 1.8	10^{-4} to 2×10^{-7}	430	67	100 – 125	0.3 cutoff filter	Slight visible damage, greater infrared damage than unfiltered samples
AC		10	air		0.3 to 1.8	10^{-4} to 2×10^{-7}	430	67	100 – 125		
AA	42	10	air		0.3 to 1.8	10^{-4} to 2×10^{-7}	0	67	100 – 125	0.4 cutoff filter	No damage in visible, slight in infrared
↓ AD		10	air		0.3 to 1.8	10^{-4} to 2×10^{-7}	0	67	100 – 125		
14873 A		10	air	SP500	0.3 to 1.8	10^{-4} to 2×10^{-7}	860	67	100 – 125		Same as standard sample exposed simultaneously
↓ AA		10	air	SP500	0.3 to 1.8	10^{-4} to 2×10^{-7}	860	67	100 – 125		
14874 A	49	10	air	Cu doped	0.3 to 1.8	10^{-4} to 2×10^{-7}	860	67	100 – 125		Lower initial reflectance than standard samples; less damage
↓ AA		10	air	Cu doped	0.3 to 1.8	10^{-4} to 2×10^{-7}	860	67	100 – 125		
14875 A	43	10	10 μ pressure		0.3 to 1.8	10^{-4} to 2×10^{-7}	860	67	100 – 125		Visible and infrared increased; a large amount of zinc was evolved
↓ AA		10	10 μ pressure		0.3 to 1.8	10^{-4} to 2×10^{-7}	860	67	100 – 125		
14876 A		10	argon		0.3 to 1.8	10^{-4} to 2×10^{-7}	860	67	100 – 125		Same as standard before and after irradiation
↓ AA		10	argon		0.3 to 1.8	10^{-4} to 2×10^{-7}	860	67	100 – 125		
14884		10	air		0.3 to 2.4	CONTAMINATED				BDR	
14907 A		10	air		0.3 to 2.4	3×10^{-7} to 8×10^{-7}	960	54	150	BDR	Slightly lowered in visible and infrared
↓ AA		10	air		0.3 to 2.4	3×10^{-7} to 8×10^{-7}	960	54	150		
14908 A	49	10	air	precipitated ZnO	0.3 to 1.8	3×10^{-5} to 1×10^{-6}	1000	134	100 – 125		Very large decrease in visible, no change in infrared
14909 A		10	air	Cu doped	0.3 to 1.8	3×10^{-5} to 1×10^{-6}	1000	134	100 – 125		Large decrease in visible, no change in infrared; contamination from adjacent samples (14908A and 14963A) suspected
↓ AA		10	air	Cu doped	0.3 to 1.8	3×10^{-5} to 1×10^{-6}	1000	134	100 – 125		
14926		10	air		0.3 to 2.4	2×10^{-6} to 4×10^{-7}	990	55	220	BDR	Readout difficulties made data unreliable

(a) All samples are formed in air and sintered at 600° C for 15 min. Further sample preparation information is given in Sec. 4.1.
(b) One sun-hr is defined as the total irradiation in the wavelength range 2000 to 4000 Å incident during 1 hr on a unit surface area normal to the solar vector at 1 AU from the sun.
(c) BDR signifies in situ bidirectional reflectance measurements.

Table 2 (concl'd)

Thermophysics Sample Number	Figure Number	Preparation[a]			Optical Measurement Wavelength Range (μ)	Ultraviolet Exposure Conditions				Other Remarks	Difference between reflectance spectrum before and after irradiation
		Forming Pressure (1000 psi)	Sintering Atmosphere	Other Remarks		Pressure (Torr)	Total Exposure[b] (sun-hr)	Irradiation Time (hr)	Nominal Sample Temperature (°F)		
14951	16, 17	10	air		0.3 to 2.4	10^{-6} to 2×10^{-7}	970	52	200	BDR[c]	Slightly lowered in visible and infrared
14962 A		10	air		0.3 to 1.8	3×10^{-5} to 1×10^{-6}	1000	134	100 – 125		Marked inconsistency in extent of visible and infrared decrease; probably due to contamination from samples 14908A and 14963A; repeat of this test done with sample 17390
AA		10	air		0.3 to 1.8	3×10^{-5} to 1×10^{-6}	1000	134	100 – 125		
AB		10	air		0.3 to 1.8	3×10^{-5} to 1×10^{-6}	740	134	100 – 125	ndf[d] τ=0.74	
AC		10	air		0.3 to 1.8	3×10^{-5} to 1×10^{-6}	740	134	100 – 125		
AD		10	air		0.3 to 1.8	3×10^{-5} to 1×10^{-6}	550	134	100 – 125	ndf τ=0.55	
AE		10	air		0.3 to 1.8	3×10^{-5} to 1×10^{-6}	550	134	100 – 125		
AF		10	air		0.3 to 1.8	3×10^{-5} to 1×10^{-6}	240	134	100 – 125	ndf τ=0.24	
AG		10	air		0.3 to 1.8	3×10^{-5} to 1×10^{-6}	240	134	100 – 125		
14963 A		10	air	precipitated ZnO	0.3 to 1.8	3×10^{-5} to 1×10^{-6}	1000	134	100 – 125		Large decrease in visible, no change in infrared
14991 A	43	10	air		0.3 to 1.8	1×10^{-5} to 3×10^{-7}	2020	184	100 – 125		Visible and infrared lower change decreases with decreasing exposure
AA		10	air		0.3 to 1.8	1×10^{-5} to 3×10^{-7}	2020	184	100 – 125		
AB		10	air		0.3 to 1.8	1×10^{-5} to 3×10^{-7}	490	184	100 – 125	ndf τ=0.24	
AC	43	10	air		0.3 to 1.8	1×10^{-5} to 3×10^{-7}	490	184	100 – 125	ndf τ=0.24	
AD	43	10	air		0.3 to 1.8	1×10^{-5} to 3×10^{-7}	1120	184	100 – 125	ndf τ=0.55	
AE	43	10	air		0.3 to 1.8	1×10^{-5} to 3×10^{-7}	1120	184	100 – 125	ndf τ=0.55	
AF		10	air		0.3 to 1.8	1×10^{-5} to 3×10^{-7}	1510	184	100 – 125	ndf τ=0.74	
AG		10	air		0.3 to 1.8	1×10^{-5} to 3×10^{-7}	1010	184	100 – 125	0.3 cutoff filter	Slight visible damage, greater infrared than unfiltered samples with equal exposure
17387	33, 34	Unpressed, unsintered particulate sample			0.3 to 2.4	10^{-6} to 2×10^{-7}	970	52	450	BDR	
17390 A	44	10	air		0.3 to 1.8	1×10^{-5} to 2×10^{-7}	1000	93	100 – 125		Visible and infrared lower; change decreases with decreasing exposure
AA		10	air		0.3 to 1.8	1×10^{-5} to 2×10^{-7}	1000	93	100 – 125		
AB		10	air		0.3 to 1.8	1×10^{-5} to 2×10^{-7}	740	93	100 – 125	ndf τ=0.74	
AC		10	air		0.3 to 1.8	1×10^{-5} to 2×10^{-7}	500	93	100 – 125	0.3 cutoff filter	Slight visible damage, greater infrared than unfiltered samples with equal exposure
AD	44	10	air		0.3 to 1.8	1×10^{-5} to 2×10^{-7}	550	93	100 – 125	ndf τ=0.55	
AE		10	air		0.3 to 1.8	1×10^{-5} to 2×10^{-7}	550	93	100 – 125	ndf τ=0.55	
AF	44	10	air		0.3 to 1.8	1×10^{-5} to 2×10^{-7}	240	93	100 – 125	ndf τ=0.24	
AG		10	air		0.3 to 1.8	1×10^{-5} to 2×10^{-7}	240	93	100 – 125	ndf τ=0.24	
AH		10	air		0.3 to 1.8	1×10^{-5} to 2×10^{-7}	0	93	100 – 125	0.4 cutoff filter	No damage in visible, slight in infrared
17391	21, 22, 23	10	air		0.3 to 2.4	10^{-6} to 10^{-7}	925	48	70	BDR	No damage
17406	37	10	air		0.3 to 2.4	10^{-6} to 10^{-7}	800	47	-225	BDR	Moderate damage in visible, slight in infrared
17434	38	10	air		0.3 to 2.4	10^{-6} to 10^{-8}	765	47	-225	BDR	Large damage in visible, slight in infrared
17606	27, 30, 31	10	air		0.3 to 2.4	6×10^{-7} to 8×10^{-7}	710	41	525	BDR	Large damage throughout

(a) All samples are formed in air and sintered at 600° C for 15 min. Further sample preparation information is given in Sec. 4.1.
(b) One sun-hr is defined as the total irradiation in the wavelength range 2000 to 4000 Å incident during 1 hr on a unit surface area normal to the solar vector at 1 AU from the sun.
(c) BDR signifies in situ bidirectional reflectance measurements.
(d) ndf signifies electroformed nickel neutral density filter.

sintered form is essentially the same as the unsintered ZnO. Therefore, it can be expected that effects related to the particle surfaces should not be altered by this sintering procedure. The reproducibility of the sample preparation technique, as manifested by the optical properties of the individual samples, is good. Reflection spectra of samples prepared under the same conditions routinely agree to within 1%.

Experiments relating to the effect of ambient oxygen on the optical properties of the sintered material have demonstrated the importance of this parameter. Although samples sintered at 600° C in 1 atm of air, nitrogen, and argon show similar reflection spectra, vacuum sintered ZnO shows drastically different properties. Pressed pellets of zinc oxide sintered at 600° C for 15 min at a pressure of 10^{-3} Torr appeared dark gray with evidence of a substantial amount of free zinc on the surface. In addition, metallic zinc was found to deposit on the cool portion of the glass chamber containing the samples, (see Sec. 4.4).

These vacuum sintered samples were stored in vacuum in the dark until used.

The primary index of sample characterization throughout this program has been the reflectance spectra of the samples. Although characterization of particulate samples by means of electrical measurements (conductivity, Hall effect, Seebeck coefficients) was considered, it was felt that this approach would be unfruitful due to the idiosyncrasies of non-single-crystal samples. Measurements of this type appear to be risky, at best, and provide relatively little insight into the properties of the bulk material.

4.3 ULTRAVIOLET EXPOSURES WITH IN SITU MEASUREMENTS

Ultraviolet irradiation tests on sintered zinc oxide with in situ bidirectional reflectance measurements were conducted in an apparatus constructed for that purpose under this contract. To our knowledge, this is the first apparatus devised with the capability for measuring spectral reflectance during ultraviolet irradiation in vacuum. The apparatus is described in detail in Appendix B. The experimental results will be given in this section, while the theoretical discussion will be described in Sec. 6. Reflectance measurements are used to detect optical property damage. For the region 0.3 to 2.0 μ,

The standard particulate samples are thick enough (~ 0.070 in.) to be opaque. Hence, a change in reflectance is necessarily a change in absorptance, not transmittance when reflectance measurements are made before and after irradiation, directional reflectance is measured on the Cary Model 14. When reflectance measurements are made in situ, bidirectional reflectance is measured and then related to directional reflectance. The tests were performed on standard particulate zinc oxide discs, formed at 10,000 psi and sintered at 600° C in air (Sec. 4.1). The samples were irradiated in vacuum at a lamp-to-sample distance of 3.2 in. for nominally 50 hr. The sample temperature was controlled and maintained nearly constant. Temperatures from -225 to 500° F were achieved. Under this contract, zinc oxide samples have been exposed to ultraviolet radiation at three or more temperatures distributed over this range.

Sample Temperature Effects. Measurement and control of sample temperature throughout the test period, including the time before and after irradiation, are important in the in situ evaluation of optical property changes. Zinc oxide in vacuum exhibits a decrease in visible and infrared reflectance with increasing temperature. In addition, there is the well-known shift in the absorptance band edge to longer wavelengths with increasing temperature. In order to determine the ultraviolet-induced changes in spectral reflectance of a sample at a given temperature, one must also determine the spectral reflectance of the sample at the same temperature but without irradiation. The first problem in this determination is the measurement of sample temperature, particularly during irradiation. The methods used to measure and control sample temperature are discussed in Appendix B.

The second problem is that reflectance is not a function of temperature alone, but rather a time-temperature parameter. This is shown in Figs. 26 and 27 and is discussed in connection with them. The determination of in situ bidirectional spectral reflectance of unirradiated samples from -300 to 495° F, of samples under irradiation from -225 to 525° F, and of the recovery of samples from -250 to 70° F has been completed. The results are presented in the following figures and discussion.

Exposure at 200° F. The damage and recovery histories of a sample exposed at 200° F are presented in Figs. 16 and 17. The general procedure for this and subsequent

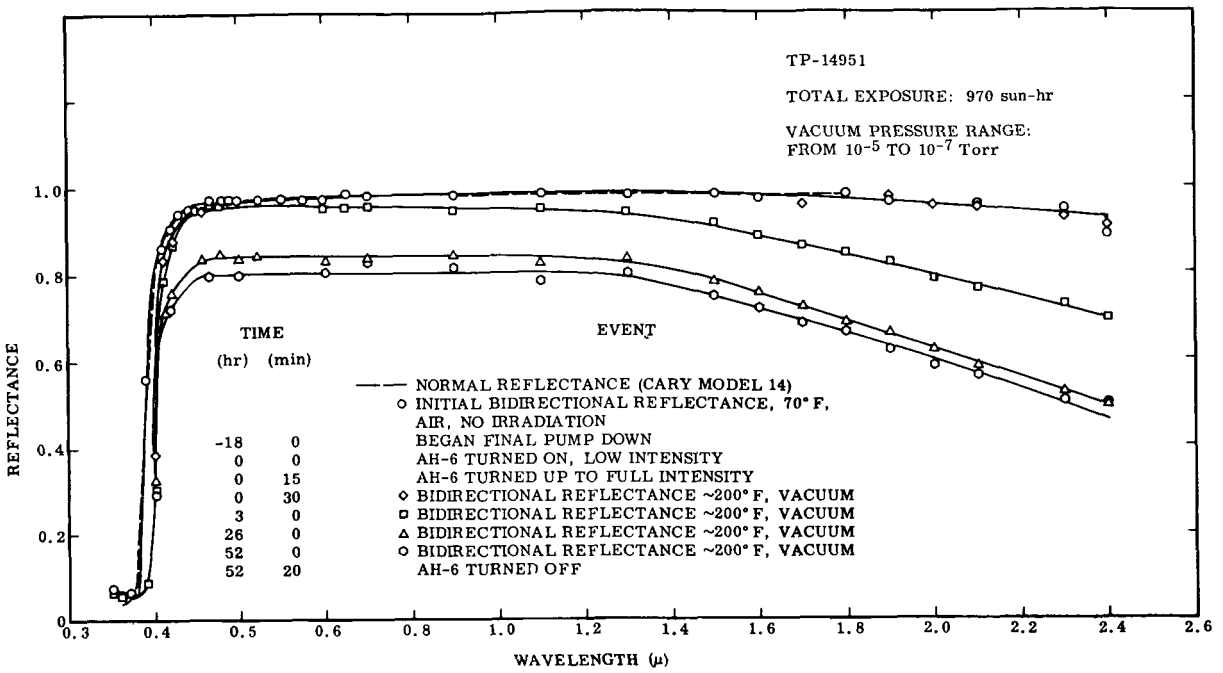

Fig. 16 Damage to Sintered ZnO at 200° F

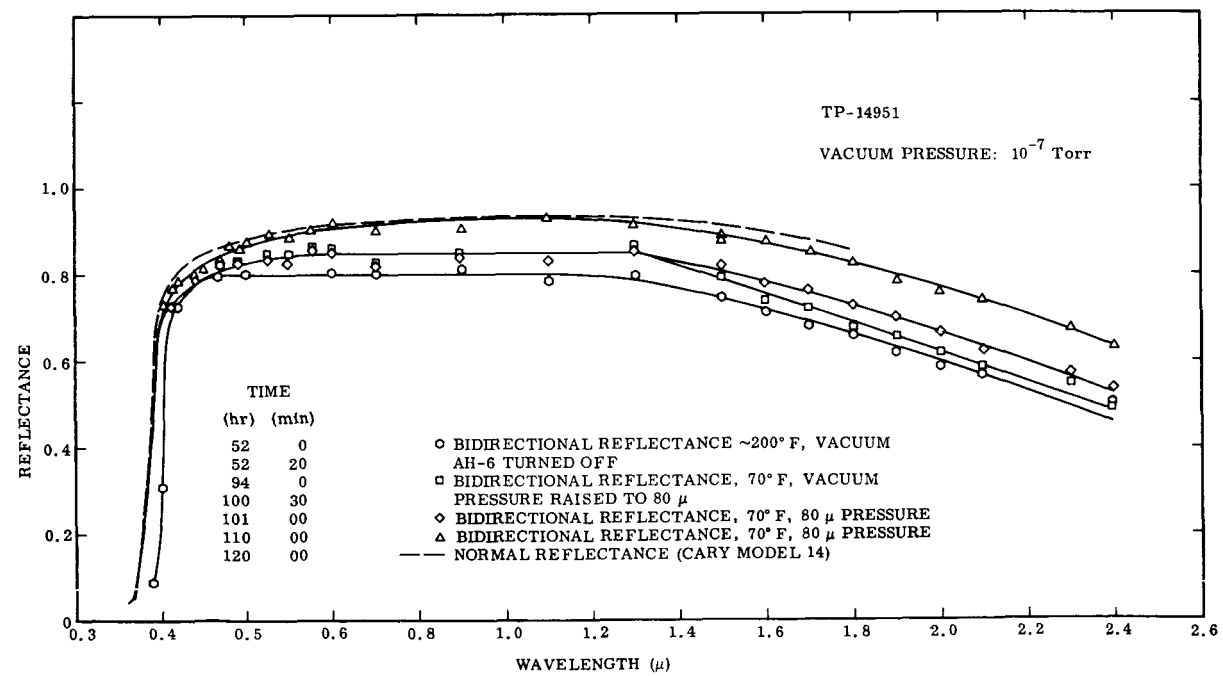

Fig. 17 Recovery of Sintered ZnO at 70° F

experiments is to find a normalization factor that adjusts the ordinate of the initial bidirectional spectrum to coincide with that of the initial normal reflection spectrum. This same factor is then used throughout on the ordinate of the bidirectional spectra. If the final bidirectional spectrum, then, agrees with the final normal reflectance measurement, it can be said that the bidirectional spectra throughout must have been representative of the total reflectance.

All the spectra from the in-air spectrum taken during the interval 15 to 45 min after the lamp was turned on agree quite well with the initial normal reflectance measurement. It is not until 3 hr after the A-H6 lamp was turned on that damage appears, and then the damage is effectively zero in the visible, increasing toward the infrared. The spectra at 26 and 52 hr show a more uniform grayness through the visible and very near infrared. The shift of the edge shown is due to temperature, as will be shown in subsequent sections.

When the A-H6 was turned off, no immediate recovery was observed. The sample was then allowed to remain in a high vacuum for 42 hr. The wavelengths near the ultraviolet absorption edge, and out into the infrared are shown to be relatively insensitive to this treatment, whereas the wavelengths in between are seen to have recovered substantially. The immediate effect of raising the pressure in the chamber to 80 μ was to partially recover the infrared, but no other part of the spectrum was changed. The entire spectrum increased substantially in reflectance over the next 9 hr in air. The final bidirectional and final normal reflectance agree in substance; the discrepancies are probably due to recovery while the normal reflectance measurement was being made with the Cary spectrophotometer. This is discussed further in connection with the second 500° F sintered sample run, Fig. 31. Plots of reflectance as a function of time during irradiation and recovery are shown in Figs. 18 and 19. Figure 20 gives the shape of the infrared recovery when air was admitted. There is a steep rise in the first 2 min, followed by a much less pronounced rise, over a longer period of time.

Exposure at 70° F With Recovery at -250° F. The history of a sample damaged at 70° F is presented in Fig. 21 and that of its recovery in high vacuum at -250° F is in Fig. 22

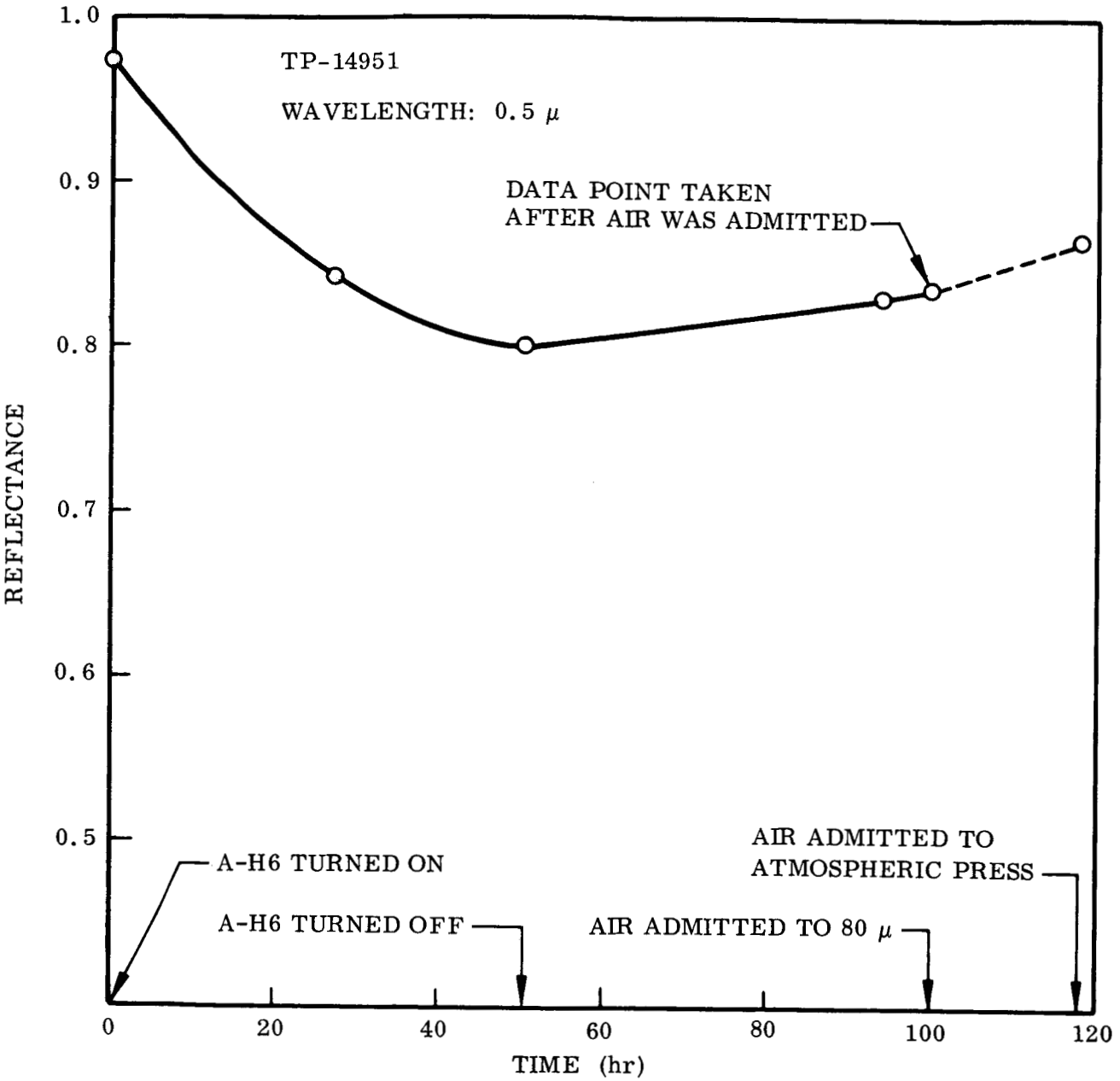

Fig. 18 Time Plot of Visible Reflectance of Sintered ZnO During Irradiation at 200° F and Recovery at 70° F

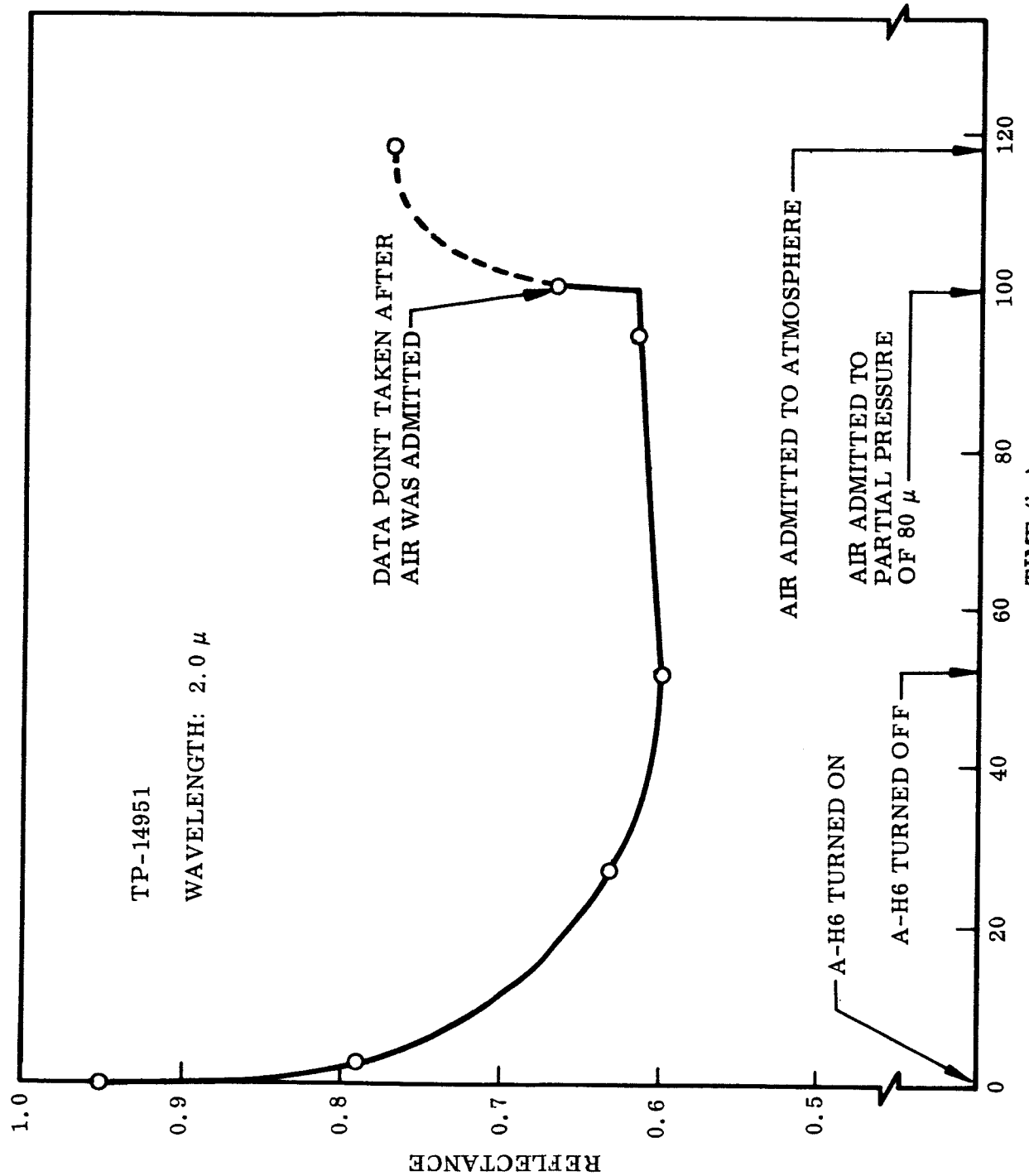

Fig. 19 Time Plot of Infrared Reflectance of Sintered ZnO During Irradiation at 200° F and Recovery at 70° F

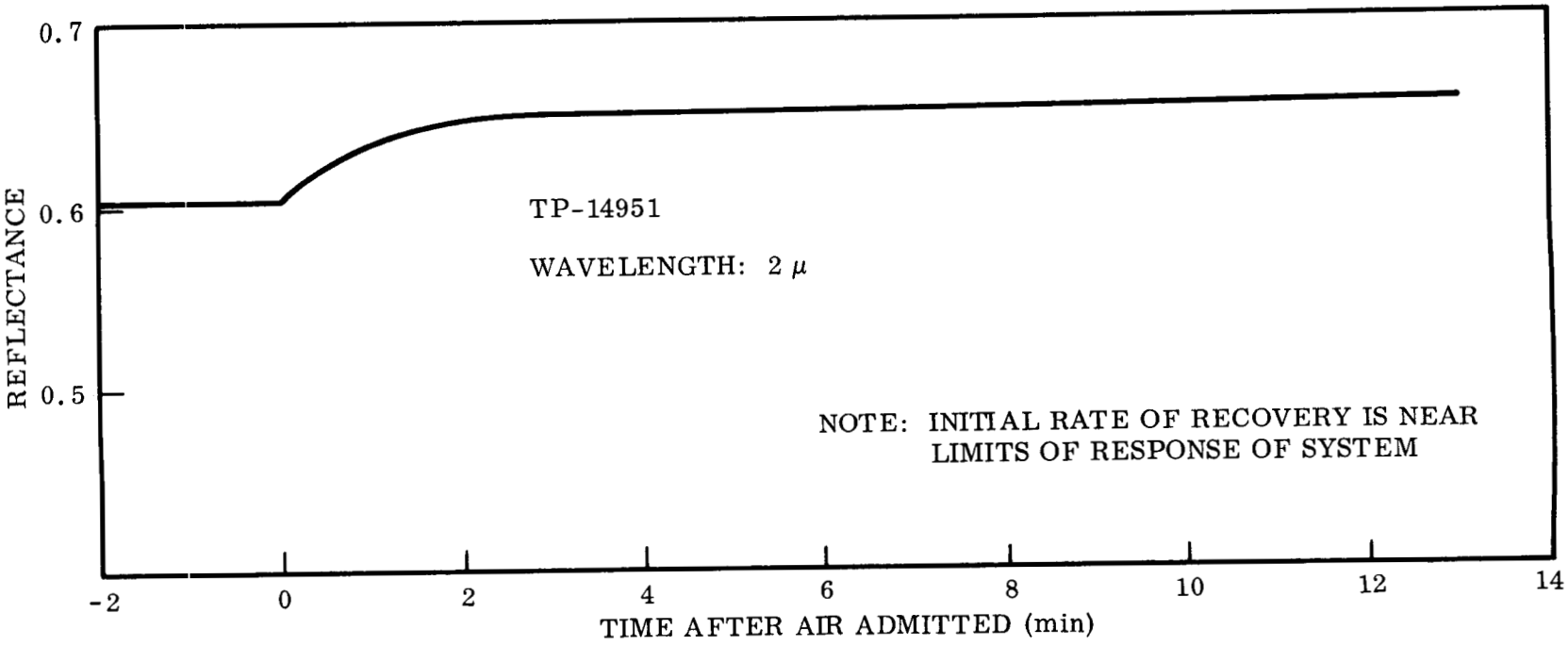

Fig. 20 Time Plot of Initial Infrared Recovery of Sintered ZnO at 70° F

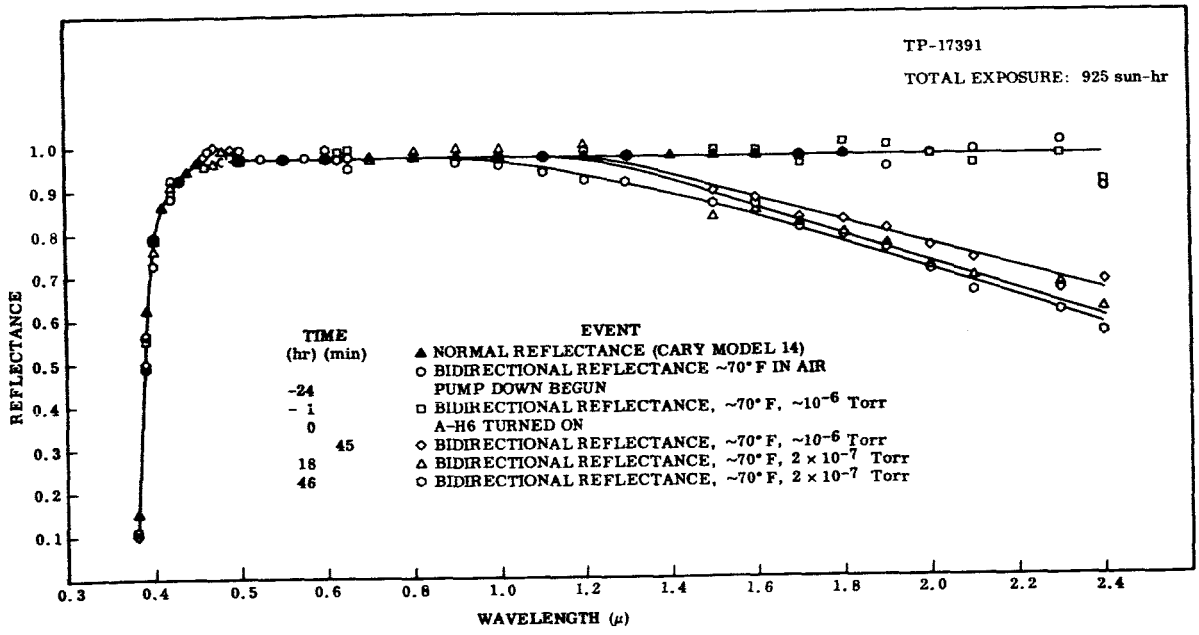

Fig. 21 Damage to Sintered ZnO at 70° F

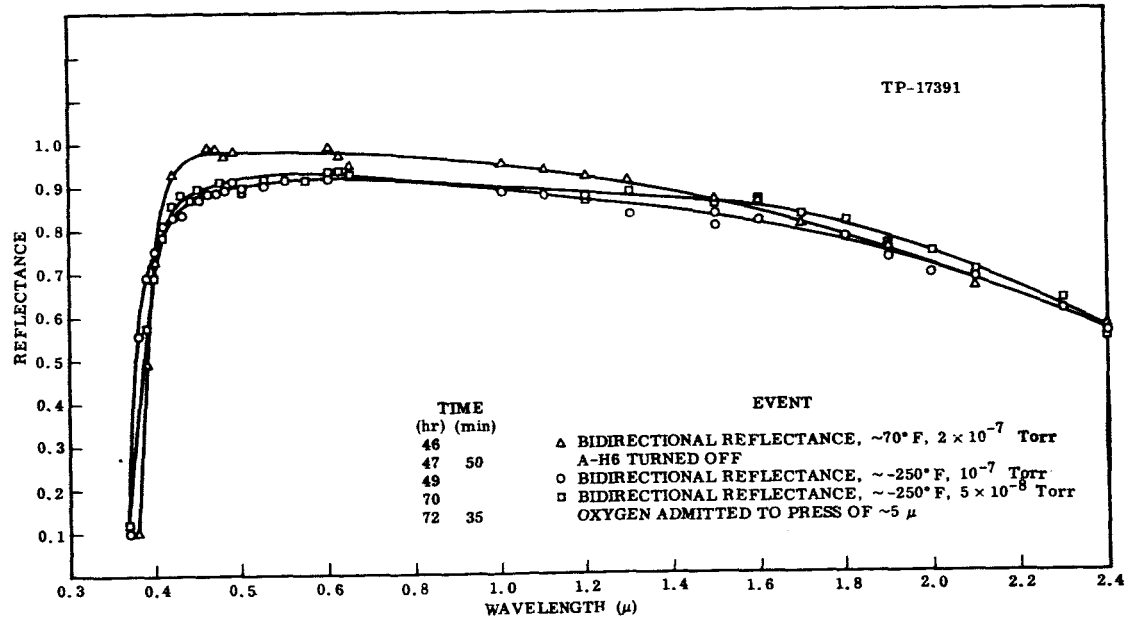

Fig. 22 Recovery of Sintered ZnO In High Vacuum at -250° F

and in low vacuum and in air is shown in Fig. 23. The ordinates for all bidirectional spectra are derived from the single normalization with the initial normal reflectance measurement.

All spectra would appear to coincide in the visible, if Fig. 21 is taken without further consideration. It is presented here in its uncorrected form. The reflectance at 0.47 μ was monitored continuously when the A-H6 was turned on, and it was observed that the apparent reflectance rose immediately to a value greater than its original value, but then decayed about 8%, so that by the time the first spectrum under irradiation could be taken, no apparent increase was shown. An example of this behavior is demonstrated in Fig. 32. All subsequent spectra under irradiation coincided with the first. The explanation for this lies in the interference of the A-H6 with the detection system. The intense reflected A-H6 radiation from the sample increases the apparent reflectance while the A-H6 is on, then, of course, the reflectance drops to its proper value when the A-H6 is turned off. This is seen in Fig. 22. The damage in the infrared appears to occur largely in the first 15 min, with only comparatively slight increases in damage subsequently. This produces a quite interesting change of slope if reflectance is plotted as a function of time, as in Fig. 24. Figure 22 shows some recovery due to 21 hr in vacuum at - 250° F. The effect of the temperature on the wavelength of the absorption edge may be noted.

Recovery at - 250° F is presented in Fig. 23. It is seen that the infrared recovers significantly when air is admitted, as it did in the room temperature recovery previously discussed. However the rate has been slowed considerably by the decreased temperature, as may be seen in the plot of Fig. 25. A 17-hr exposure in air brings the visible and very near infrared back to their original values of reflectance, while leaving the infrared damaged. Then, with the chamber brought up to atmospheric pressure, and the sample warm, the original reflectance is obtained throughout. If initial and final normal reflectance measurements were compared, there would appear to have been no measurable damage.

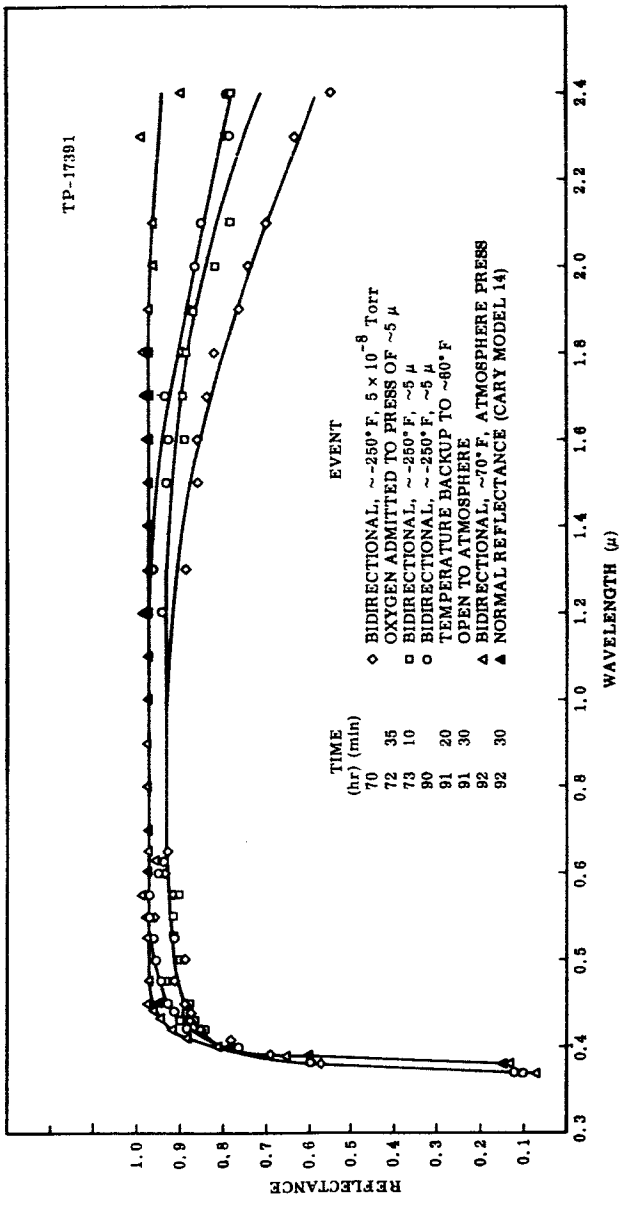

Fig. 23 Recovery of Sintered ZnO in Low Vacuum and in Air at -250° F

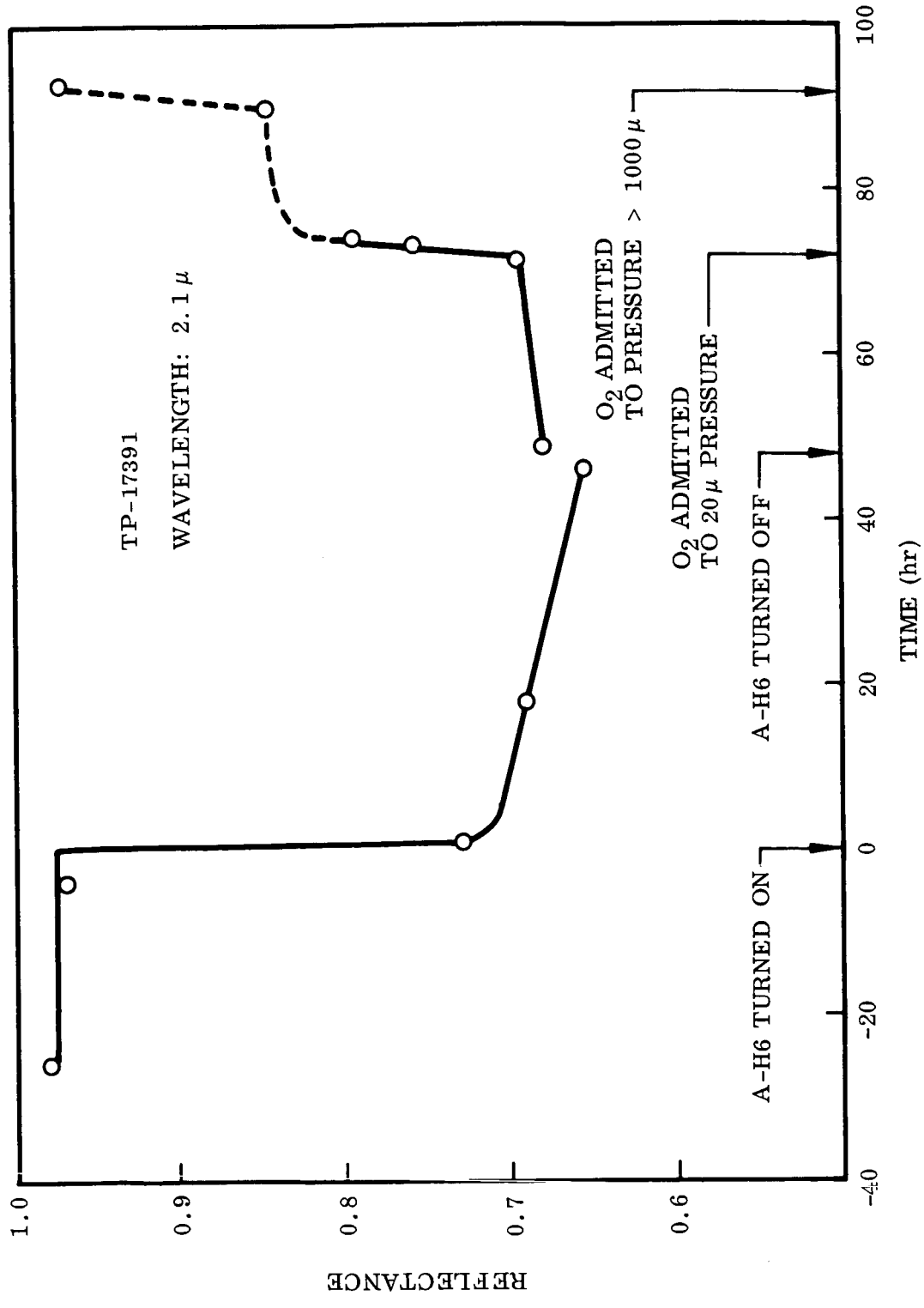

Fig. 24 Time Plot of Infrared Reflectance of Sintered ZnO During Irradiation at 70° F and Recovery at - 250° F

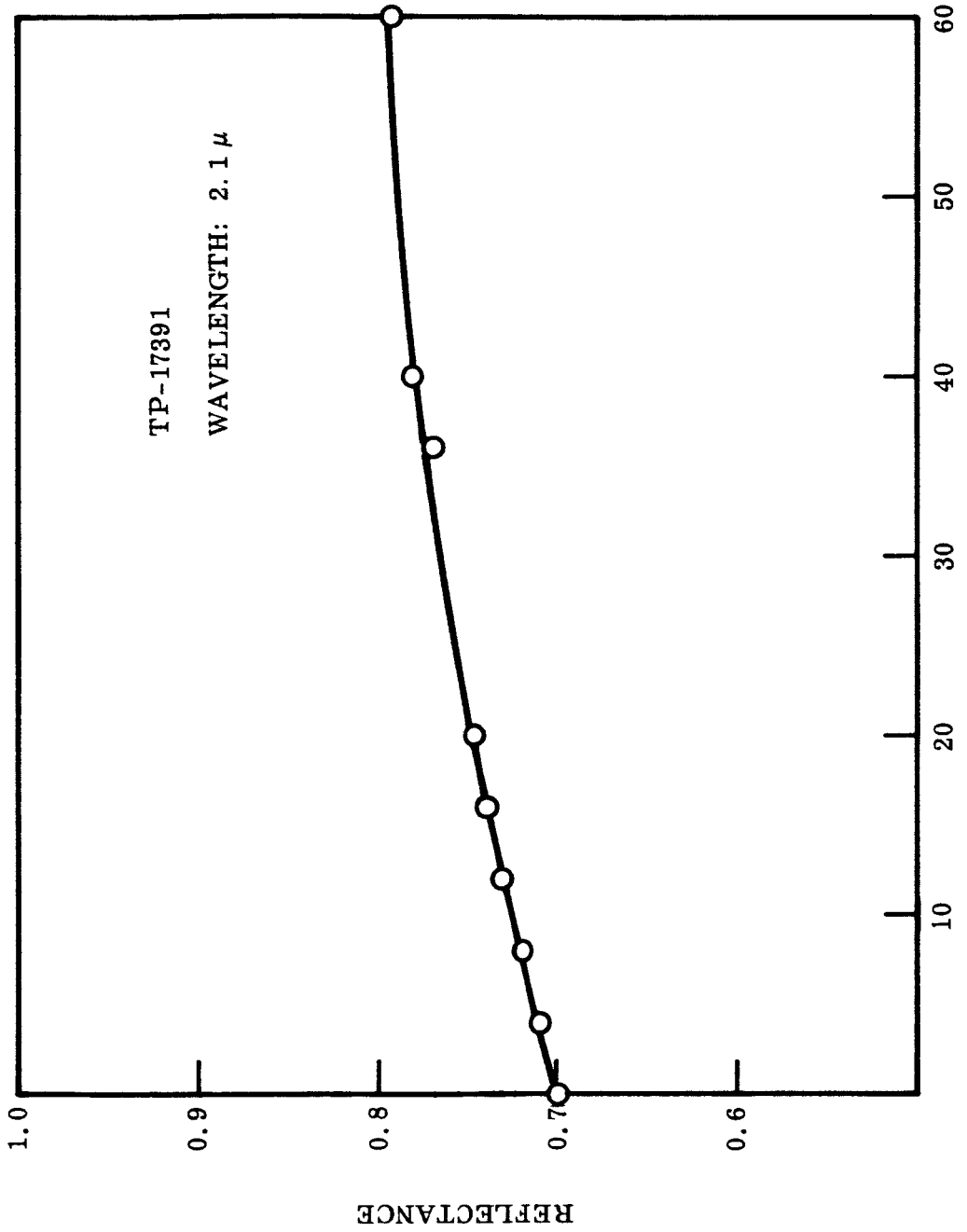

Fig. 25 Time Plot of Initial Infrared Recovery of Sintered ZnO at - 250° F

Effect of Temperature on Ultraviolet Absorption Edge. From Fig. 26, it is clear there is a definite shift of the absorption band edge toward longer wavelengths and a decrease of the visible reflectance due to increasing temperature. The wavelength of the true absorption band edge is observed to be only a function of sample temperature. In situ bidirectional reflectance measurements have shown that neither vacuum nor ultraviolet irradiation have an effect on the band edge during or after irradiation except to the extent that sample temperature is affected. In fact, the band edge location may serve as a convenient check for sample temperature measurements. It is evident that a small band edge shift produces a large percentage change in spectral or bidirectional reflectance at a wavelength in the region of the edge. The observed temperature-dependence of the band edge is similar to that reported in Ref. 33.

The temperature range from - 275 to 495° F is presented in Fig. 27. The most remarkable feature here is that the reflectance in the vicinity of the edge did not decrease as much as it did in Fig. 26. These spectra may be used to illustrate the point that ZnO damages as a result of being in vacuum for a time. The 70 and 210° F spectra in Fig. 27 were taken the same day, and could be drawn with a single line. The sample was then left to heat overnight to 495° F where the next spectrum was taken the next morning. The sample then cooled to 385° F and a spectrum taken that afternoon. The 495 and 385° F spectra were also drawn with a single line in the visible. Thus it seems probable that the time in vacuum at the elevated temperatures caused the damage in both Figs. 26 and 27. The fact that when temperature was lowered from 495 to 385° F there was no recovery in the visible, and in fact further damage was observed in the infrared, shows that the damage is not reversible with lowering of temperature. The liquid nitrogen curve is from a different experiment on a different sample, and so the infrared is omitted for clarity.

Exposures at 500° F. After evaluating the magnitude of the effect of temperature and vacuum on the spectral reflectance of unirradiated zinc oxide, an ultraviolet exposure test was performed on a sample maintained at 490 ± 20° F. The chronological variation of spectral reflectance up to the termination of the 54-hr irradiation period is shown in

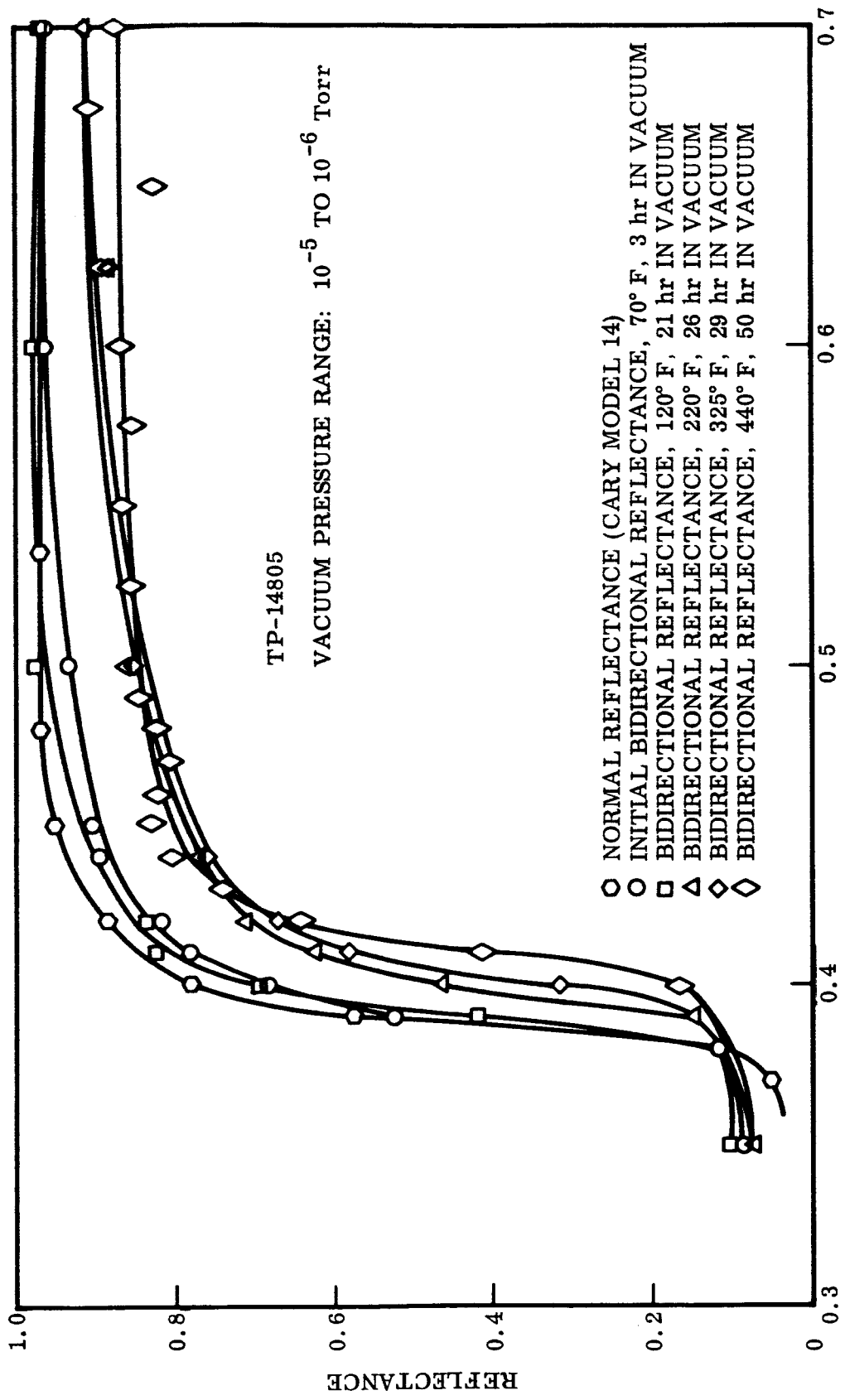

Fig. 26 Effect of Temperature on Reflectance of Sintered ZnO From 70 to 440° F

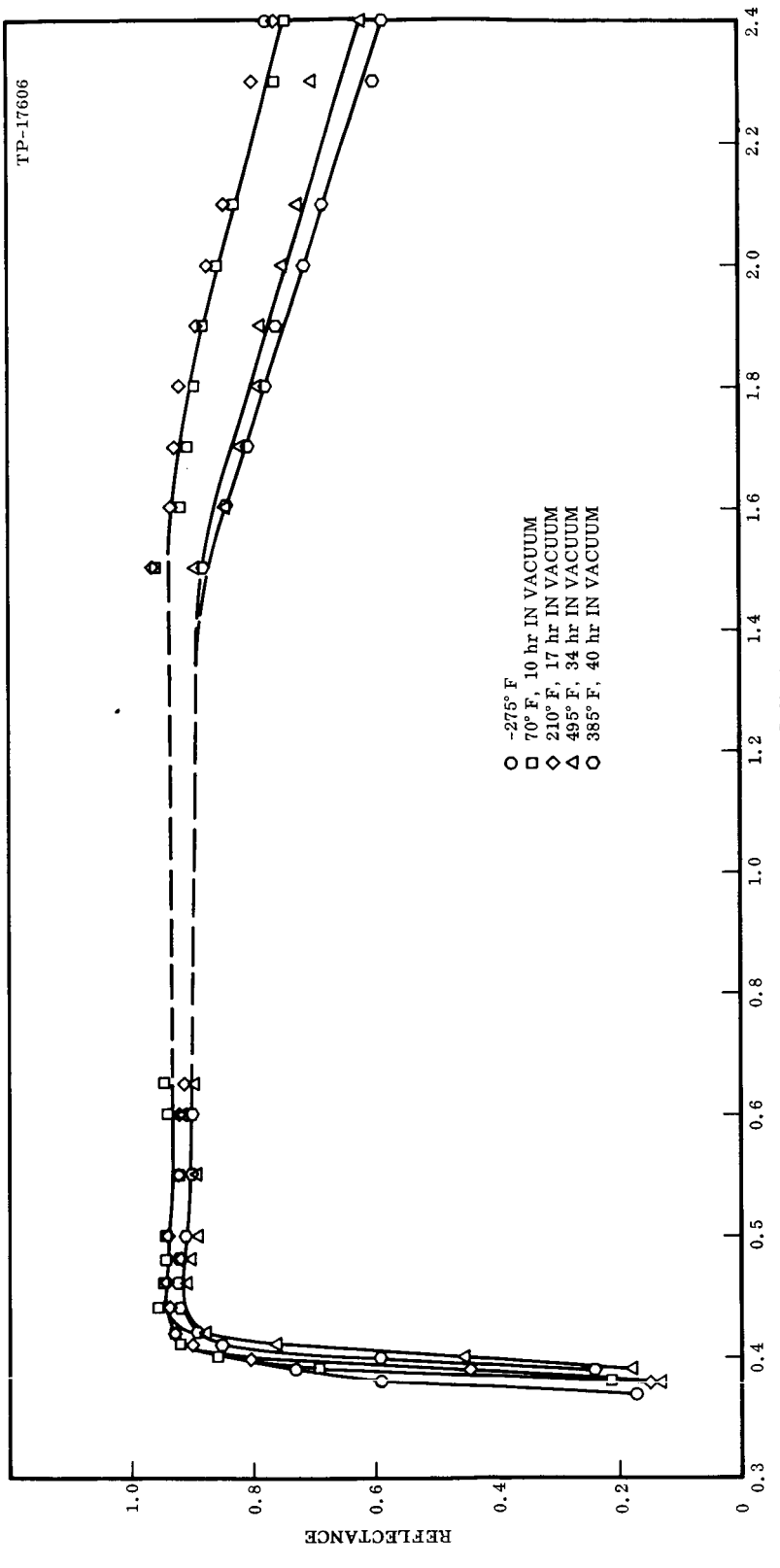

Fig. 27 Effect of Temperature on Reflectance of Sintered ZnO From -275 to 495° F

Fig. 28. The variation of spectral reflectance from the end of exposure to the final measurement with the Cary spectrophotometer is shown in Fig. 29. All of the bidirectional reflectance data on both Figs. 28 and 29 are normalized with respect to the initial Cary reflectance curve at 0.65 μ.

The initial bidirectional reflectance at 70° F in vacuum is lower than the Cary reflectance in the regions 0.4 to 0.6 μ and 1.6 to 2.4 μ. This departure from the Cary measurement is repeatedly observed (also see Fig. 26) for bidirectional reflectance measurements taken in vacuum, but not for those taken in air. Checks have been made to ensure that these departures were not associated with mechanical displacement of the optical system during pump-down. It is probable that this observation is related to the desorption of oxygen from the zinc oxide, and is not instrumental.

Ten minutes after initiation of ultraviolet irradiation, a full reflectance spectrum was measured. Figure 28 indicates that the band edge has not fully shifted, so the sample has not quite reached steady state temperature. The visible reflectance has decreased from the room temperature values. However, comparison of these data to those for a 440° F sample in Figs. 26 or 27 indicates that this decrease may be partially due to the increased temperature under irradiation. The shape of the infrared reflectance spectrum 10 min after initiation of irradiation is unexpected, in that it does not have the same general form as the remaining infrared reflectance spectra. This has not been explained, and has not been repeated, but may be connected with the rapid change in sample temperature during this run, or the unusual thermal and vacuum history of this particular sample.

The last two bidirectional reflectance spectra show a progressive and definite degradation of sample reflectance with continued irradiation. The total degradation is only slightly greater in the visible range than in the infrared if the lowest reflectance curve (after 49-hr irradiation) is compared to the initial room temperature reflectance. However, the relative rates of degradation in the visible and infrared cannot be meaningfully compared because of the one irregular infrared spectrum discussed above.

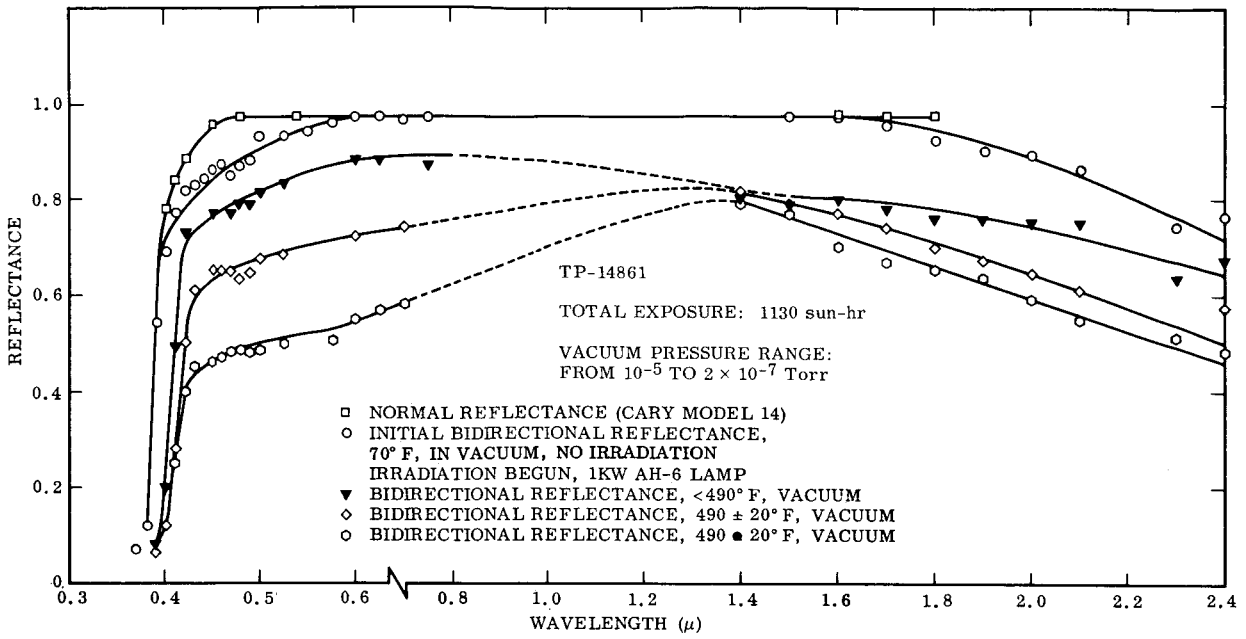

Fig. 28 Damage to Sintered ZnO at 490° F

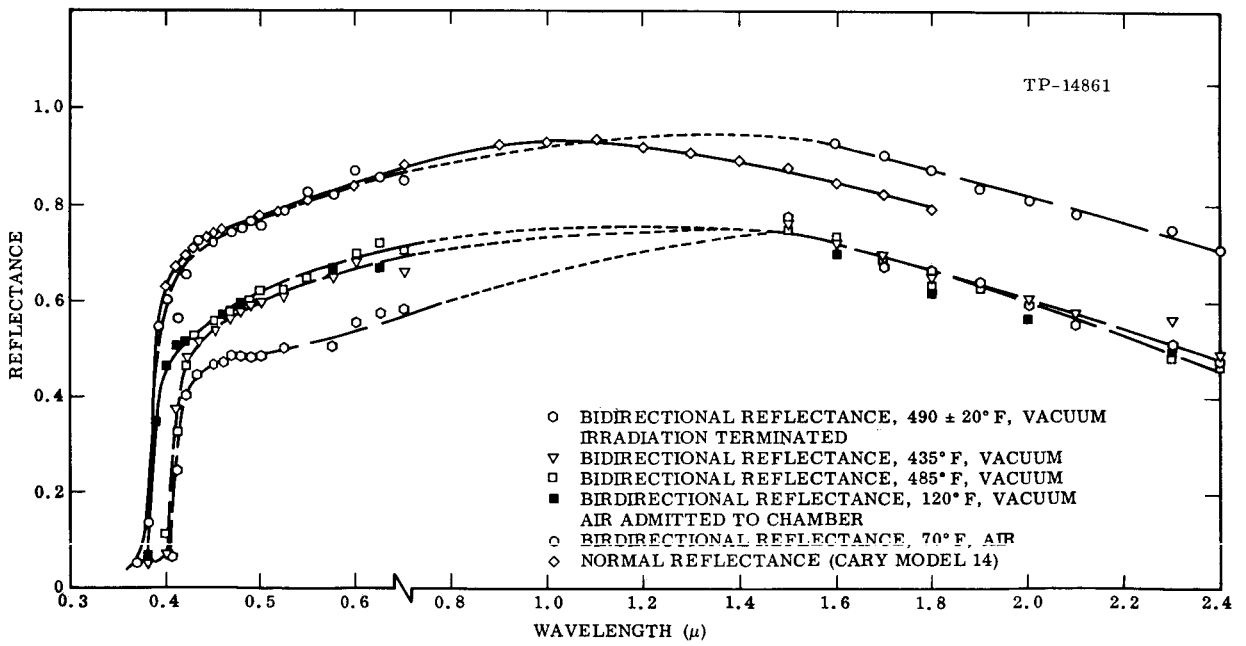

Fig. 29 Recovery of Sintered ZnO at 70° F

After 54 hr of irradiation the lamp was extinguished and "recovery" measurements made. The first post-irradiation spectrum was recorded 1 hr after stopping irradiation; sample temperature had decreased to 435° F. For the second post-test spectrum, taken 23 hr after the termination of radiation, the sample temperature was approximately that maintained during irradiation (490° F). Note that there was no recovery in the infrared region (1.4 to 2.4 μ), but there appears to have been significant recovery in the visible and very near infrared. This may be attributed partially, if not wholly, to the procedure for taking data. A reference technique was used in this experiment whereby the A-H6 irradiation source decreased the apparent sample reflectance. This technique was corrected for all other tests reported, and recovery in the visible has not been observed again due to the irradiation source being extinguished. The final spectrum in vacuum, taken 25 hr after irradiation was terminated and after the sample had cooled to room temperature, is essentially identical to those taken 1 hr at 435° F and 23 hr at 490° F after termination of irradiation. The only significant change is the shift in the band edge, which is due to the decrease in sample temperature from 490 to 120° F.

From these three spectra, it appears that very little reflectance recovery occurs in vacuum, at temperatures from 490 to 70° F, for many hours after the termination of irradiation.

After 26 hr in vacuum and comparative darkness, the damaged sample (having reached room temperature) was re-exposed to air; 15 hr later the bidirectional reflectance was measured. After an additional 6 hr the final normal reflectance was measured on the Cary spectrophotometer. These final two spectra indicate that significant recovery of spectral reflectance has occurred upon re-exposure of the sample to air. The total recovery is generally uniform in the visible and infrared.

The fact that the final infrared reflectance measured as bidirectional reflectance was higher than the normal reflectance measured on the Cary was certainly not expected. The phenomenon did not recur, and so was assumed to be instrumental and peculiar to the particular experiment.

A second experiment at high temperatures was performed in order to resolve the questions brought up by the first. The damage history is shown in Fig. 30, and the recovery in Fig. 31. The same sample was used here as was used in Fig. 27; thus no initial normal reflectance can be shown. Also, instrument modifications between the two parts of the experiment made it impossible to use the same normalization for the two, and so all spectra in Figs. 30 and 31 are normalized with respect to the final normal reflectance measurement. Experience with several experiments where a single normalization was used throughout indicated this procedure was permissible. Also, the damage spectra agree quite well with those in Fig. 28.

The first spectrum in Fig. 30 was taken at high vacuum, at 365° F, shortly before the A-H6 was turned on. The second was taken at 520° F in the period between 20 min. and 1 hr after the A-H6 was turned on. It shows rapid damaging in both visible and infrared. This must be attributed primarily to the ultraviolet, since Fig. 27 shows temperature alone does not give changes in as short a time as observed here. Reflectance at 0.47 μ is plotted as a function of time in Fig. 32. The apparent reflectance increased when the A-H6 was turned on due to the increase d-c level in the photomultiplier, then decreased as the sample damaged. Subsequent spectra show progressive damage in the visible, but the infrared remains the same for the second and third spectra. At 26 hr, a vacuum problem developed in the apparatus, and the pressure rose to 10^{-3} for 5 min. This evidently was enough to recover the infrared to the level shown in the last spectrum in Fig. 30, as a check immediately after the pressure rise showed the reflectance at 2.0 μ to have risen from 59 to 64% where it is shown in the final spectrum. The pressure remained close to 10^{-5} for the rest of the experiment, and as a result no further damage in the infrared took place, though the visible did damage further. The last spectrum was taken with the lamp off, due to further experimental difficulties.

Air was allowed back into the chamber 48 hr after the lamp was turned on. There was no immediate recovery, as had been observed on all previous experiments, probably due to the high pressures the samples had been at for some time prior to admission of air. However, a slower recovery rate was observed, as it has been on

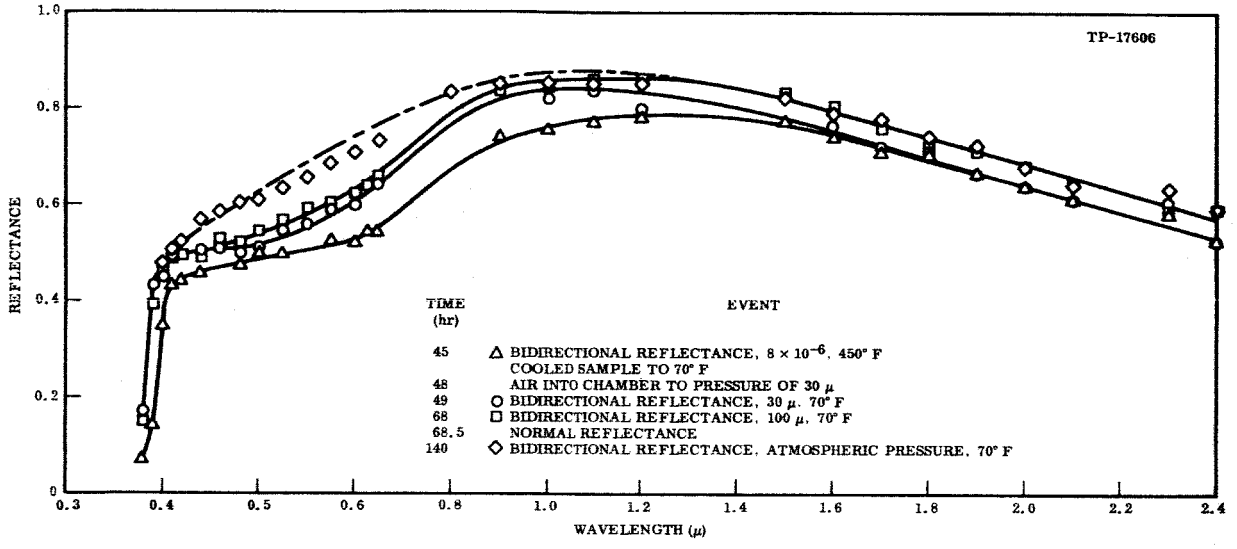

Fig. 30 Damage to Sintered ZnO at 525° F

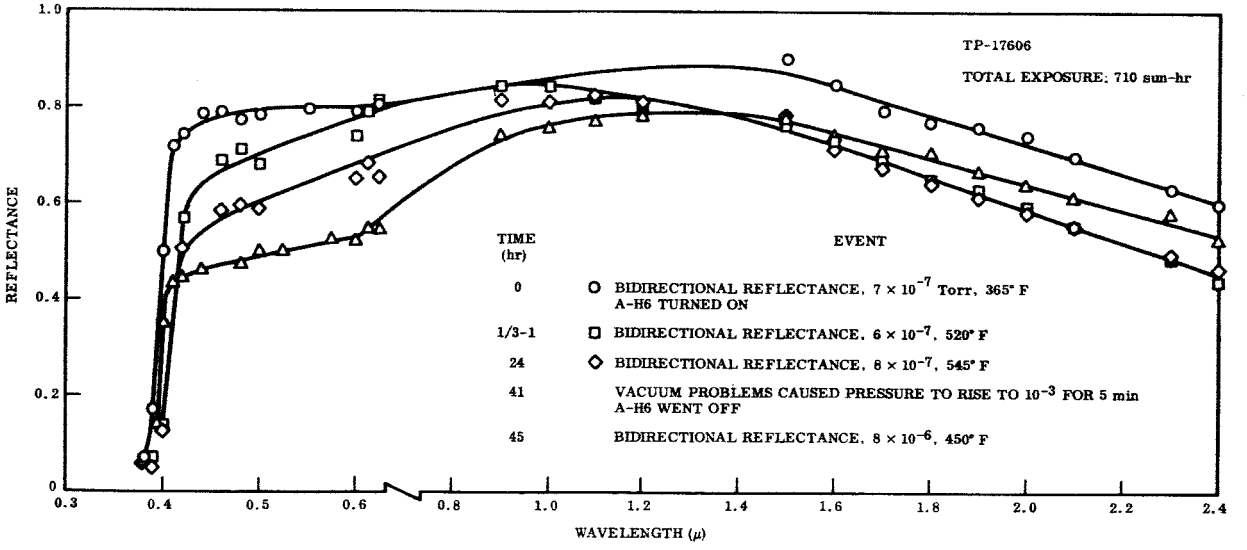

Fig. 31 Recovery of Sintered ZnO at 70° F

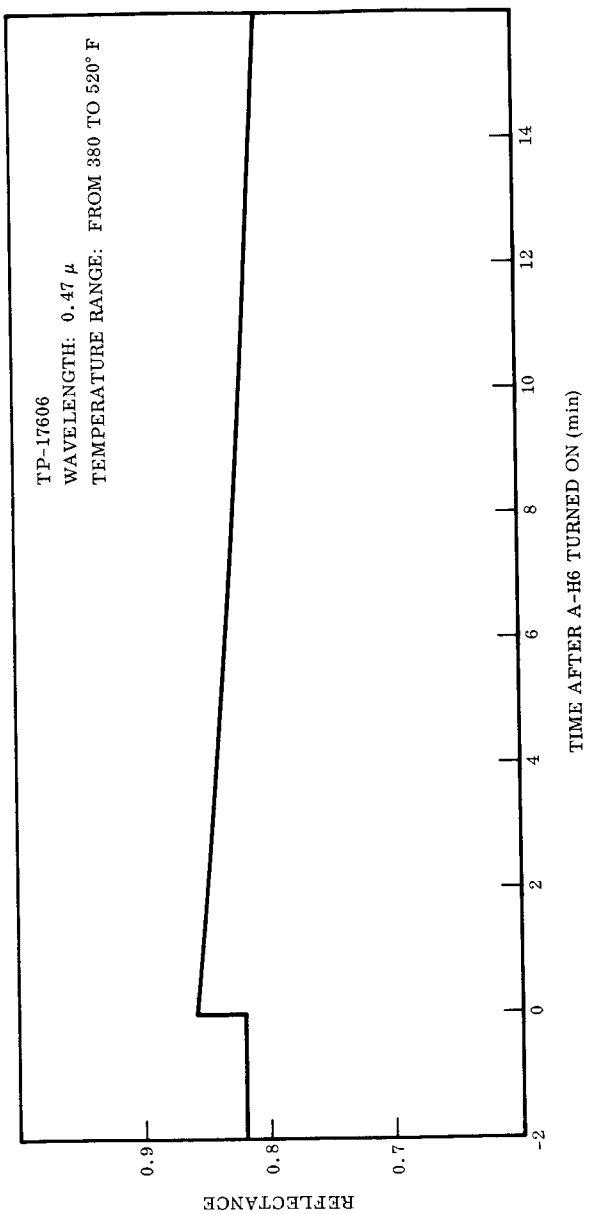

Fig. 32 Time Plot of Initial Visible Damage to Sintered ZnO at 520° F

previous experiments and is shown by the second and third bidirectional curves. The normal reflectance curve was taken immediately after the third bidirectional, yet the discrepancy between the two is quite marked. This same effect is noticed on virtually every run. It is evidently a bleaching effect caused by the intense light used in the normal reflectance device, since the recovery observed in the bidirectional for a comparable elapsed time is negligible. The final bidirectional spectrum demonstrates that the final recovery is indeed recovery of the sample, and not simply an artifice of the apparatus.

Figures 33 and 34 refer to a sample of unpressed, unsintered ZnO which has been irradiated. In this case the ordinate was arbitrarily picked to coincide with a pressed and sintered sample, and the spectrum of a sintered sample is shown for comparison. It may be noticed that the bidirectional spectrum shows a sharper edge for the loose powder than the normal reflectance shows for the sintered sample. The sintered sample used was the same one used in Figs. 16 and 17, and the sintered and unsintered samples were run side by side, using the same reference (see Appendix B for the description of data taking techniques). The normal reflectance and initial bidirectional spectra in Fig. 16 have identically the same shape through the absorption edge. Thus the slight difference between the shapes in Fig. 33 may be indicative of the small amount of mechanical damage introduced during the pressing operation.

There was no change up until the time the A-H6 lamp was turned on. When the irradiation source was turned on, the particles came to a temperature that was in radiation equilibrium with the irradiation source. This situation is very difficult to avoid in a loose powder sample because the contact conductance from one grain of the powder to the next is very small, resulting in little if any heat being conducted away from the sample. To confirm this, a sample was tested with the sample table at liquid nitrogen temperatures. The powder reached the same temperature under irradiation as it did in this test.

In Fig. 33, spectra are displayed for 20 and 40 min after irradiation commenced. Rapid dimunition in the visible and infrared is seen to have taken place, while at wavelengths in between the reflectance remained unchanged. Further irradiation retained

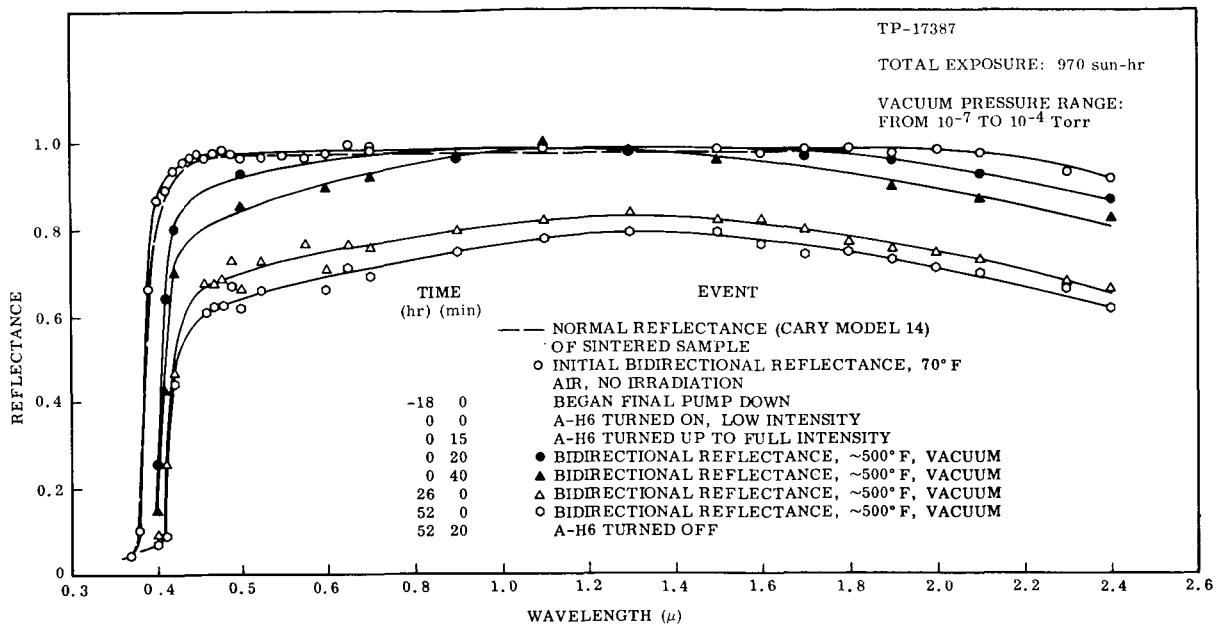

Fig. 33 Damage to Unpressed, Unsintered ZnO at 500° F

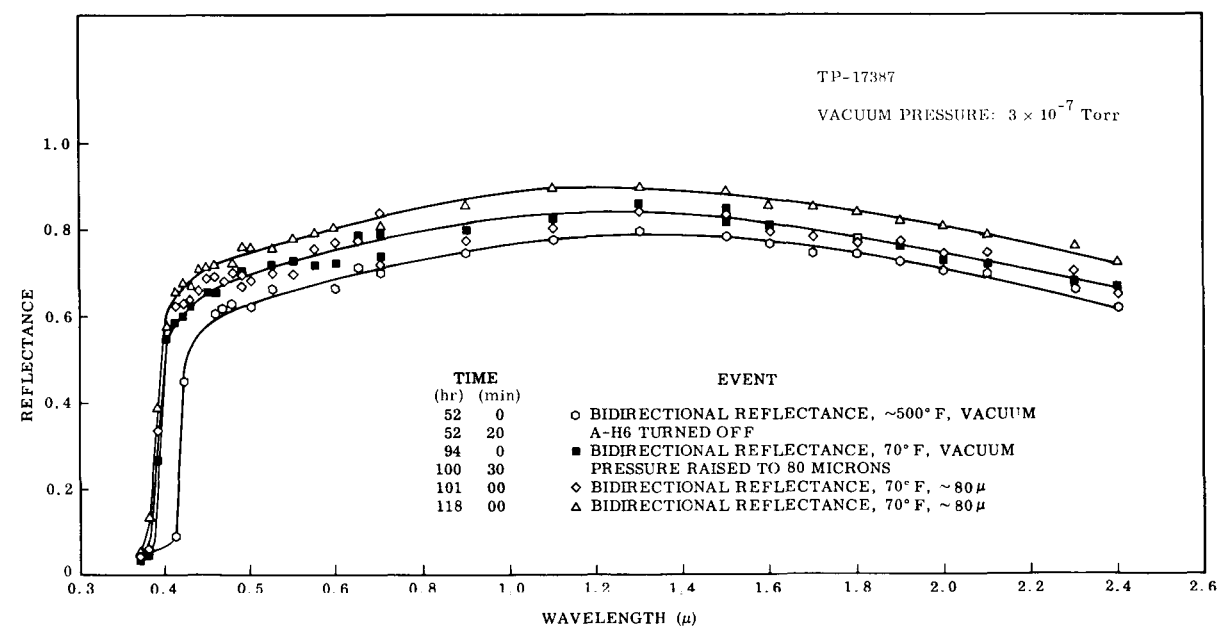

Fig. 34 Recovery of Unpressed, Unsintered ZnO at 70° F

this shape, but lowered the over-all reflectance. Plots of reflectance as a function of time in the visible and infrared may be found in Figs. 35 and 36.

The entire spectrum in Fig. 33 is seen to have lowered considerably in reflectance after irradiation. However, if the damage is compared to that in Figs. 28 or 30, reflectance is seen to be higher in Fig. 33 in the visible and infrared, while being comparable at intermediate wavelengths.

With this sample, as with that in Fig. 17, recovery during 42 hr in vacuum was not great, and consisted of a small, fairly uniform increase in reflectance over the measured spectrum. When air was admitted, there was no immediate recovery in reflectance at any wavelength, except adjacent to the absorption edge. However, with further time in air there was a gradual, uniform increase in reflectance over the measured spectrum.

Irradiation at liquid nitrogen temperatures. The results of two irradiations of ZnO at liquid nitrogen temperatures are presented in Figs. 37 and 38. These experiments were of somewhat shorter duration than prior runs at higher temperatures. However the 21.5 and 24 hr of irradiation shown in the figures suggests what would be found with further irradiation. As usual, the ordinates for the bidirectional are adjusted to coincide with those of the normal reflectance measurement.

Figure 37 shows no effect of the vacuum, but marked decrease in reflectance due to the chilling of the sample. Whether this is a temperature effect of the sample or not may be discovered by looking at Fig. 38. Here there was no effect of chilling the sample holder on reflectance. In both figures the infrared damaged due to vacuum alone. In Fig. 37, reflectance diminished uniformly, though slightly, for wavelengths $< 1.6\ \mu$ under irradiation. For wavelengths $> 1.6\ \mu$, it is interesting to compare damage with that observed in previous experiments. Minimum reflectance at $2.4\ \mu$ was typically 45% for the high temperature test, and 200° F test, 55% for the room temperature test, and 70% for the liquid nitrogen temperature test.

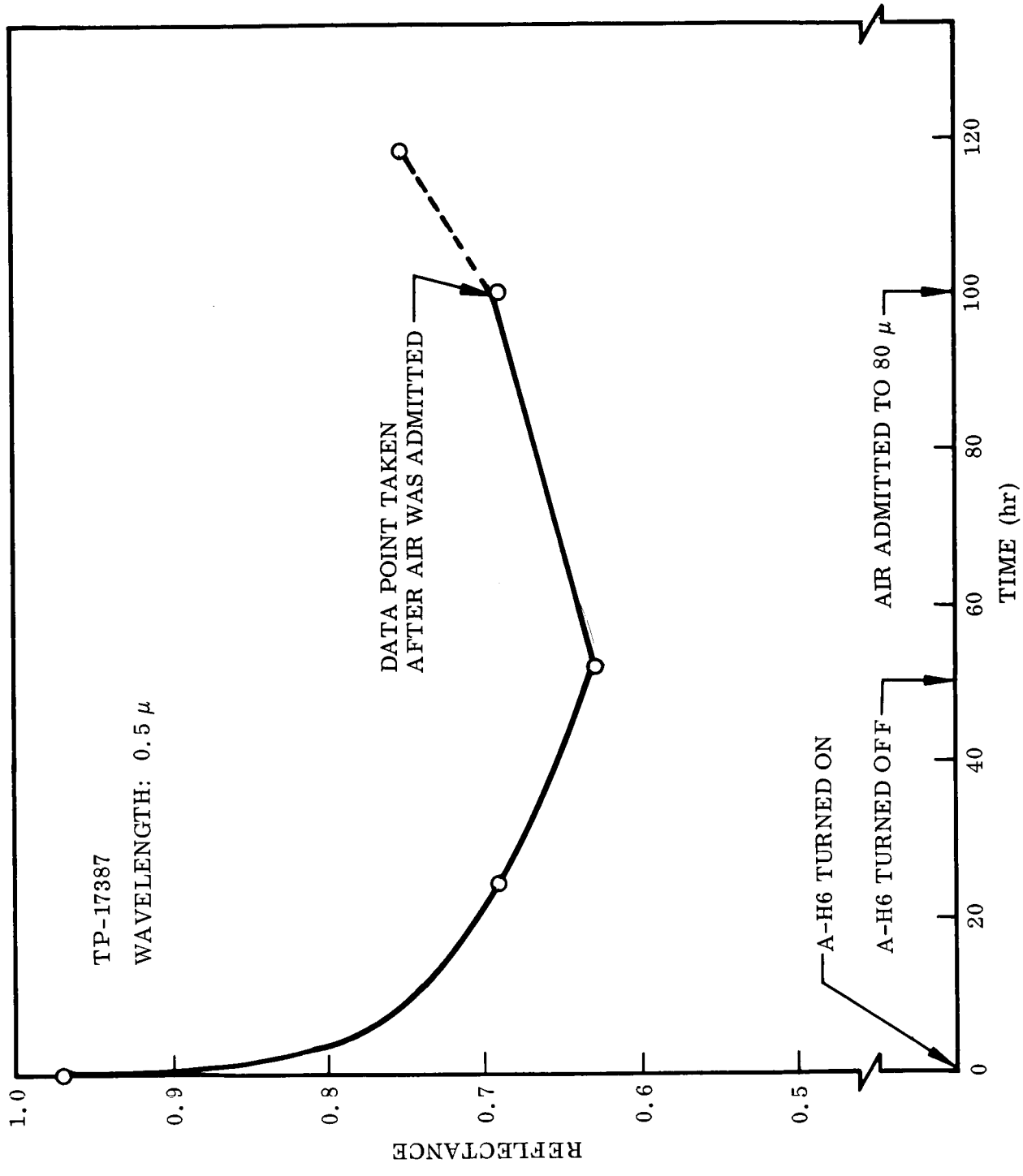

Fig. 35 Time Plot of Visible Reflectance of Unpressed, Unsintered ZnO During Irradiation at 500° F and Recovery at 70° F

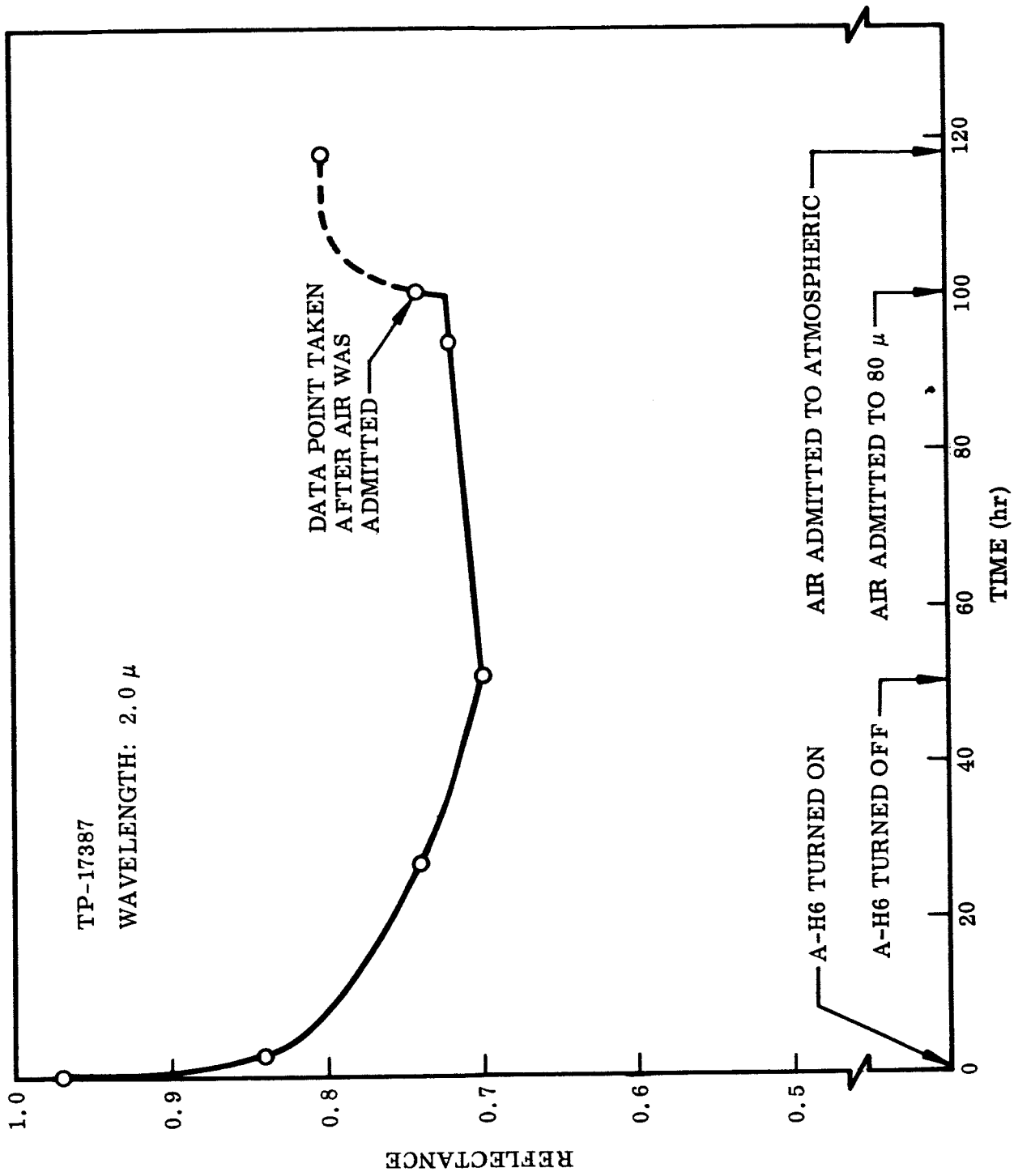

Fig. 36 Time Plot of Infrared Reflectance of Unpressed, Unsintered ZnO During Irradiation at 500° F and Recovery at 70° F

The infrared damage in Fig. 38 compares well that in Fig. 37. However, Fig. 38 shows slightly greater damage in the visible region than Fig. 37. This discrepancy is of relatively minor significance in view of the great preponderance of damage in the infrared region. This result is compatible with the premise that infrared damage is related to bulk processes while ultraviolet and visible damage is associated with oxygen desorption. Obviously, desorption will be inhibited at the low temperatures encountered in this series of experiments (as it was at room temperature), leading to an increased stability in the visible portion of the spectrum.

4.4 STATIC ULTRAVIOLET IRRADIATION TESTS

Ultraviolet irradiation tests without in situ optical measurements are termed "static" tests in this report; information on sample behavior is based on before-test and after-test examination of the sample. These tests are performed with the apparatus described in Appendix C. Static tests were performed on particulate zinc oxide samples, under various test conditions, throughout the last 12 months. Before proceeding to presentation of the data, a few comments qualifying the value of static exposure techniques are in order. The theoretical implications of these comments are discussed in Sec. 6.

The in situ bidirectional reflectance data presented in Sec. 4.3 show that significant post-test "recovery" from ultraviolet damage, as measured by decrease in sample reflectance, occurs upon exposure of the damaged samples to air. Through prompt post-test measurement of reflectance with the Cary or Beckman spectrophotometers, the effect of such recovery on evaluation of the damage is minimized. In practice, the elapsed time between opening the vacuum chamber to air and the measurement of the last of a series of samples has been no longer than 1 hr. It must be kept in mind however, that in this first hour of exposure to air, it is very likely that measurable recovery occurs. Additional recovery takes place due to the intense source in the spectrophotometer. Valid qualitative data are gained, but precise quantitative data are difficult to obtain. As an example, two samples were prepared and irradiated under nominally identical conditions. One (TP-14872AB) suffered a 12% decrease in spectral reflectance at 0.45 μ, the other (TP-14507AA) an 8% decrease.

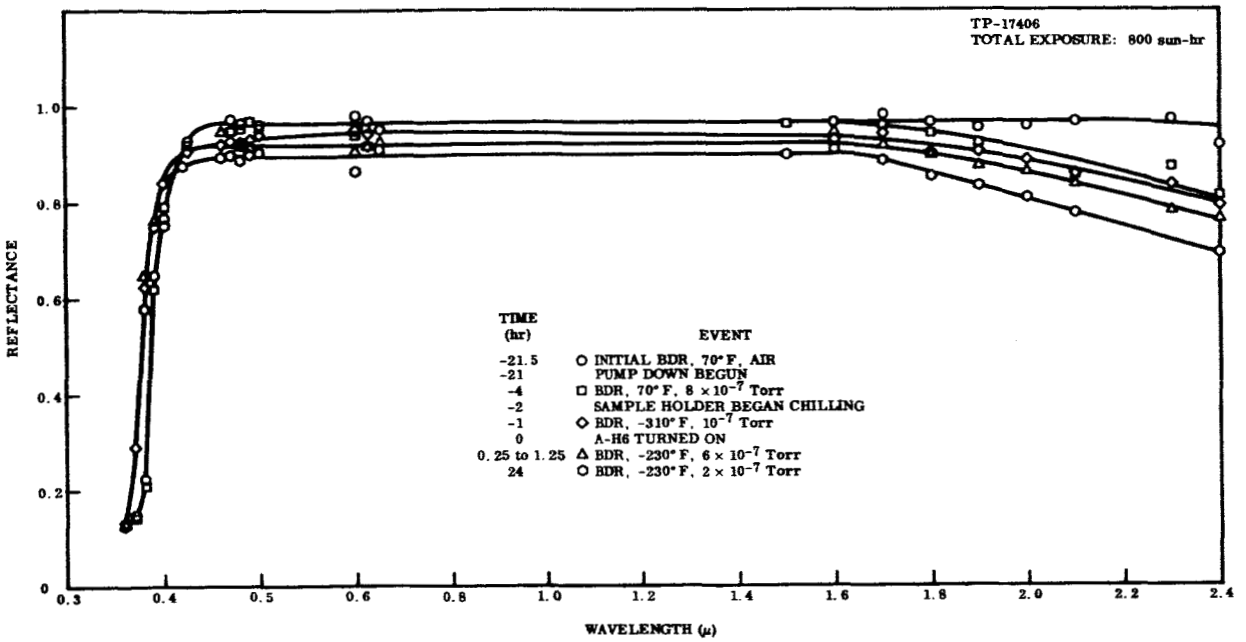

Fig. 37 Damage to Sintered ZnO at -230° F

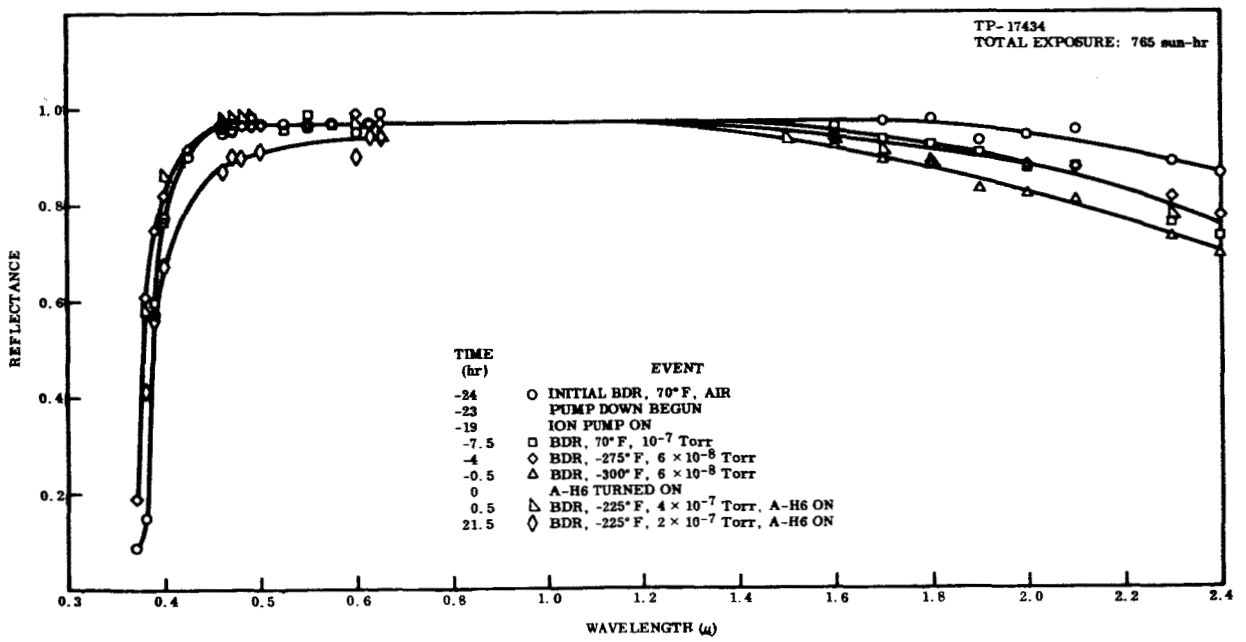

Fig. 38 Damage to Sintered ZnO at -225° F

The first post-test measurement was performed within 1 hr after exposure to air, and the second within 2 hr after exposure to air. A probable explanation for the different behavior of the two samples is the different time that each sample was allowed to recover in air before being measured. Nevertheless, through static tests, valuable information has been obtained of the influence of sample preparation and ultraviolet exposure parameters on the behavior of particulate zinc oxide during irradiation. With these qualifications in mind, it is now appropriate to review the results of the static tests.

The basic parameters considered in the static tests have been the preparation conditions (forming pressure and sintering atmosphere) and the exposure conditions, (pressure, sample temperature, and irradiation spectrum). The data presented are representative of each condition. All of the tests have been repeated with more than one sample. A full tabulation of test samples and test conditions are presented in Table 2 Unless otherwise specified, the test parameters of the static exposures are as follows:

- Irradiance source: A-H6 (PEK Lab Type) Lamp
- Distance of sample from lamp: 3.9 in.
- Nominal irradiation flux density: 10 suns. A flux density of 1 sun near ultraviolet radiation is defined as the flux density of extraterrestial radiation at 1 AU from the sun, in the wavelength interval from 2000 to 4000 Å
- Sample temperatures from 100 to 125° F
- Pressures of 2×10^{-7} Torr except during initial ultraviolet exposure, when sample and chamber wall outgassing causes pressures as high as 1×10^{-5} Torr

Standard Samples. Figure 39 shows the spectral reflectance of a standard particulate zinc oxide sample from 0.3 to 20 μ. A standard sample is prepared by forming at 10,000 psi in air for 1 min. and then sintering at 600° C in air for 15 min. (Sec. 4.2). The spectral reflectance of these standard samples before irradiation was found to be highly repeatable, that is within 1% in the range 0.3 to 1.8 μ throughout the program. For wavelengths larger than 1.8 μ the transmission of particulate zinc

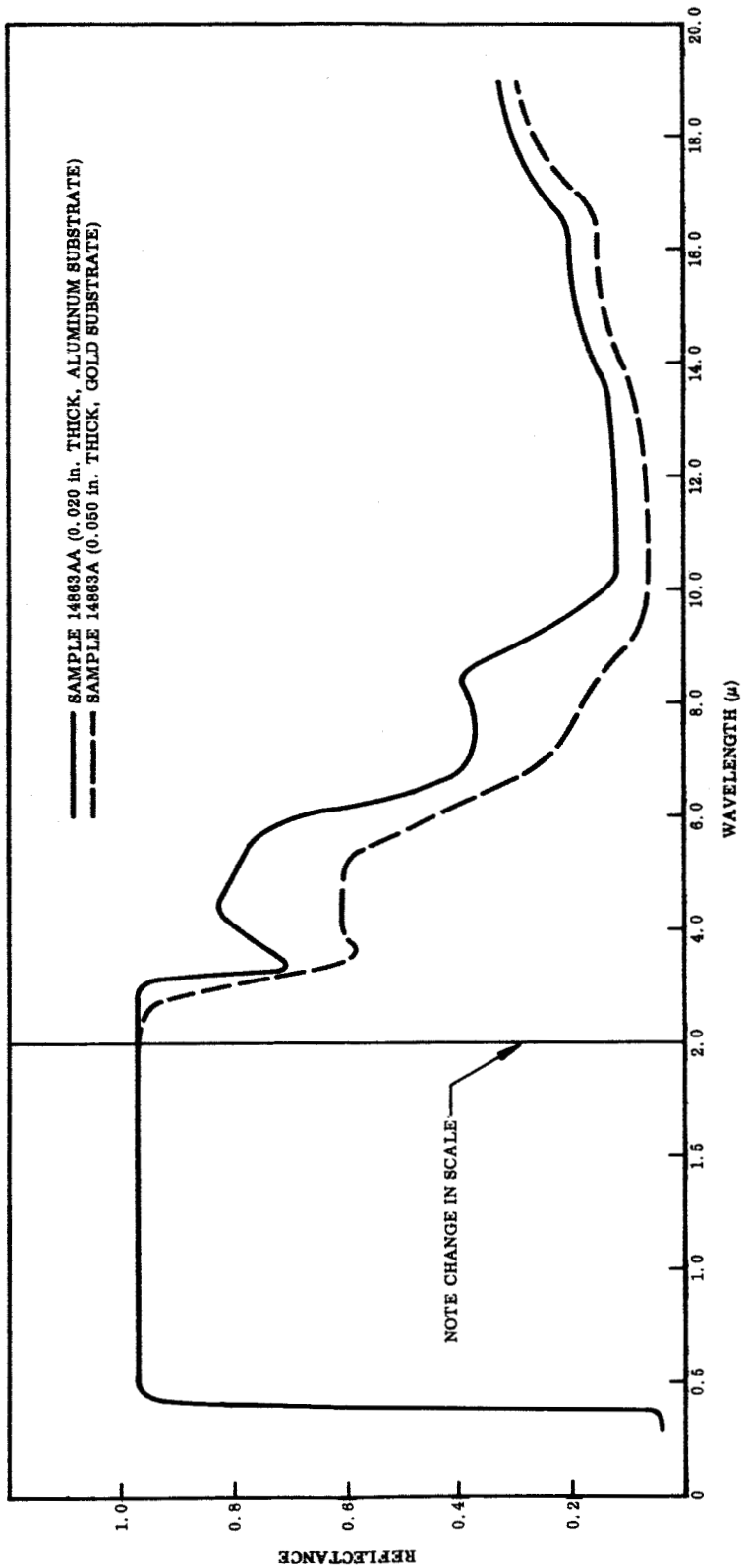

Fig. 39 Normal Spectral Reflectance of Particulate ZnO (Unirradiated)

oxide increases, so the reflectance is affected by sample thickness (Ref. 20). Two different sample thicknesses are depicted to show this effect. Spectral reflectance for samples prepared under the same forming and sintering condition of SP-500 zinc oxide are identical to these reflectance curves for the interval 3.0 to 1.8 μ. Comparative measurements were not taken at longer wavelengths.

Standard Samples – Standard Exposure. Standard samples and samples made of SP-500 (New Jersey Zinc Co.) zinc oxide exposed to 860 sun-hr of ultraviolet irradiation in vacuum over a period of 67 hr underwent decreases in reflectance as shown in Fig. 40. It can be seen that the reflectance decrease is a maximum near the absorption band edge at 0.4 μ. The decrease is less in the visible and near infrared region, but becomes greater in the region of 1.5 to 1.8 μ. Data on the Beckman to 2.6 μ shown in Figs. 45 and 46 show the decrease in reflectance becomes still larger in the region 1.8 to 2.6 μ. Three post-test reflectance curves are presented to show the range of variation in measured reflectance due to sample variation and more importantly to "recovery" time in air between cessation of exposure and final measurement.

Standard Sample – Filtered Exposure. Standard samples were irradiated in vacuum simultaneously with those reported above, but behind selective wavelength filters. The normal transmission characteristics before and after the test are shown in Fig. 41. One filter (microsheet) transmits radiation of wavelength longer than 0.3 μ. The other (approximately equivalent to Corning Filter 3-73) transmits radiation of wavelength longer than 0.4 μ, that is radiation less energetic than the band-gap energy for zinc oxide. The effects of this selective wavelength irradiation are shown in Fig. 42. As expected, the samples protected by the 0.4-μ cut-on filter showed relatively slight damage increasing in the near infrared. It is significant that the samples protected by the 0.3-μ cut-on filter show less damage than the unprotected samples in the visible region, but more in the infrared. The 0.3-μ cut-off filter not only changes the spectral distribution of the ultraviolet irradiation, but also consequently reduces the total ultraviolet exposure of the sample. It is clear that the former effect is the cause of the different character of the damage for the samples covered by this

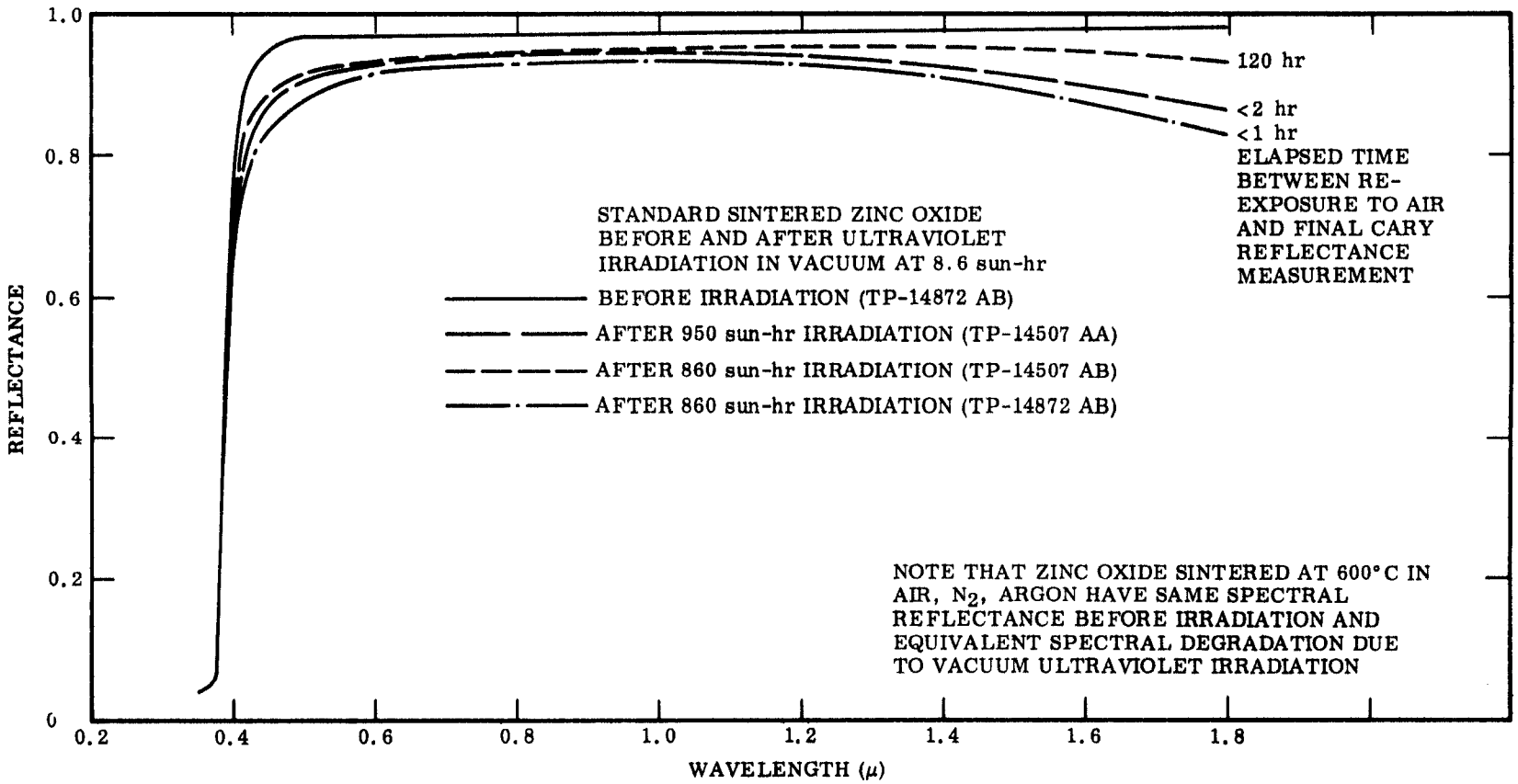

Fig. 40 Spectral Reflectance of Particulate ZnO Before and After UV Irradiation in Vacuum

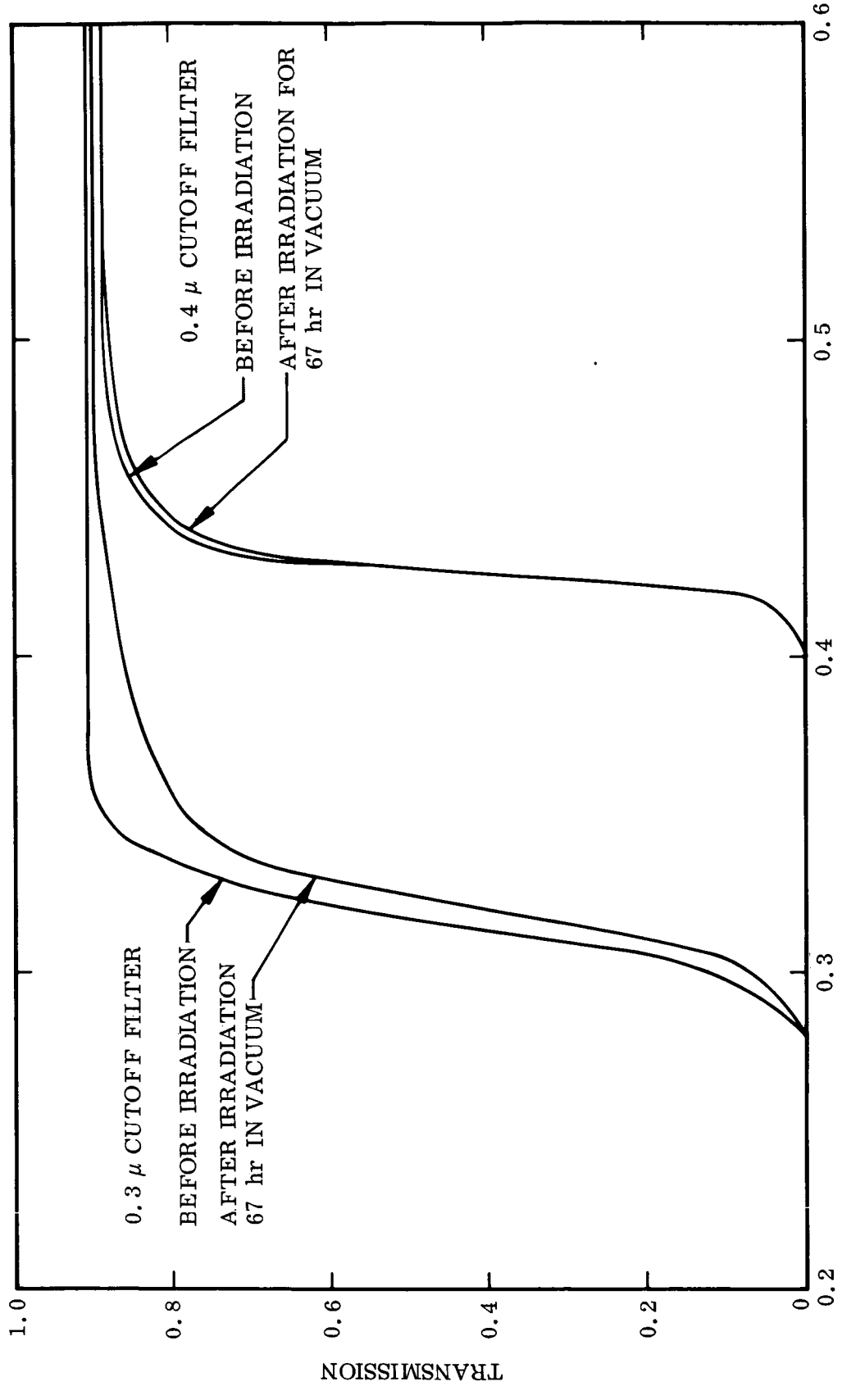

Fig. 41 Normal Spectral Transmission of Selective Wavelength Filters Before and After UV Irradiation in Vacuum

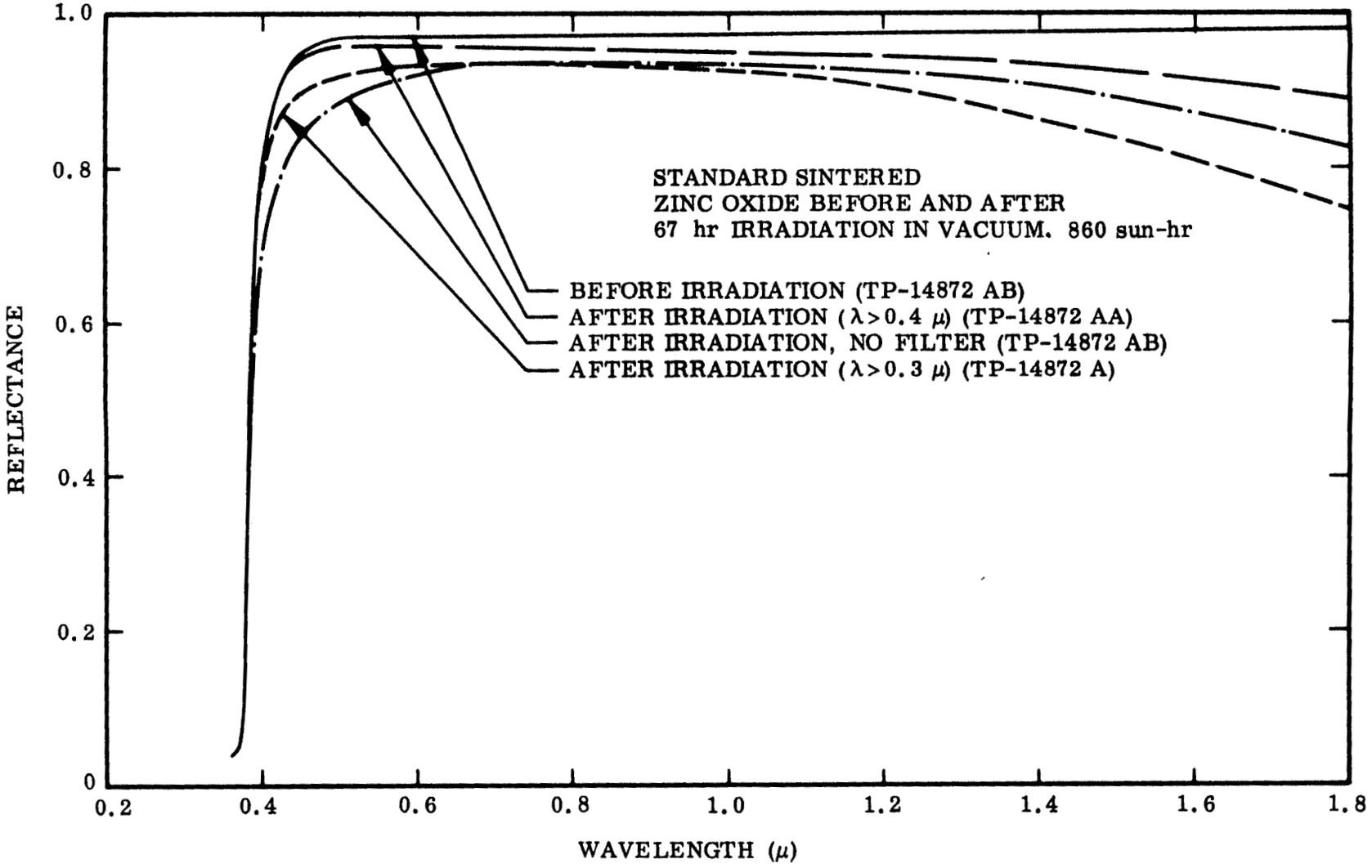

Fig. 42 Effect of Selective Wavelength Irradiation in Vacuum on Spectral Reflectance of Particulate ZnO

as compared to those without filtering. Samples subjected to a range of total irradiation exposures of the same spectral distribution are presented in Figs. 43 and 44. The magnitude but not the relative visible-to-infrared reflectance degradation varies with total exposure. The implications of this are discussed in Sec. 6.

Standard Samples – Effect of Irradiation Flux Density. Standard sintered samples were exposed to a range of ultraviolet irradiation flux densities of 4:1 (11 suns:2.7 suns) and total equivalent exposures of approximately 8:1 (2020 sun-hr:240 sun-hr) in vacuum. The pre- and post test spectral reflectances are shown in Figs. 43 and 44. The samples exhibited progressively more degradation in both the visible and infrared regions with increased total exposure up to the maximum exposure tested. The magnitude of degradation correlated approximately with the intensity-time product. That is, a sample irradiated for 184 hr at a flux density of 6 suns exhibited approximately the same degradation as a sample irradiated for 93 hr at 11 suns. However, post-exposure recovery of all samples between the time of readmission of air to the chamber and post-test reflectance measurements makes a quantitative correlation impossible. To adequately ascertain whether a correlation of degradation with total exposure for a range of irradiation flux densities is valid, the bidirectional reflectance apparatus should be employed.

Standard Samples – Exposed in Air. Standard samples exposed to 1070 sun-hr of ultraviolet irradiation over a period of 88 hr in ambient air did not show any change in spectral reflectance. Consequently, no data on this test are presented in graphical form.

Effects of Sample Forming Pressure. The effect of forming pressure on the spectral reflectance of irradiated samples is shown in Fig. 45. Samples were pressed at pressures from 10,000 to 100,000 psi and sintered at 600° C in air. The reflectance of the same samples after 100 hr and 860 sun-hr of irradiation in vacuum is shown in Fig. 46. Note that the decreases in reflectance due to increased forming pressure and to ultraviolet radiation are in the same spectral regions. The magnitude of the spectral reflectance decrease was found difficult to reproduce consistently because of

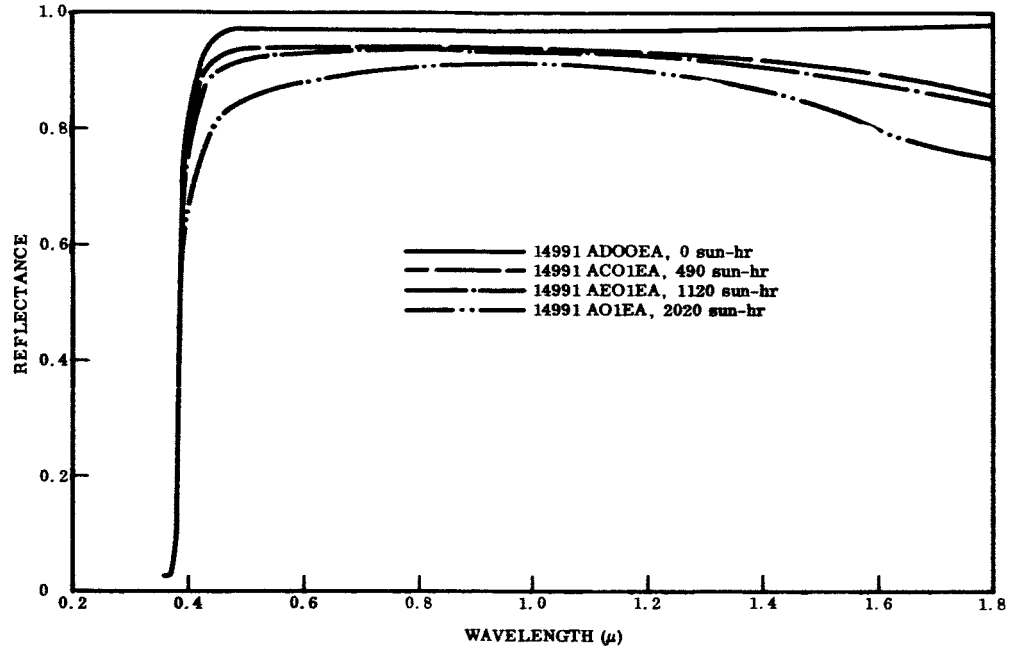

Fig. 43 Effect of UV Irradiation Flux Density in Vacuum for 184 hr on Spectral Reflectance of ZnO

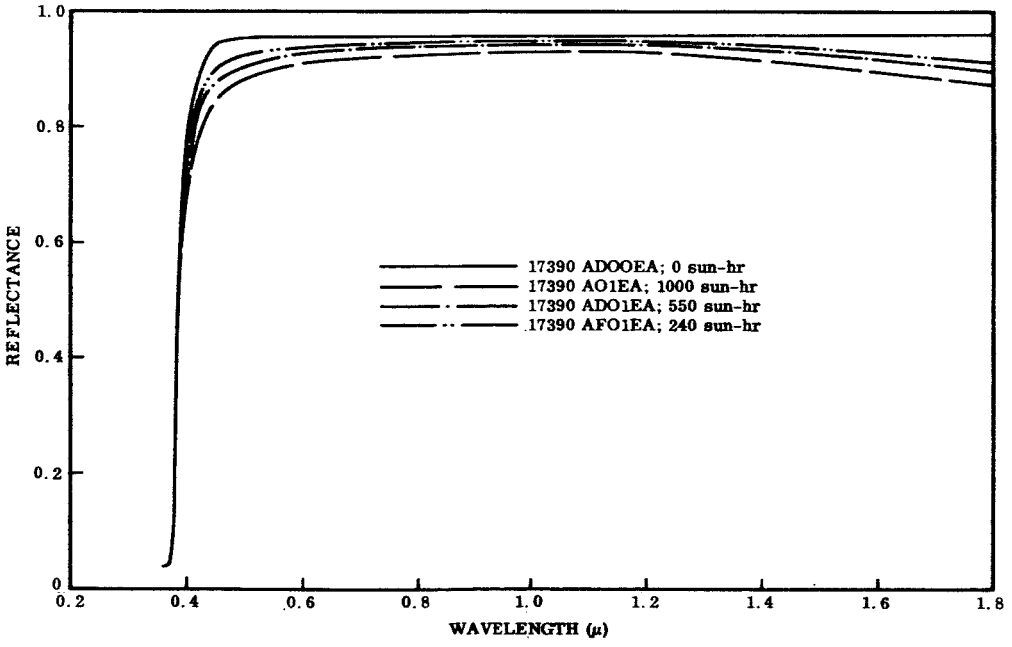

Fig. 44 Effect of UV Irradiation Density in Vacuum for 93 hr on Spectral Reflectance of ZnO

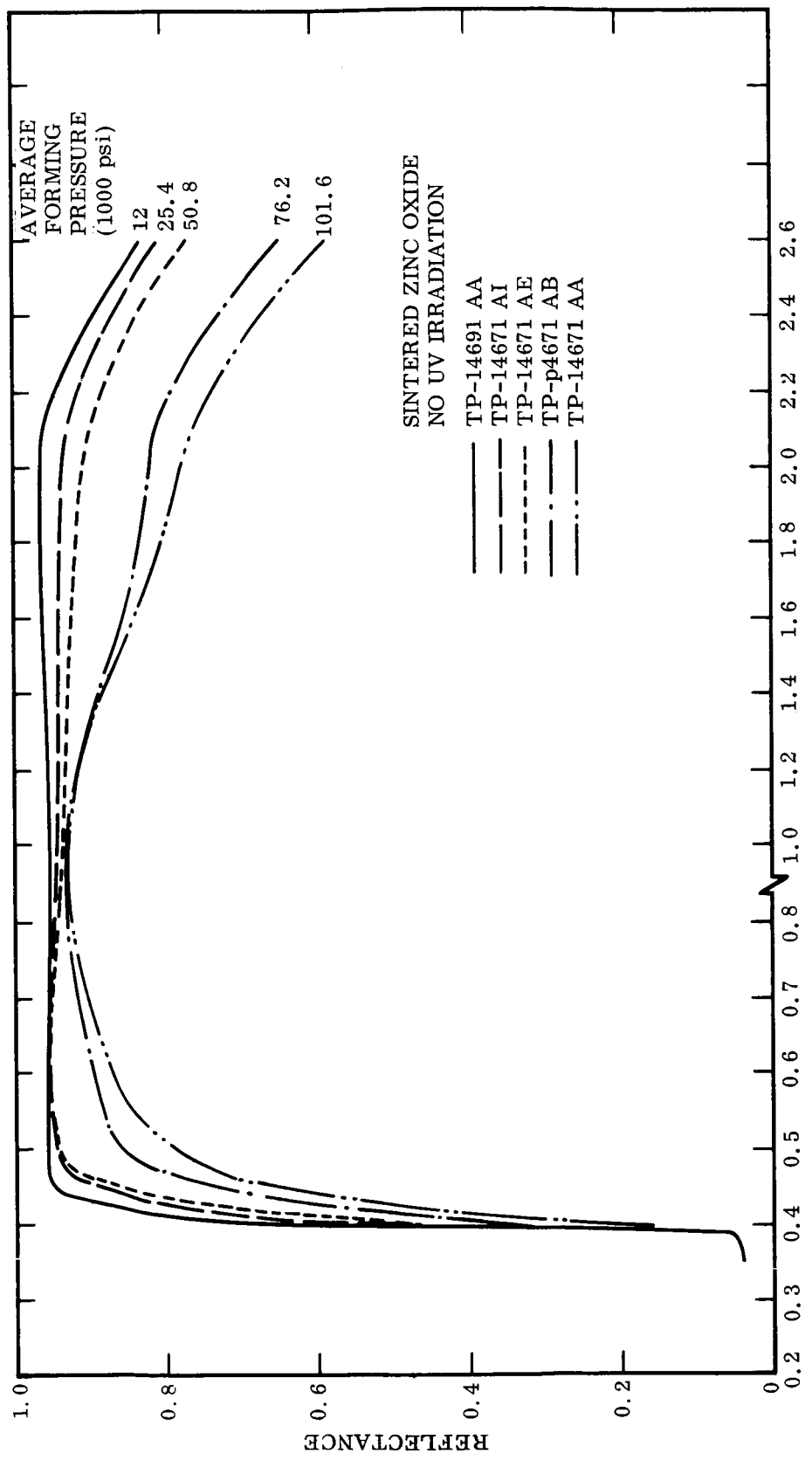

Fig. 45 Effect of Forming Pressure on Spectral Reflectance of Unirradiated Particulate ZnO

the large variations in local pressure on any sample at high forming pressures. Consequently, the observed effect of pressure and ultraviolet irradiation depended to some extent on the precise region of the sample viewed by the Beckman spectrophotometer. However, these variations were generally small compared to the overall trend shown in Figs. 45 and 46.

Effects of Sintering Atmosphere. Particulate samples prepared at a forming pressure of 10,000 psi and sintered at 600° C in various atmospheres were exposed to ultraviolet irradiation in vacuum and in air. Those samples sintered in air, nitrogen, and argon exhibited: (1) the same initial spectral reflectance, (2) the same magnitude of spectral reflectance degradation when irradiated in vacuum, and (3) no degradation when irradiated in air. Therefore, Fig. 40 is representative of all these conditions. On the other hand, samples sintered at 600° C in a residual air pressure of 10^{-2} to 10^{-3} Torr exhibited markedly different characteristics. When irradiated for 1070 sun-hr and 88 hr in air, the vacuum sintered samples showed a marked increase in reflectance in the visible region, but only a slight increase in the infrared.

These results are shown in Fig. 47. Similar samples sintered at approximately 10^{-3} Torr and irradiated in vacuum for 860 sun-hr and 67 hr showed only a slight increase in reflectance at all wavelengths. This result is not surprising, considering the relative lack of oxygen in the vacuum irradiation test (see Sec. 6). These results are presented in Fig. 48. The vacuum sintered samples for which spectral reflectance data are presented in Figs. 47 and 48 have different spectral reflectances before irradiation. The sample presented in Fig. 47 has higher reflectance throughout the infrared region than that presented in Fig. 48. At this time no particular significance can be attached to these differences. Although all vacuum sintered samples were prepared in nominally identical fashion, it is recognized that sintering oven pressure variations and temperature gradients through each sample can have marked effects. Variations in surface appearance, not only between samples but on the same sample, have consistently occurred, for those sintered in vacuum.

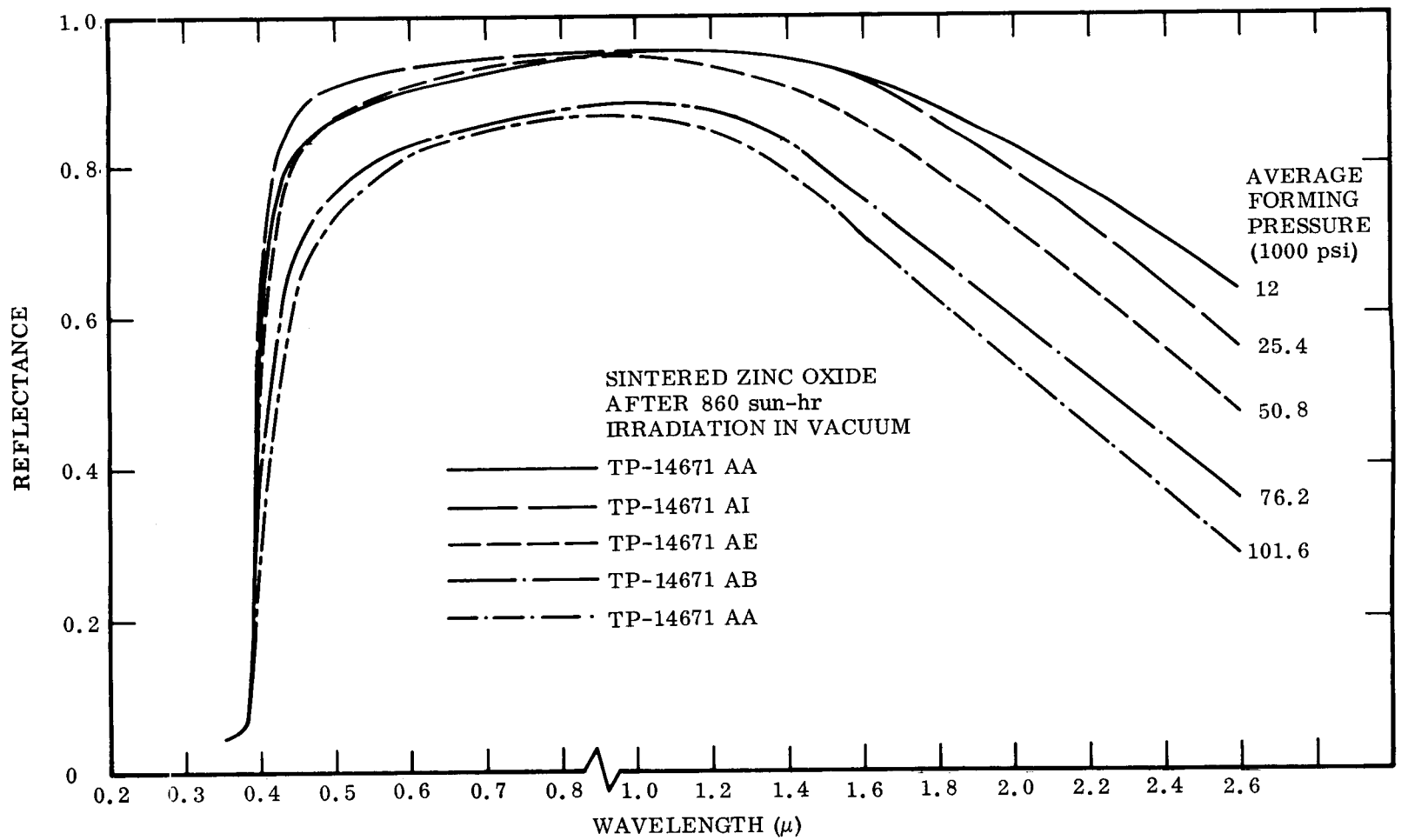

Fig. 46 Effect of Forming Pressure and UV Irradiation in Vacuum on Spectral Reflectance of Particulate ZnO

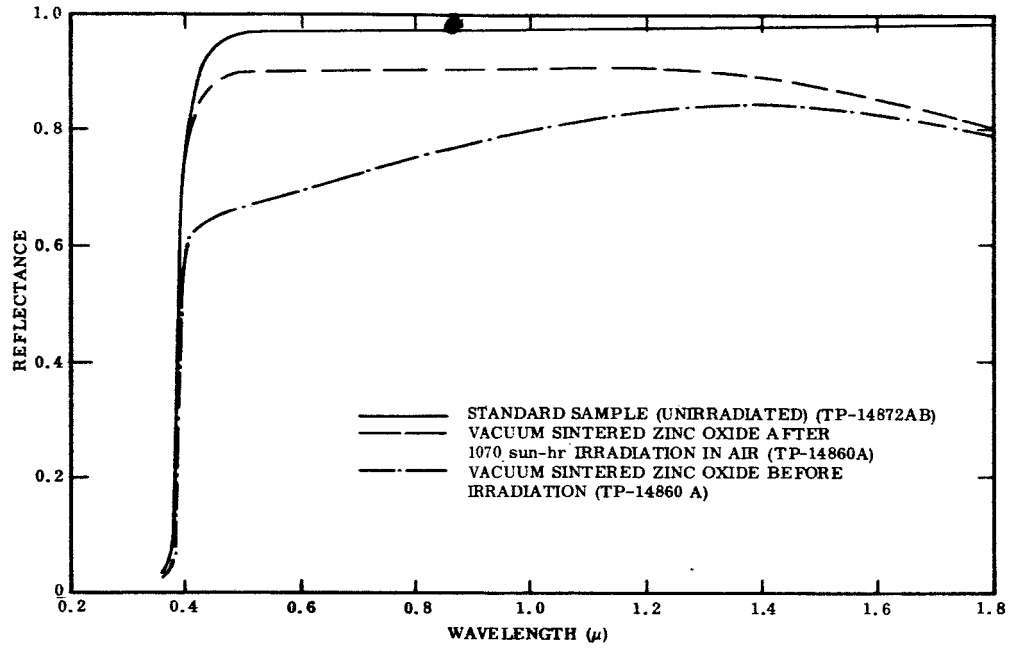

Fig. 47 Spectral Reflectance of Vacuum Sintered Particulate ZnO Before and After UV Irradiation in Air

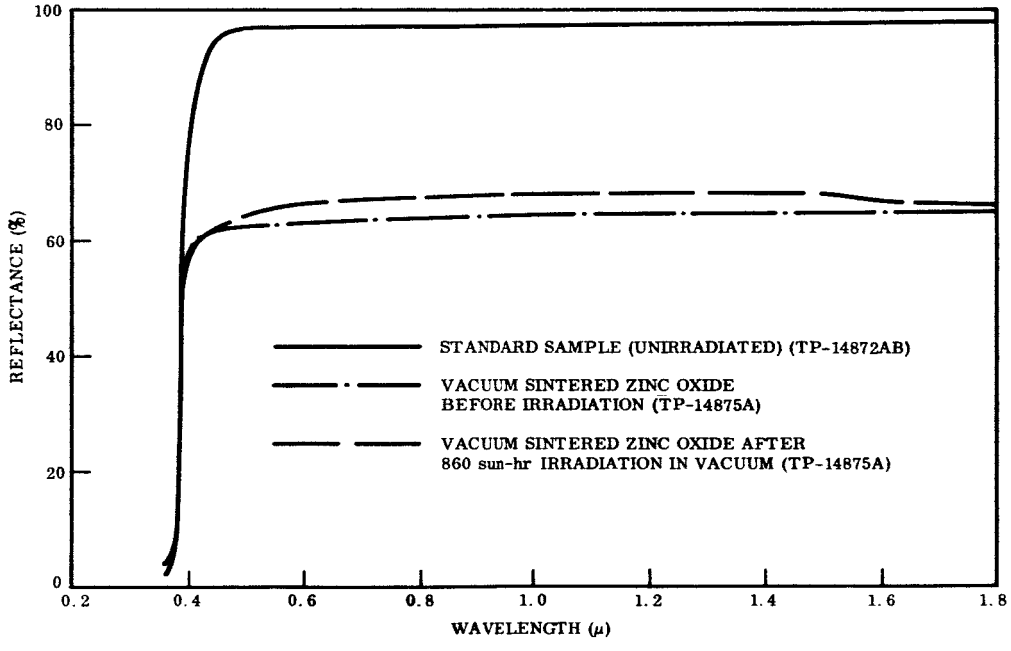

Fig. 48 Spectral Reflectance of Vacuum Sintered Particulate ZnO Before and After Ultraviolet Irradiation in Vacuum

Cu/ZnO Samples. Samples prepared by co-precipitating copper and zinc oxide as described in Sec. 3.1, were irradiated for 860 sun-hr and 67 hr in vacuum. The pre- and post-test spectral reflectance data are presented in Fig. 49. The effect of the 0.1% copper doping is to lower the initial reflectance throughout the visible and infrared. However, the ultraviolet stability of copper doped samples is markedly better than for the pure zinc oxide. For comparison with the copper-doped sample spectral reflectance two undoped zinc oxide spectral reflectance curves are presented. One is of the standard sample, and the other is for undoped, precipitated zinc oxide prepared in identical fashion to the copper-doped sample. Precipitated zinc oxide samples were exposed to 1000 sun-hr of irradiation in vacuum over a period of 134 hr. The post-test reflectance data for one of these samples are presented in Fig. 49. Both samples exhibited a large decrease in visible reflectance and no change in infrared reflectance. It is interesting to note that the copper doping improves the ultraviolet stability of the precipitated zinc oxide markedly in the visible region, whereas neither doped nor undoped precipitated zinc oxide degrades in the infrared region. This may be simply attributable to the low initial infrared reflectance of the undoped precipitated zinc oxide; that is, the infrared region of the material spectrum is apparently stable under ultraviolet irradiation because those defects which cause infrared absorption are already numerous.

Oxygen Photodesorption. During irradiation of zinc oxide samples it has been routinely observed that the pressure in the vacuum chamber increases when the lamp is turned on after initial pumpdown. This has been attributed to photodesorption of gases from the chamber walls as well as from the sample surfaces. In order to determine if oxygen desorption from the zinc oxide contributed significantly to this pressure rise, the photodesorption process was investigated. The quantity of oxygen evolved was determined by employing a stabilized zirconia ($Zr_{0.85}Ca_{0.15}O_2$) solid electrolyte cell, which produces an emf that is proportional to the logarithm of the partial pressure of oxygen present in the cell. Due to difficulties encountered in maintaining a satisfactory and stable vacuum level in the cell, the results obtained were only of a qualitative nature. Several repetitions of igniting and extinguishing the ultraviolet lamp showed conclusively that there was a photodesorption-adsorption of oxygen on the zinc oxide

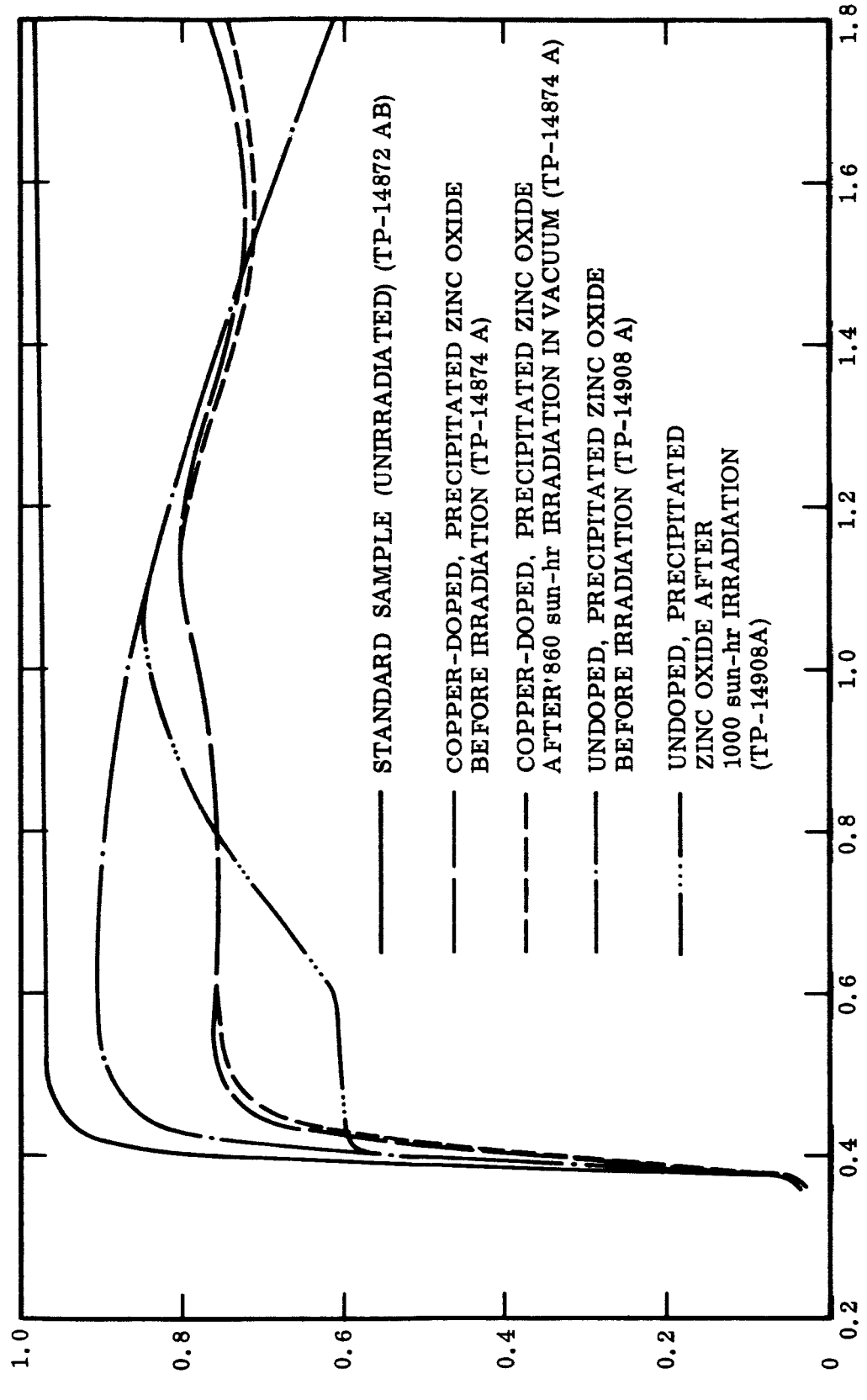

Fig. 49 Spectral Reflectance of Precipitated ZnO and Cu-Doped ZnO Before and After UV Irradiation in Vacuum

surface occurring during and after irradiation (see Sec. 2.4). The results of this exploratory test are not adequate to distinguish among desorption of physically adsorbed oxygen,chemisorbed oxygen,and lattice dissociation. However, it has been conclusively demonstrated that there is a photoinduced exchange of oxygen between the zinc oxide and the gaseous environment that, in all likelihood, is related to changes in optical properties.

Section 5
BAND STRUCTURE STUDIES

A thorough understanding of the electronic energy band structure (Ref. 21) of a crystal is a necessary prerequisite for the detailed interpretation of many important transport and optical properties. We have, therefore, initiated theoretical band structure studies of ZnO to complement the experimental program.

To the best of our knowledge, no serious attempt has previously been made to elucidate the electronic band structure of ZnO. We thus feel that our efforts will prove to be both useful and unique. Although the results to be presented here are of a preliminary nature, a number of interesting inferences can be made on the basis of this work.

The initial attempt to determine the band structure of ZnO was based on the pseudopotential method (Ref. 22). The essential feature of this approach is that it provides a parametrized form of $E(\underline{k})$ throughout the entire Brillouin zone. The correct band structure is then obtained by adjusting the parameters so that certain features of the calculated band structure agree with experiment. At certain points of the zone, for instance, one might choose to fit experimentally determined band gaps, or individual band slopes or curvatures.

Our pseudopotential calculation was carried out for several points of high symmetry in the Brillouin zone using five parameters and an average of about twenty plane waves. Proceeding on this basis, it was not possible to obtain an energy band scheme in agreement with the relevant experimental data. This was initially somewhat puzzling, since in the case of the Column IV semiconductors only three pseudopotential parameters are needed to obtain excellent results. The key to this difficulty is likely to be found in some recent work by Falicov and Golin (Ref. 23). In a paper reporting on an investigation of the band structure of the Group V semimetals, these authors made an

interesting speculation concerning the construction of pseudopotentials. If their procedure is adapted to the wurtzite-type crystals, it would imply that approximately fifteen pseudopotential parameters are needed in this case. The parametrization of the band structure is thus very complex for wurtzite-type crystals. Furthermore, because of the paucity of experimental band parameters for ZnO, there is clearly insufficient information available to fit such a large number of parameters. The pseudopotential calculation was therefore temporarily put aside for a more promising method. However, we did gain a great deal of physical insight into the ZnO band structure problem in the course of this initial study.

In particular, it became evident that the band structure of ZnO should be quite similar to that of ZnS. Both compounds crystallize in the wurtzite structure, have nearly the same c/a ratio, and 16 valence electrons per unit cell. Furthermore, sulfur is adjacent to oxygen in Column VI of the periodic table and both elements have only s and p valence states occupied. The direct band gaps at $\underline{k} = (000)$ are similar in ZnS and ZnO (3.94 and 3.44 eV at 0° K), and exciton studies of Dietz, Hopfield, and Thomas (Ref. 24) have given a band edge structure for ZnO at $\underline{k} = (000)$ which is identical to that determined for ZnS by the exciton studies of Wheeler and Miklosz (Ref. 25). This latter work is also in agreement with the band edge ordering calculated for ZnS by Herman and Skillman (Ref. 26) using the orthogonalized-plane-wave (OPW) method.

During the course of his early investigation of ZnS, Herman studied the behavior of the energy bands when all of the core energy levels are shifted by a common amount – the so-called "core shift." The core shift was originally intended as a diagnostic device; however, it can be used to great advantage to relate the band structures of similar systems. Stated briefly, certain energy band levels are extremely sensitive to changes in the crystal potential while other levels are relatively insensitive. As one proceeds in a systematic fashion through a series of closely related crystals, it is the shifts of the sensitive levels which provide the most significant changes in the electronic properties throughout the sequence. As an example, Phillips (Ref. 27) has

shown that the band structure of Si can be obtained from that of Ge by applications of a suitable core shift to the band structure of Ge. Thus, given a band structure and the knowledge of how the important valence and conduction bands vary as a function of the core shift we have, in fact, an "adjustable" band structure which can be chosen to determine other, closely related band structures. This describes the "method of corresponding states."

We have carried out this core shift procedure and have succeeded in obtaining the band structure of ZnO from that of ZnS thereby. The results of this calculation, given in Fig. 50 , were obtained by using that core shift yielding the correct direct gap at $\underline{k} = (000)$. Of interest here is the relative flatness of the upper valence bands, the presence of a subsidiary conduction band minimum at K , and the presence of a valence band maximum at H . The nearly parallel conduction and valence bands along the A-H axis should give rise to a marked increase in the optical absorption at $\sim$ 5.5 to 6.0 eV.

The reliability of our results, of course, can be no better than that of the ZnS calculation used as a basis for this work. The photoemission studies of Kindig and Spicer (Ref. 28) on CdS add to our confidence here. For many of the same reasons already noted, the band structure of CdS should be similar to both that of ZnS and ZnO. These authors have shown that the valence and conduction band densities of states are in good agreement with Herman's ZnS calculation. We do expect, however, that a self-consistent band structure calculation may lead to results which differ from Fig. 50 in some respects.

For the sake of comparison, the free electron (or "empty lattice") band structure (Ref. 29) for wurtzite-type crystals is given in Fig. 51. This represents the band structure in the limit of zero crystal potential. As the crystal potential is "turned on" to its true value, the free electron bands evolve into the actual band structure as shown in Fig. 50.

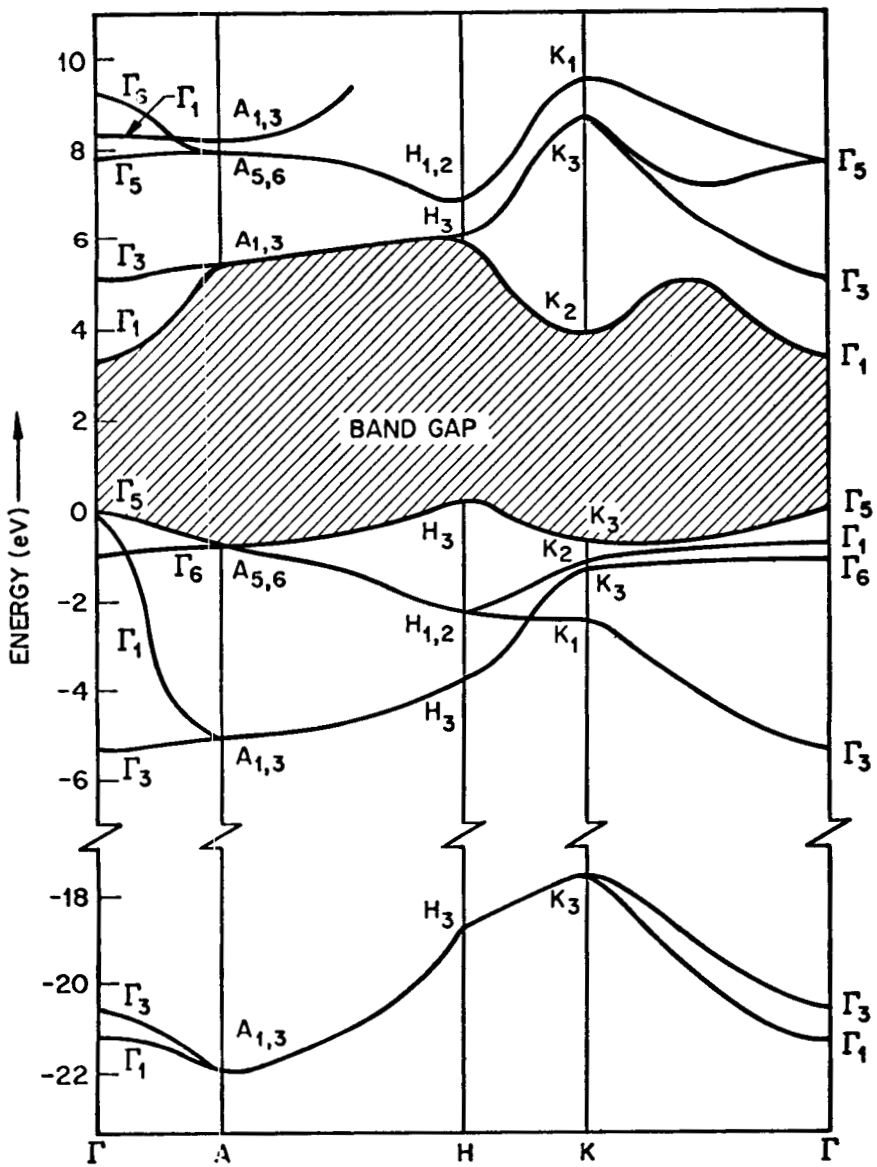

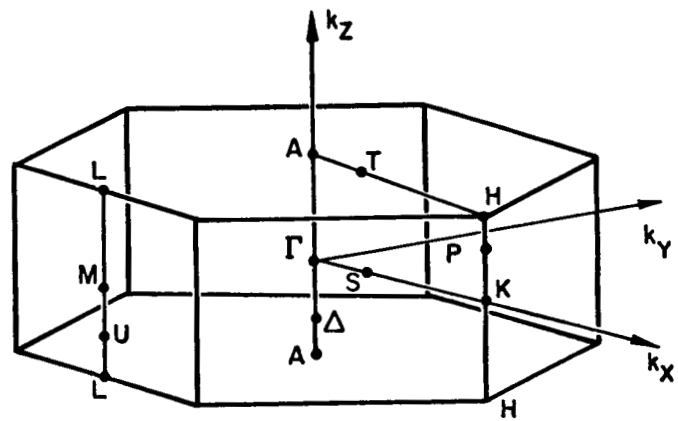

THE FIRST BRILLOUIN ZONE SHOWING LINES AND POINTS OF SYMMETRY

Fig. 50 Energy Band Structure of ZnO Along the Γ-A-H-K Directions

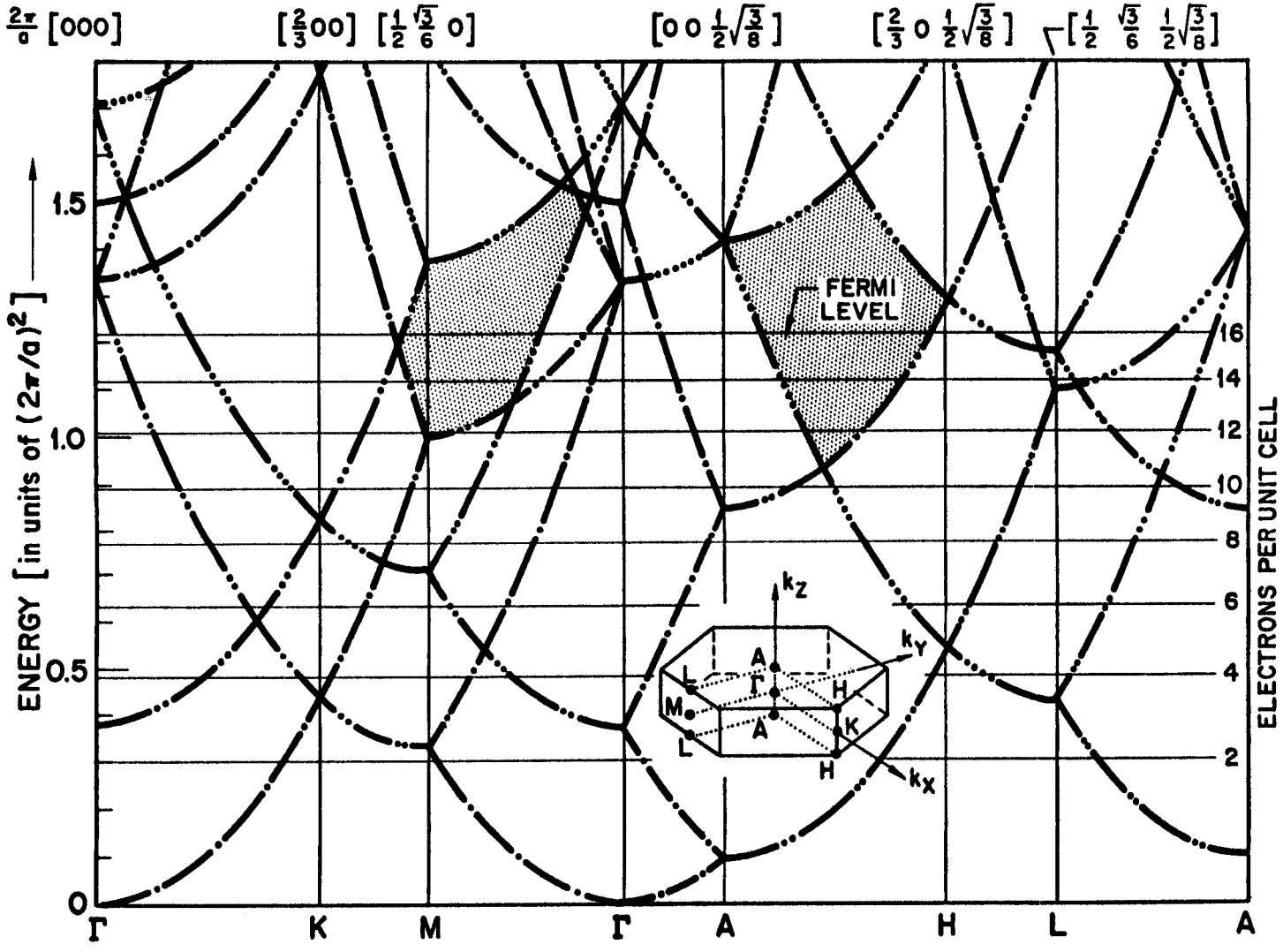

Fig. 51 Wurtzite Free Electron Band Structure. Free electron band structure for close-packed hexagonal or wurtzite-type crystals, drawn for the ideal c/a ratio. The heavy lines denote the positions of the highest valence band and lowest conduction band for crystals having 16 valence electrons per unit cell. The dots denote the degeneracy of each band (not including spin degeneracy) and the shaded region shows the band gap.

Another interesting comparison is given in Fig. 52. Here we have compared the energy levels at the center of the zone Γ as given by three different methods: the free electron model, our preliminary results for the band structure, and a tight binding model (to be discussed below). In the left-hand column, we have taken the set of plane waves corresponding to each degenerate eigenstate and have formed linear combinations (designated by Γ_i) transforming as the irreducible representations of the group of the wave vector $\underline{k} = (000)$ (Ref. 30). In this way, it is shown how the free electron levels split as the crystal potential is "turned on" and the correspondence between the free electron and actual band structures at Γ is established.

In the right-hand column, we have assumed that the electronic wave functions are simply the orbitals of the constituent neutral atoms. The energy levels were obtained from the work of Herman and Skillman (Ref. 31). This would serve, for instance, as the starting point for a linear-combination-of-atomic-orbitals (LCAO) calculation (Ref. 32). As in the case of the plane wave states, we have taken the atomic orbitals corresponding to each degenerate eigenstate and have determined linear combinations transforming as the irreducible representations of the group of the wave vector $\underline{k} = (000)$. In explanation of the notation used here, $[4s, Zn]_2$ identifies the 4s states of the two (subscript) Zn atoms in the unit cell.

In both the free electron and tight binding cases, states having the same irreducible representation will be mixed as the crystal potential is "turned on." The lowest conduction band is thus a mixture of Zn 4s-orbitals and O 2p-orbitals as is the second highest valence band. The highest valence band arises from O 2p-orbitals.

Our assignment of an atomic orbital character to the various bands is subject to the following limitations. In the first place, we have neglected all states of higher (or lower) energy than those indicated. We can therefore expect that the energy bands of interest (subject to the rules of group theory) will contain small admixtures of these states. Secondly, the 3d levels of Zn, which lie between the oxygen 2s and 2p levels, have for the sake of simplicity been treated as core rather than valence states.

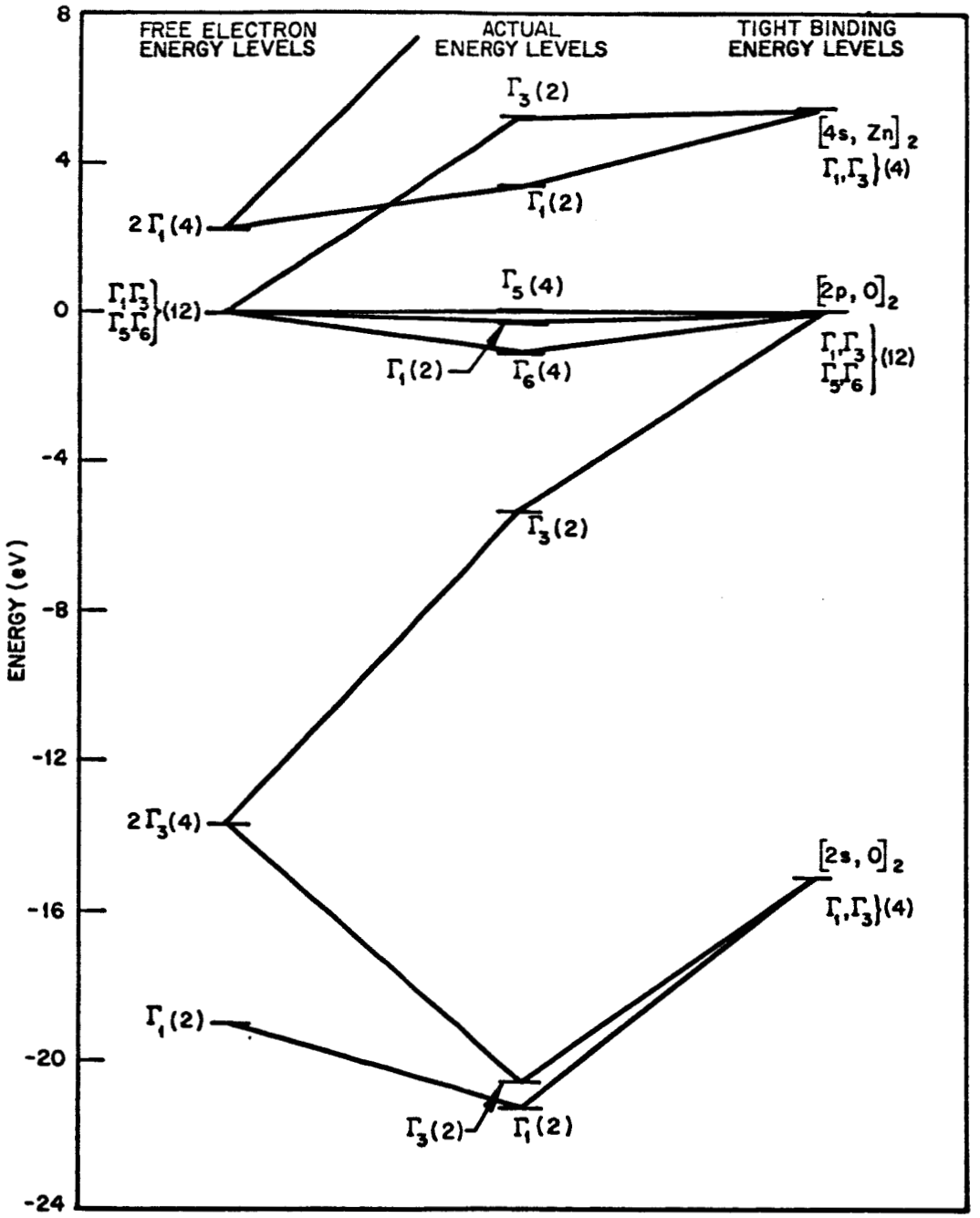

Fig. 52 Comparison of Band Structure Models at Center of Brillouin Zone. Comparison of the energy levels as given by the free electron, tight binding, and "actual" band structure models at $\underline{k}$ = (000) . The top of the valence band has been chosen as the zero energy for all three models. Numbers in parentheses denote the degeneracy of the levels, including spin degeneracy.

Actually, the 3d orbitals fall into a class that is between true "core states" (virtually no nearest neighbor overlap) and "valence states" (significant overlap). Finally, the atomic character of the bands will vary somewhat as $\underline{k}$ varies over the Brillouin zone.

The energy band structure of ZnO has been examined in a preliminary manner on the basis of four different theoretical models: the method of pseudopotentials, the method of weak binding, the method of tight binding, and the method of corresponding states. The pseudopotential method was used to gain some physical insight into the nature of the band structure. While it was found that insufficient experimental information was available at present to make possible a detailed band calculation on the basis of the pseudopotential method, the work we carried out led us to the conclusion that the band structures of ZnO and hexagonal ZnS were probably closely related, and that the former could be deduced from the latter by the method of corresponding states. Starting from an earlier study of the band structure of hexagonal ZnS by Herman and Skillman, and making suitable adjustments in scale, an energy band model for ZnO was derived. The plausibility of the derived model was then tested by the method of weak binding (nearly-free-electron model) and by the method of tight binding (LCAO model). These tests indicated that our derived band structure for ZnO was probably a good first estimate. Further work in this area may prove to be quite valuable because of the crucial role that the energy band structure can play in estimating the energy levels of both surface states and bulk defect states.

Section 6
DISCUSSION

During the course of this program, the primary characterization of the solar-radiation-induced damage to zinc oxide has been made in terms of the changes in optical properties of the samples. The relationships existing between the zinc oxide employed in this work and the material employed in thermal control paints is of particular interest. Although no binder materials were included with the pressed and sintered samples, the reflectance spectra were found to be quite similar, over the wavelength range of 0.27 to 2.5 μ, to those of zinc oxide paints. This observation, in connection with the findings that the average particle sizes of the original zinc oxide powder and the sample compacts were approximately the same, indicates that the sample preparation procedures did not alter the properties of the material to an appreciable extent. Therefore, it is to be expected that, exclusive of binder effects and pigment-binder interactions, the damage processes observed in this study are similar to those occurring in zinc oxide paint systems. The relative simplicity of the pure pigment system has led to a better understanding of those processes characteristic of the pigment, without the added complexities of pigment-binder interactions.

Throughout the course of the experimental studies, one unifying trend in the data has been apparent: many of the changes in the optical properties of zinc oxide appear to be connected with the loss and gain of oxygen by the crystal. This is borne out not only by the results of irradiation in vacuum and air, but also by the changes in optical properties induced by sintering in vacuum. Evidence in support of this point lies in the observation that both the ultraviolet-radiation-induced damage and mechanically-induced damage can be reversed by exposure to air. These results emphasize the need for in situ measurements of sample reflectance, since recovery and bleaching effects greatly limit the quantitative significance of post-exposure reflectance measurements.

A major portion of the effort in this program has been devoted to development of the in situ bidirectional reflectance measurement and ultraviolet exposure apparatus, and to learning the strengths and limitations of this new analytical tool. Excessive quantitative importance should not be attributed to the preliminary in situ data accumulated to date; however, the trends and qualitative behavior observed are extremely significant. Further exposures with in situ measurements will play a crucial role in the construction and evaluation of a model for the mechanisms of optical damage. Because of the complications involved in observation of the spectral and temporal dependence of recovery, in situ measurements are mandatory for accurate determination of the kinetics of damage and recovery. In situ tests afford much greater flexibility than static tests involving only pre- and post-test property measurements. For instance, conditions can be altered during the course of a run as a result of data being obtained. In addition, the in situ tests provide a means for observing behavior of samples when in the simulated orbital environment, and thus are the best practical means for observing phenomena predicted on the basis of a postulated damage model.

Of particular importance in diagnosing the degradation effects in ZnO are the characteristics of the degradation observed in various spectral regions. In most of the degradation observed, a gray absorption occurs throughout the spectral range studied (0.4 to 1.8 μ). This absorption is very likely due to a surface layer of Zn in some form. Such a deposit has been observed in the vacuum chamber and is an expected consequence of the degradation process. In addition to this gray absorption, additional damage-induced absorption occurs in the 0.4 to 0.6 μ (visible) region and in the 1.0 to 2.6 μ (infrared) region.

Samples damaged by ultraviolet irradiation in vacuum, and by vacuum sintering both develop marked absorption in the visible and infrared regions, as well as exhibiting the generalized lowering of reflectance throughout the spectral range studied. Samples damaged mechanically by means of high forming pressures also exhibit damage in the same regions, which is further enhanced by irradiation. The qualitative similarity among the various types of damage suggests one predominant underlying cause, which appears to be the presence or absence of oxygen.

The first experiments to be discussed are those involving filtering of the damaging radiation source. Two filters were used, a yellow filter and a Pyrex filter. The yellow filter cut off radiation below 0.40 μ and has a 50% transmission near 0.425 μ, and the Pyrex filter cut off radiation below 0.28 μ with a 50% transmission at 0.32 μ (see Sec. 4.4).

The yellow filter removes all radiation with energy greater than the band gap, and in this case only damage in the infrared was produced. The Pyrex filter passes significant amounts of radiation with energy greater than the band gap, and in this case visible damage occurred and increased infrared damage was observed. The unfiltered radiation produced increased visible damage but less infrared damage in comparison to the results of the Pyrex filter. The lack of visible absorption in the 0.4 μ filter run and its subsequent increase with increasing intensity of band-gap radiation in the other filter runs indicate that this damage requires band-gap radiation. Because band-gap radiation is absorbed very near the surface (<0.1 μ) the visible absorption is presumably associated with damage generated near the surface.

Since the yellow filter only passes radiation with energies less than the band gap, this radiation is rather penetrating, and the infrared damage resulting from this radiation must, therefore, be generated in the bulk of the particles. By penetrating radiation is meant radiation which can penetrate deeply into the bulk of the particles because of its relatively low absorption coefficient. This experiment only shows that the damage is <u>generated</u> throughout the bulk of the particles. The resulting infrared absorbing species may not necessarily, on the basis of this experiment, reside throughout the particle.

In comparison to the yellow filter, the Pyrex filter passes a greater amount of radiation less than the band gap (penetrating radiation) in addition to passing radiation of energy greater than the band gap. Apparently this increased penetrating radiation increases the infrared damage. The relatively large change in infrared damage produced by radiation between the absorption edge and 0.425 μ would indicate that the radiation producing the infrared damage is rather near the absorption edge in energy.

The relative decrease in the infrared absorption with no filtering is presumably the result of a self-filtering action which comes about from the increased visible damage for this case. The lack of the gray absorption in the yellow filter run and its appearance in the other runs indicates it also required band-gap radiation.

The next important series of experiments are those involving the ultraviolet irradiation in air of vacuum sintered samples which show recovery in the visible region, but not in the infrared, after exposure. Because the visible absorption observed in vacuum sintered samples and samples degraded by ultraviolet radiation are similar, the disappearance of visible absorption by bleaching a vacuum sintered sample would indicate that this visible absorption and its elimination is primarily a surface phenomenon. Also the lack of bleaching in the infrared would indicate that the infrared damage is located in the bulk; its bleaching would presumably require a much longer time because of the requirement for a diffusion process.

The next related series of experiments we wish to discuss involve the time and temperature dependence of the ultraviolet-induced degradation and its recovery both in the visible and infrared regions; these are the ultraviolet exposures performed with in situ bidirectional reflectance measurements (Sec. 4.3). In the exposures at 500, 200, and -250° F the damage in the infrared region appeared to increase slightly with increasing temperature, reaching a saturation level during irradiation. However, decreases in reflectance in the visible region showed a much stronger temperature dependence, with little change being observed at the lowest temperature. This observation in conjunction with the observed recovery in air supports the thesis that the visible damage occurs close to the surface, whereas the infrared damage is initiated in the bulk. The comparative lack of visible damage at -250° F is therefore attributed to the inhibition of the desorption process at low temperatures which requires a small but finite activation energy. The primary process for the creation of bulk defects by solar radiation is considered to be essentially temperature independent, with activated secondary processes such as diffusion accounting for the decreasing infrared reflectance with increasing sample temperature.

In all cases in situ bidirectional reflectance measurements indicated significant recovery of both visible and infrared damage upon admission of air to the exposure chamber. At this time it is not possible to present a detailed kinetic analysis of the recovery process, since many of the samples investigated had significantly different thermal and vacuum histories. However, it must be emphasized that in situ measurements have unambiguously demonstrated that post exposure measurements performed in air yield erroneously low values for reflectance changes of particulate zinc oxide, due to recovery of the damage upon exposure to oxygen.

The involvement of oxygen with the solar radiation-induced damage to zinc oxide has been verified by the positive identification of the photodesorbed gas as O_2. By the use of a solid electrolyte electrochemical cell which generates an emf dependent solely upon the partial pressure of oxygen, it has been demonstrated that the changes in pressure associated with the ignition and extinguishing of the AH-6 ultraviolet lamp are associated with an adsorption-desorption process involving oxygen and zinc oxide.

The next experiments to be discussed are the studies of particulate samples of Cu-doped zinc oxide. These studies were based on consideration of certain aspects of the damage model and on the observed behavior of single crystals doped with copper and lithium. On the basis of conductivity measurements, it has been shown that the Fermi level can be depressed by 1 eV or more through doping with Group I acceptor impurities (i.e., lithium or copper). Lowering of the Fermi level by a sufficient amount may lead to an emptying of the surface states, and consequently to stabilization of the surfaces of the ZnO particles by reduction of the field-aided drift of optically injected holes toward the surface. It might therefore be possible that copper or lithium doping of ZnO would result in a retardation of the solar-radiation-induced optical damage. The available data on the Cu-doped particulate samples were shown in Fig. 49; these samples exhibited a marked reduction in damage, as compared to that incurred by "standard" samples as well as to undoped ZnO prepared in the same manner as the doped samples. These data must be interpreted with caution since the initial absorptances of the doped and undoped samples were considerably higher than that of the "standard" samples, indicating that the initial defect character of these samples was substantially different.

In Sec. 2.5, the possible impurity mechanisms which give rise to the observed visible and infrared damage were discussed. On the basis of the existing knowledge of ZnO and the experiments carried out here on particulate samples to date, it has not been possible to clearly define the specific impurity transitions giving rise to the observed absorptions.

The single crystal degradation studies were undertaken in order to determine if single crystals can be degraded by the ultraviolet irradiation. If degradation can be observed in single crystals, the mechanisms of the degradation can be more clearly characterized. As an example, surface and bulk effects can be separated, important parameters such as the Fermi level and defect distributions can be determined, and definitive techniques can be used to characterize defects and surface state properties. One important point is that the type of information that can be obtained from single crystal studies yields significant information leading to an understanding of the basic mechanisms of the degradation process. Because of the limited amount of experimental data available to date, firm conclusions cannot be drawn from the single crystal degradation runs. However, the existing data can be tentatively interpreted to yield certain gross features of the degradation processes. For example, the visible damage appears to result from greater than band-gap irradiation absorbed near the surface and appears to be due to acceptor type defects which have diffused into the bulk. The infrared damage appears to result from less than band-gap irradiation and appears to be due to donor type defects created within the bulk. Furthermore, the single crystal degradation effects appear to be quite similar to those observed with the particulate samples.

Section 7

CONCLUSIONS AND RECOMMENDATIONS

7.1 CONCLUSIONS

- An apparatus for performing in situ bidirectional reflectance measurements has been constructed and successfully operated.
- The initial reflectance spectra of the pressed and sintered particulate samples were quite similar to those of zinc oxide-pigmented thermal control paints, over the wavelength range 0.27 to 2.5 μ (except for binder absorptions in the infrared).
- Solar-radiation-induced reduction in reflectance of the particulate samples over the same wavelength range was similar to that observed for zinc oxide paints.
- The zinc oxide optical property changes observed in the visible region of the spectrum appear to be connected with the loss and gain of oxygen by the ZnO.
- Solar-radiation-induced reduction in reflectance spectra of particulate samples recovers upon exposure to air.
- The solar-radiation-induced reduction in the reflectance for visible energy is apparently initially generated near the surface, whereas reduction in infrared reflectance appears to be more of a bulk phenomenon.
- The effect of sample temperature on the degradation of particulate zinc oxide indicates that the visible damage is enhanced at elevated temperatures, while the infrared damage is relatively insensitive to temperature.
- The effects in the particulate sample reflectance spectra produced by (1) solar-radiation in vacuum, (2) high sample forming pressure, and (3) sintering in vacuum are similar enough to suggest one predominant underlying cause.
- Sintering in vacuum appears to produce free zinc at the surface of the particulate samples.
- A working model for solar-radiation-induced damage to the optical properties of zinc oxide has been formulated.

- Conclusive evidence for the photodesorption and adsorption of oxygen on particulate zinc oxide has been obtained.
- The information available on diffusion rates in zinc oxide and the complex diffusion conditions near the surface prevent quantitative prediction of the time dependence of the damage processes.
- A band structure for zinc oxide was derived in a preliminary manner by the method of corresponding states.
- Ultraviolet irradiation of ZnO single crystals in vacuum appears to produce damage in the visible and infrared regions of the spectrum reminiscent of damage to particulate samples.
- Ultraviolet exposures with in situ bidirectional reflectance measurements play a crucial role in the construction and evaluation of a model for the mechanism of optical damage to zinc oxide.

7.2 RECOMMENDATIONS FOR FUTURE WORK

The ultimate goal of elucidating the mechanisms involved in the solar radiation-induced damage to the optical properties of zinc oxide could be approached by the successful execution of the following tasks:

- Performance of an experimental study of the effects produced by exposure to solar radiation.
- Particulate and single crystal samples should be exposed to radiation of wavelengths between 0.2 and 2.0 μ. Irradiation parameters including flux density, spectrum, and exposure time should be varied. Samples should be exposed in vacuum and inert atmospheres at various temperatures between -250 and 500° F.
- In situ spectral bidirectional reflectance measurements on particulate samples should be performed during irradiation. In situ spectral transmittance measurements should be performed on single crystals during irradiation. Particular emphasis should be placed on measuring the rates of the damage processes as a function of temperature, in order to clarify the role of diffusion of lattice defects.

- Investigations of the dependence of radiation damage on wavelength by interposition of selective wavelength filters should be performed, employing in situ measurements on both particulate and single crystal samples.
- Studies of the kinetics of recovery of particulate samples from radiation-induced degradation should be carried out, employing in situ bidirectional measurements. Recovery in the dark and with selected wavelength illumination in vacuum and selected atmospheres merits investigation.
- Examination of the effects of selective doping of both particulate and single crystal samples of zinc oxide on the solar radiation-induced damage processes should be carried out. These studies should serve as a diagnostic tool for elucidating the degradation mechanism and testing various aspects of the working model.
- Exploratory experiments relevant to surface states characterization and other effects should be performed in order to further elucidate the solar radiation-induced damage to zinc oxide. Continuation of the theoretical investigation of the effect of solar radiation on the optical properties of zinc oxide single crystals and pigments is warranted.
- Theoretical considerations of solar irradiation-induced degradation and recovery as affected by irradiation wavelength, flux density, material temperature, gaseous environment, and defect structure of zinc oxide should be correlated with the experimental data. This theoretical treatment in conjunction with the experimental results would serve as a basis for elucidating the nature of the damage mechanisms.

Section 8

REFERENCES*

1. Lockheed Missiles & Space Company, Thermophysics Design Handbook, Report 8-55-63-3, Sunnyvale, Calif., Jul 1963

2. R. E. Gaumer and L. A. McKellar, Thermal Radiative Control Surfaces for Spacecraft, LMSC-704014, Lockheed Missiles & Space Company, Sunnyvale, Calif., Mar 1961

3. R. L. Olson, L. A. McKellar, and J. V. Stewart, "The Effects of Ultraviolet Radiation on Low α_s/ϵ Surfaces," Symposium on Thermal Radiation in Solids, sponsored by NASA, NBS, and USAF/ASD, San Francisco, Calif., Mar 4–6, 1964

4. R. L. Olson, L. A. McKellar, and W. E. Spicer, The Energetics of Ultraviolet Radiation Damage to White Surfaces, (in preparation), Lockheed Missiles & Space Company, Sunnyvale, Calif., Mar 1964

5. "Coatings for the Aerospace Environment," Symposium sponsored by WADC, WADC TR 60-773, Wright Air Development Center, Wright-Patterson Air Force Base, Ohio

6. R. E. Gaumer, F. J. Clauss, M. E. Sibert, and C. C. Shaw, "Materials Effects in Spacecraft Thermal Control," Proceedings of WADD Conference on Coatings for Aerospace Environment, Dayton, Ohio, Nov 1960; WADD TR 60-773

7. W. F. Carroll, Development of Stable Temperature Control Surfaces for Spacecraft – Progress Report No. 1, JPL Technical Report 32-340, Jet Propulsion Laboratory, Pasadena, Calif., Nov 1962

8. G. A. Zerlaut, Y. Harada, and E. H. Tompkins, "Ultraviolet Irradiation in Vacuum of White Spacecraft Coatings," Symposium on Thermal Radiation of Solids sponsored by NASA, NES, and USAF/ASD, San Francisco, Calif., Mar 4–6, 1964

*See Appendix A for zinc oxide bibliography.

9. H. H. Hormann, Improved Organic Coatings for Temperature Control in a Space Environment, ASD-TDR-62-917, Aeron. Systems Division, USAF, Feb 1963

10. James H. Weaver, Anodized Aluminum Coatings for Temperature Control of Space Vehicles, ASD-TDR-62-918, Aeron. Systems Division, USAF, Feb 1963

11. N. Z. Searle, J. H. Daniel, R. C. Hirt, P. A. Mullen, and W. J. Stehman, Pigmented Surface Coatings for Use in the Space Environment, Report ML-TDR-64-314, Air Force Materials Laboratory, Wright-Patterson AFB, Ohio, Nov 1964

12. E. R. Streed and C. M. Beveridge, "The Study of Low Solar Absorptance Coatings for a Solar Probe Mission," Symposium on Thermal Radiation in Solids Sponsored by NASA, NBS, and USAF/ASD, San Francisco, Calif., Mar 4–6, 1964

13. J. A. Parker, C. B. Neel, and M. A. Golub, Experimental Development of a Technique for the Correlation of Flight and Ground Based Studies of the Ultraviolet Degradation of Polymer Films, NASA, TM X-54-015, National Aeronautics and Space Administration, Dec 1963

14. J. S. DeWitt, C. W. Litton, and T. C. Collins, Bull. Am. Phys. Soc., 10, No. 3, 331 (1965)

15. A. R. Hutson, Physical Review, 108, No. 2, 222 (1957)

16. G. Heiland, "Surface Properties of Zinc Oxide," International Summer Course on Solid State Physics, Ghent (1963)

17. P. H. Kasai, "Electron Spin Resonance Studies of Donors and Acceptors in ZnO," Phys. Rev., 130, 989–995 (1953)

18. G. Heiland, "Surface Conductivity of Semiconductors and its Variation by Adsorption, Transverse Electric Fields, and Irradiation," Disc. Faraday Soc., 28, 168–182 (1959)

19. J. J. Lander, "Reaction of Lithium as a Donor and Acceptor in ZnO," J. Phys. Chem. Solids, 15, 324 (1960)

20. H. E. Brown, ed., Zinc Oxide Rediscovered, The New Jersey Zinc Co., New York, N. Y., 1957

21. Frank Herman, Proc. IRE, 43, 1703 (1955). This, together with reference 29, forms an excellent introduction to energy band theory and related topics.

22. L. Kleinman and J. C. Phillips, Phys. Rev., 116, 880 (1959)
M. H. Cohen and V. Heine, Phys. Rev., 122, 1821 (1961)
F. Bassani and V. Celli, Phys. Chem., Solids, 20, 64 (1961)
David Brust, Phys. Rev., 134, A1337 (1964)

23. L. M. Falicov and Stuart Golin, Phys. Rev., 137, A871 (1964)

24. R. E. Dietz, J. J. Hopfield, and D. G. Thomas, J. Appl. Phys., 32, 2282 (1961)

25. R. G. Wheeler and J. C. Miklosz, Proceedings of the International Conference on Semiconductor Physics, Paris, 873 (1964)

26. F. Herman and S. Skillman, Proceedings of the International Conference on Semiconductor Physics, Prague, 20 (1960)

27. J. C. Phillips, Phys. Rev., 125, 1931 (1962)

28. N. B. Kindiz and W. E. Spicer, to be published

29. F. Herman, Rev. Mod. Phys., 30, 102 (1958)

30. L. P. Bouckaert, R. Smoluchowski, and E. P. Wigner, Phys. Rev., 50, 58 (1936). G. F. Koster, Solid State Physics, Vol. 5, F. Seitz and D. Turnbull (eds.), Academic Press, New York, 1957

31. F. Herman and S. Skillman, Atomic Structure Calculations (Prentice-Hall, Inc., Englewood Cliffs, New Jersey, 1963)

32. F. Bloch Z. Physik, 52, 555 (1928)
J. C. Slater and G. F. Koster, Phys. Rev., 94, 1498 (1954)

33. H. E. Brown, ed., Zinc Oxide Rediscovered, The New Jersey Zinc Co., New York, N. Y., 1957

Appendix A

A PARTIAL BIBLIOGRAPHY OF RESEARCH ON ZINC OXIDE

The published literature on the semiconducting properties of zinc oxide is very extensive (for example, one article by Heiland, Mollwo, and Stockmann quotes 130 references), and there is also a large amount of literature on catalysis at ZnO surfaces. Much information on the above subjects exists also in the form of unpublished reports (such as the University of Pennsylvania reports during the 1950's).

Additionally, there is a large body of information (both in published and in report form) on the degradation of zinc oxide paints due to electromagnetic or particulate radiation. This information has not been specifically included in this abbreviated literature bibliography, but instead, enough of the published papers on zinc oxide as a material have been included so that results which shed light on damage mechanisms will have been reported in at least one paper.

Some of these papers relate to the electrical and optical properties of single crystals, or to impurity diffusion rates in single crystals. Others are concerned with the properties of ZnO in powdered or microcrystalline form, and there are four review papers which attempt to cover the whole field.

Review Articles

G. Heiland, E. Mollwo, and F. Stockmann, Solid State Physics Vol. 8, (Academic Press, 1959), pp. 191–323.
"Electronic Processes in Zinc Oxide"

A very exhaustive and well documented survey article of results on both powdered and monocrystalline zinc oxide, with 130 references up to 1959. Describes the electrical and optical properties, adsorption phenomena, impurity diffusion, and luminescence.

G. Heiland, International Summer Course on Solid State Physics, Ghent (1963)
"Surface Properties of Zinc Oxide"

Notes associated with lectures given by Heiland at this summer school in Belgium. Contains nothing brand new, but gives a useful summary of information about processes on the ZnO surface up to 1963, field effect measurements, and adsorption.

E. Scharowsky, Z. Phys. 135, pp. 318–330 (1953)
"Optical and Electrical Properties of ZnO Single Crystals with Zn Additions" (In German)

The foundation paper of ZnO single crystal work – essentially Scharowsky's thesis in which he describes how crystals are grown from a vapor-phase reaction. Crystals were heated in Zn vapor at various temperatures and he shows how excess zinc in the lattice provides conduction electrons and produces the famous "b" optical absorption between 0.37 and 0.65 μ.

E. E. Hahn, J. Appl. Phys. 22, pp. 855–863 (1951)
"Some Electrical Properties of Zinc Oxide Semiconductor"

This is probably the earliest general review paper we should take note of. There had been much earlier work on zinc oxide – notably the work of Carl Wagner and his group before World War II – but Hahn essentially brings us up to date to 1950 with the situation on ZnO pressed powders, the n-type conduction, and the high resistance at intergranular contacts due to upturned bands.

F. F. Kenshtein (Th. Wolkenstein)
"The Electronic Theory of Catalysis on Semiconductors," Macmillan Co., N. Y., 1963 (Translated from Russian)

An excellent review and an extended version of concepts in his many papers on the subject.

H. E. Brown, ed., Zinc Oxide Rediscovered
The New Jersey Zinc Company, New York, 1957.

Extensive review of selected properties and commercial uses of zinc oxide.

Single Crystals – Electrical Properties

G. Mesnard and C. Eymann, Comptes Rendus 258, pp. 3672–3675 (1964)
"Electronic Properties of Zinc Oxide Single Crystals Containing Acceptor Elements"
(In French)

Reports on ZnO single crystals grown by the flux method – using a lead fluoride flux – rather than the conventional Scharowsky vapor-phase approach. Crystals can be grown with up to 1% of acceptor elements such as lithium, sodium, and copper. Such crystals are still not p-type, but have extremely small free electron densities, reduced infrared absorption, but a fundamental absorption edge displaced toward longer wavelengths.

A. R. Hutson, J. Phys. Chem. Solids 8, pp. 467–472 (1959)
"Electronic Properties of ZnO"

A paper given at the 1958 Rochester conference. Uses thermoelectric and magnetoresistance data in combination with existing Hall effect and conductivity data to elucidate the conduction band structure in ZnO. Finds that there should be at least 12 conduction band valleys of relatively small mass anisotropy!

G. Heiland, J. Phys. Chem. Solids 6, pp. 155–168 (1958)
"Field Effect and Photoconductivity in ZnO Single Crystals" (In German)

Uses field effect and photoexcitation to study electron mobility in the surface layer of ZnO crystals treated in hydrogen to create an N+ surface layer. Tries to measure electron lifetime from functional dependence of steady state and chopped photoresponse, while gas coverage is maintained nominally constant.

A. R. Hutson, Phys. Rev. 108, pp. 222–230 (1957)
"Hall Effect Studies of Doped Zinc Oxide Single Crystals"

A useful review of the temperature dependence of density and mobility of free electrons in ZnO crystals, to be used in conjunction with other papers.

Single Crystals – Optical Properties

D. G. Thomas, J. Phys. Chem. Solids 10, pp. 47–51 (1959)
"Infrared Absorption in Zinc Oxide Crystals"

Comments on lattice absorption bands at 10.1 and 11.5 μ, uses lithium and indium doped single crystals to show how superimposed free carrier absorption is linear in free electron density, varies as cube of wavelength from 1 to 6 μ.

R. Arneth, Z. Physik 155, pp. 595–608 (1959)
"On the Absorption of ZnO Crystals in the Infrared" (In German)

Displays infrared results in good agreement with above reference. Also shows how additions such as zinc or copper lead to additional near ultraviolet and visible absorption on the low-energy side of the "pure crystal" intrinsic absorption edge.

Single Crystals – Surface Effects

G. Heiland, Disc. Faraday Soc. 28, pp. 168–182 (1959)
"Surface Conductivity of Semiconductors and its Variation by Adsorption, Transverse Electric Fields, and Irradiation"

A review of University of Erlangen work, particularly field effect experiments, on ZnO and other semiconductors. The discussion involving Heiland and F. S. Stone brought up the point as to whether any proof exists that oxygen from the lattice itself as opposed to adsorbed oxygen is evolved on irradiation; the strongest evidence seems to be in Collins and Thomas paper, Phys. Rev. 112.

G. Heiland, Z. Phys. 142, pp. 415–432 (1955)
"The Surface Electrical Conductivity of Zinc Oxide Crystals" (In German)

Concerned with the change of conductance of single crystals due to change in the surface condition following irradiation. Used 1-keV electrons as well as ultraviolet photons for irradiation.

D. F. Anthrop and A. W. Search, J. Phys. Chem. 68, 2335–2342 (1964)
"Sublimination and Thermodynamic Properties of ZnO"

Mass spectrometric study of sublimination of ZnO. Resolves the problem of the anomalous rate of sublimative of ZnO in the presence of Zn vapor.

E. Kh. Enikeev, C. Z. Roginsky and J. H. Rufov, Proc. International Conf. on Semiconductor Phys., Prague 1960
"Study of the Influence of the Adsorption of Gases on the Work Function of Semiconductors"

Relates the work function and activation energy of adsorption and desorption of oxygen on ZnO as a function of surface coverage and Li and Zn doping.

Th. Wolkenstein, Disc Faraday Soc. 31, 209–218 (1961)

The problem of ionizing radiation in the adsorptive and catalytic properties of a semiconductor is formulated within the framework of the electron theory of chemisorption and catalysis. Discusses band-bending and bulk parameters of a semiconductor in relation to the above effects.

G. Heiland, J. Phys. Chem. Solids 22, pp. 227–234 (1961)
"Photoconductivity of Zinc Oxide as a Surface Phenomenon"

Discusses field effect and photoconductivity measurements on single crystals in terms of the motion of mobile carriers in a surface channel, and the trapping and recombination of electrons and holes. The data appear open to several interpretations.

H. J. Krusemeyer, J. Phys. Chem. Solids 23, pp. 767–777 (1962)
"The Influence of Light, Oxygen,and Nitrogen on the Field Effect Mobility of Zinc Oxide Crystals"

Suggests that a result of optical absorption in the fundamental region is the transfer of oxygen lattice ions to adsorption sites – from which they can presumably later desorb.

T. Wolkenstein and I. V. Karpenko, J. Appl. Phys. 33, pp. 460–465 (1962)
"On the Theory of the Photoadsorptive Effect on Semiconductors"

Establishes a rather complicated criterion for adsorption or desorption of oxygen upon illumination which appears to be able to reconcile the various experimental observations of Fujita, Terenin, Barry and Stone, and Barry.

R. J. Collins and D. G. Thomas, Phys. Rev. 112, pp. 388–395 (1958)
"Photoconduction and Surface Effects with Zinc Oxide Crystals"

Remarks that the surface photoconduction in single ZnO crystals is too large to be explained by photodesorption of adsorbed oxygen. Argues that actual photolysis must occur – light produces hole electron pairs, holes move to surface and discharge lattice oxygen, leaving a zinc-enriched surface region.

H. J. Krusemeyer, Phys. Rev. 114, pp. 655–664 (1959)
"Surface Potential, Field Effect Mobility, and Surface Conductivity of ZnO Crystals"

Measurements on single crystals suggest that the bulk diffusion length for holes exceeds 10^{-5} cm, and that the quantum efficiency of the hold trapping process at the surface is approximately unity for a neutral surface.

D. G. Thomas and J. J. Lander, J. Phys. Chem. Solids 2, pp. 318–326 (1957)
"Surface Conductivity Produced on Zinc Oxide by Zinc and Hydrogen"

Studies the additional conductance of single crystals of ZnO caused by adsorption of zinc or hydrogen. Zn is adsorbed at room temperature and the additional conductance is a surface effect, with evidence of impurity band conduction.

Single Crystals-Diffusion Studies

W. J. Moore and E. L. Williams, Disc. Faraday Soc. 28, pp. 86–93 (1959)
"Diffusion of Zinc and Oxygen in Zinc Oxide"

A quite small diffusion coefficient for zinc, governed by an activation energy of 165 K cal, is found by using radioactive tracer techniques with single crystals. A mechanism based on thermally produced Frenkel defects is suggested. Radioactive techniques for oxygen yield a diffusion coefficient which is even smaller than for zinc. Vigorous discussion following presentation of this paper at an Ottawa symposium brought out the diversity of views on how zinc can propagate through the ZnO lattice.

D. G. Thomas, J. Phys. Chem. Solids 3, pp. 229–237 (1957)
"Interstitial Zinc in Zinc Oxide"

ZnO single crystals heated in zinc vapor, and the temperature dependence of the interstitial zinc solubility and diffusion coefficient inferred from the added conductivity. This method implies much faster diffusion than radioactive methods suggest.

D. G. Thomas, J. Phys. Chem. Solids 9, pp. 31–42 (1959)
"The Diffusion and Precipitation of Indium in Zinc Oxide"

Indium coated on ZnO single crystals is dissolved and diffused in at temperatures from 800 to 1300° C. This precipitates out on dislocations at lower temperatures when the solubility limit is surpassed, at rates indicating dislocation densities ranging from 10^6 to 10^7 cm^{-2}.

Single Crystals-Doped

G. Bogner and E. Mollwo, J. Phys. Chem. Solids 6, pp. 136–143 (1958)
"On the Production of Zinc Oxide Single Crystals with Definite Additions" (In German)

Describes adaptation of the Scharowsky method for making doped single crystals of ZnO. Shows how the conductivity increases with indium addition and decreases with copper addition, and how doping affects the infrared free carrier optical absorption.

H. Rupprecht, J. Phys. Chem. Solids 6, pp. 144–154 (1958)
"On the Concentration and Mobility of Electrons in Zinc Oxide Single Crystals with Definite Additions" (In German)

Conductivity and Hall effect measured and analyzed for the indium- and copper-doped crystals of Ref. 14.

J. J. Lander, J. Phys. Chem. Solids 15, p. 324 (1960)
"Reaction of Lithium as a Donor and Acceptor in ZnO"

Contains recipes for obtaining Li donor and acceptor states in ZnO and discusses the thermodynamic and kinetic aspects of the problem.

P. H. Kasai, Phys. Rev., 130, pp. 989–995 (1963)
"Electron Spin Resonance Studies of Donors and Acceptors in ZnO.

Identifies levels and gives estimates for them from an analysis of ESR experiments on Li and Zn doped polycrystalling ZnO.

Powders – Surface Effects

Y. Fujita and T. Kwan, Bull. Chem. Soc. Japan 31, pp. 379–380 (1958)
"Photodesorption and Photoadsorption of Oxygen on Zinc Oxide"

Report direct observations of gas – presumably oxygen – given off by ZnO powder in vacuum under UV illumination.

D. B. Medved, J. Chem. Phys. 28, pp. 870–873 (1958)
"Photodesorption in Zinc Oxide Semiconductor"

Also reports evolution of gas – presumably oxygen – by ZnO powder on UV illumination. Compares simultaneous curves of gas evolution and photoconductivity as a function of time.

D. B. Medved, J. Phys. Chem. Solids, 20, 255–267 (1961)
"Photoconductivity and Chemisorption Kinetics in Sintered ZnO Semiconductor"

Relates the "slow photoconductivity process to the chemisorption process which obeys the Elovich rate equation."

S. R. Morrison, Advances in Catalysis VII (Academic Press, 1955), pp. 259–301
"Surface Barrier Effects in Adsorption, Illustrated by Zinc Oxide"

Explains time-dependent events in ZnO as the consequence of chemisorption with electron transfer across the surface potential barrier as the rate-determining step. Suggests that ionization of surface states is the primary rather than secondary result of absorption of light.

H. J. Gerritsen, W. Ruppel, and A. Rose, Helv. Phys. Acta 30, pp. 504–512 (1957)
"Photoproperties of Zinc Oxide with Ohmic and Blocking Contacts"

Studies fast and very slow photoconductive response for the finely divided powders of Ruppel et al.

T. I. Barry and F. S. Stone, Proc. Roy. Soc. A. 255, pp. 124–144 (1960)
"The Reactions of Oxygen at Dark and Irradiated Zinc Oxide Surfaces"

Adsorption techniques including use of 180 used to keep track of oxygen on and off the surface of zinc oxide with a large surface to volume ratio. Results suggest that UV irradiation usually results in photodesorption, but that oxygen photoadsorption can occur when the ZnO has a large zinc excess – a not unreasonable result but one in direct conflict with Terenin et al.

T. I. Barry, Proc. 2nd Int. Cong. Catalysis (Paris, 1960), pp. 1449–1457
"The Adsorption of Oxygen on Zinc Oxide. The Effect of γ Radiation"

The kinetics of oxygen chemisorption on ZnO surfaces studied as a function of temperature, and two processes separated, interpreted as chemisorption of O^- at low temperatures and of $O^=$ above 200° C. Gamma radiation produces desorption of oxygen adsorbed at low temperatures, but there are complications when oxygen is pre-adsorbed at higher temperatures.

W. Ruppel, H. J. Gerritsen,and A. Rose, Helv. Phys. Acta 30, pp. 495–503 (1957)
"An Approach to Intrinsic Zinc Oxide"

Studies extremely finely divided zinc oxide powder, which can have an apparent resistivity of up to 10^{17} Ω-cm. The grain size of about 10^{-5} cm resulted in enormous effects of adsorbed oxygen.

S. R. Morrison and P. H. Miller, Jr., J. Chem. Phys. 25, pp. 1064–1065 (1956)
"Adsorption of Oxygen on Zinc Oxide"

Measures directly the volume of oxygen adsorbed by powdered ZnO. The variation of this with the prior time-temperature-oxygen pressure history is suggestive of the ready diffusion of interstitial zinc away from and toward the surface at about 500° C.

P. H. Miller, Jr., Photoconductivity Conference (Wiley, 1956), pp. 287–297
"The Role of Chemisorption in Surface Trapping"

A report to the Atlantic City conference on the work of the University of Pennsylvania group up to 1954. Reviews the experiments of Melnick and Medved on very slow and non-exponential decay of photoconductance in pressed powders in the light of Morrison's model for surface barrier and adsorption effects.

E. Mollwo, Photoconductivity Conference (Wiley, 1956), pp. 509–528
"Electrical and Optical Properties of ZnO"

Review the work of Scharowsky and Heiland. Discusses both the rapid and the slow photoconductive response observable in pressed sintered layers.

D. A. Melnick, J. Chem. Phys. 26, pp. 1136–1146 (1957)
"Zinc Oxide Photoconduction, an Oxygen Adsorption Process"

Much concerned with the very slow and non-exponential decay of photoconductance in pressed powders, and its interpretation on the basis of Morrison's model.

Appendix B
BIDIRECTIONAL REFLECTANCE APPARATUS

B.1 INTRODUCTION

The effects of the space environment on the optical properties of materials are generally evaluated by exposing materials to a simulated environment and measuring the preexposure and postexposure optical properties using standard optical instrumentation. This approach permits selection of the measuring technique best suited to definition of the operational parameters required of the optical material. However, such "static" test data (i.e., with pre-test and post-test measurements only) cannot account for possible postexposure recovery of the damaged material during the period preceding the final optical measurements. Exposure to ultraviolet or high-energy radiation in vacuum generally reduces the solar reflectance of white paints; this damage is known to recover upon exposure of the irradiated specimens to air. Previous work at LMSC also indicated that white metallic oxide pigments without a surrounding paint binder might recover quite rapidly. Furthermore, such recovery could occur in vacuum upon cessation of irradiation. It is evident that precise information on ultraviolet degradation of these materials can be assured only by optical property measurements performed in vacuum both during and after irradiation (i.e., in situ). A study of the mechanisms of radiation-induced damage to the optical properties of zinc oxide itself, with no surrounding paint vehicle, is presently underway at Lockheed. Basic to this study are in situ measurements of ultraviolet-induced optical damage to particulate zinc oxide samples, including determination of both the extent and the kinetics of recovery from damage under various conditions.

The apparatus for in situ bidirectional reflectance measurements consists of a vacuum enclosure containing a sample table. The intense source of damaging ultraviolet and visible radiation is external to the vacuum chamber and is incident on the sample

through a high-purity quartz window in the top of the chamber. The chopped radiation source for the reflectance measurements is also external to the vacuum chamber; the radiation passes through a light pipe which penetrates the chamber walls and illuminates the sample at an angle of incidence of approximately 45 deg. A fraction of the energy reflected from the sample enters another light pipe and passes out the opposite side of the chamber to a monochromator. After passing through the monochromator, the dispersed signal is detected, amplified, and filtered in frequency and phase, corresponding to the chopper frequency and phase. This reflected signal is compared with a reference signal obtained by manipulating the light pipes so that they view each other directly. The ratio of these two signals is normalized by a procedure which will be described in subsection B.4.

The apparatus measures an approximation of spectral bidirectional reflectance that can be defined as follows. Consider a differential surface element irradiated with essentially unidirectional, monochromatic energy. The bidirectional reflectance gives the fraction of that energy that is reflected in a given direction. Proper integration of the spectral bidirectional reflectance over the hemispherical space above the surface element gives the spectral directional reflectance of the surface for the specified unidirectional irradiation. For a true measurement of bidirectional reflectance, the directions, areas, and solid angles involved in both incident and reflected energy must be accurately specified and controlled. In this apparatus, the incident and reflected radiant energy are guided by unfocused quartz light pipes which are directed at the center of the sample surface. The incident energy is diverging – not unidirectional – and reflected energy collected and transmitted to the detector by the receiver light pipe is reflected from a large portion of the sample surface. However, the term "bidirectional reflectance" most nearly describes the optical property measured by this technique and is used here for simplicity.

B.2 DESCRIPTION OF APPARATUS

A side view of the apparatus is shown in Fig. B-1. In the center of the picture is the cylindrical vacuum chamber with an electronic high-vacuum pump mounted below it.

A. Terenin and Yu. Solonitzin, Disc. Faraday Soc. 28, pp. 28–35 (1959)
"Action of Light on the Gas Adsorption by Solids"

Results suggest that photodesorption of oxygen occurs when ZnO with zinc excess is illuminated with UV, but that oxygen photosorption occurs if the ZnO has excess oxygen!

Powders – Optical Properties

V. N. Filimonov, Optika i Spektr. 5, pp. 709–711 (1958)
"Electronic Absorption Bands of ZnO and TiO_2 in the Infrared Region of the Spectrum" (In Russian)

Describes how infrared absorption by ZnO powder increases under ultraviolet irradiation in vacuum, and how it decreases again when oxygen is admitted to the system.

Thin Films

V. K. Miloslavskii and N. A. Kovalenko, Optika i Spektr. 5, pp. 616–617 (1958)
"Absorption by Zinc Oxide in the Infrared Region of the Spectrum" (In Russian)

Measurements of infrared optical transmission for sputtered films of ZnO apparently with a large excess of zinc, showing a strong absorption peak at 5 μ which is attributed to an impurity band.

Catalysis

F. Romero-Rossi and F. S. Stone, Proc. 2nd Int. Cong. Catalysis (Paris 1960), pp. 1481–1496
"The ZnO-Photosensitized Oxidation of Carbon Monoxide"

It is involved with the effect of dopants such as Li and Cr in ZnO on the adsorption and photoadsorption characteristics of the surface. Results are discussed relative to oxygen adsorption.

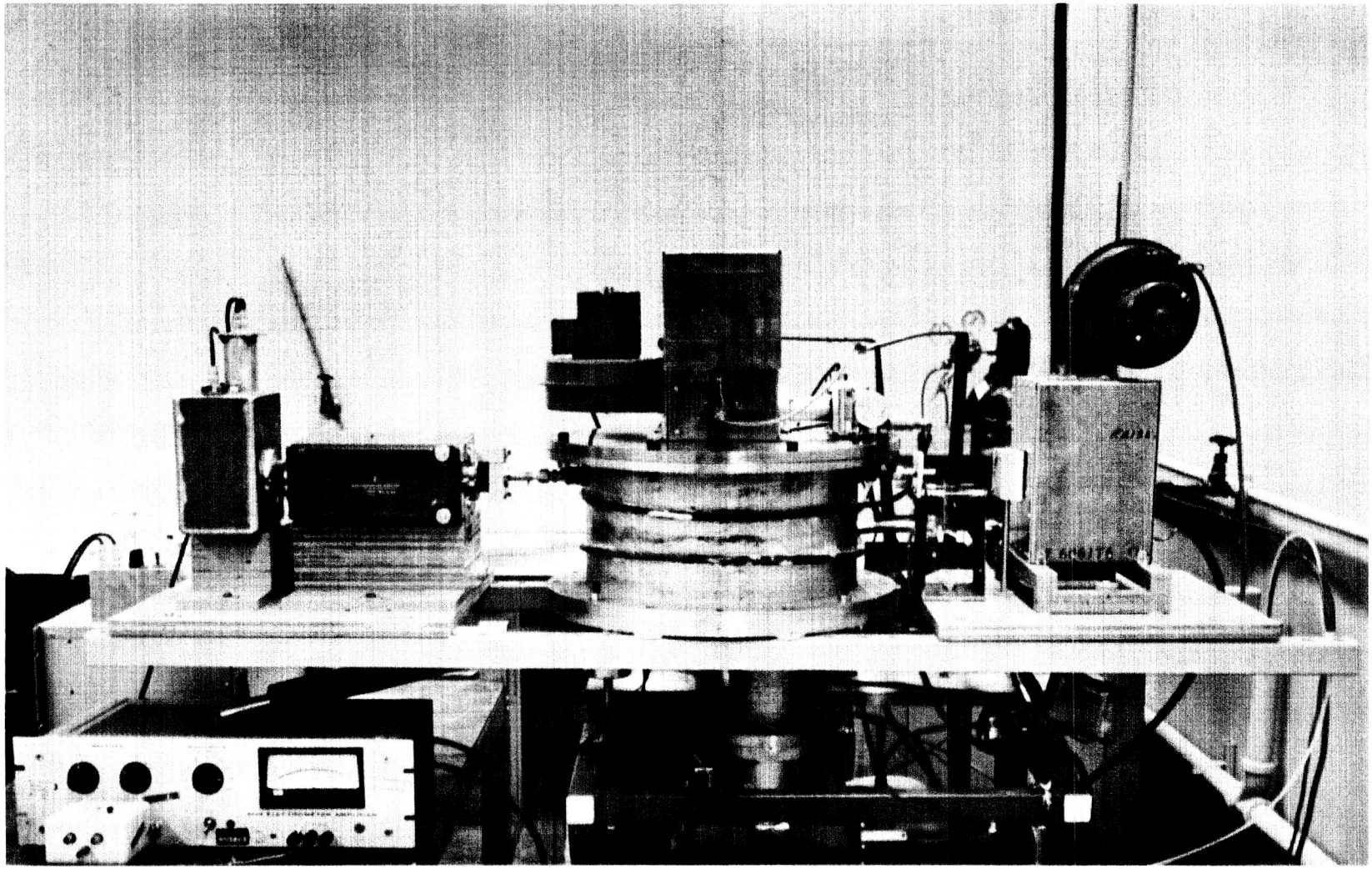

Fig. B-1 Ultraviolet Radiation – High Vacuum Exposure Apparatus for In Situ Measurement of Bidirectional Reflectance

A liquid nitrogen cold trap is located in the lower portion of the chamber. Chamber pressures of 10^{-6} to 10^{-8} Torr are maintained during vacuum-ultraviolet irradiation of typical thermal-control materials.

On top of the chamber are mounted the ultraviolet irradiation source and its convection-cooled housing, with an automatic lamp-intensity monitor. The housing is constructed to accommodate xenon, mercury-xenon, or mercury-argon ultraviolet arc lamps, either air- or water-cooled. Ultraviolet radiation enters the chamber through a Suprasil (Engelhard Industries, Inc.) window, 4 in. in diameter and 1/2 in. thick, located on the center of the removable top plate. The lamp-to-sample distance can be varied from 3-1/4 to 6 in. to achieve the nominal ultraviolet irradiation flux density desired. The location of the lamp cannot be changed during operation. All the ultraviolet irradiation tests reported in subsection 4.2 were run with an A-H6 water-cooled source and a lamp-to-sample distance of 3-1/4 in. The sample irradiation intensity was determined with a secondary photosensitive detector standard calibrated against an Eppley thermopile using an A-H6 source. Simultaneously, the automatic lamp-intensity monitor (RCA 935 phototube) was calibrated so that preceding and subsequent test intensities could be determined. The reported total ultraviolet exposures are based on manufacturers' reports that 35% of the A-H6 output is in the near-ultraviolet wavelength region, 2000 to 4000 Å. Based on this assumption, the nominal test ultraviolet irradiation flux density was 20 "suns" for all tests in the bidirectional reflectance apparatus. The accuracy of the intensity calibration is believed to be approximately ± 10%.

Material samples are mounted on a horizontal 3-in.-diameter stainless steel table (Fig. B-2) located 2 in. below the Suprasil window. Attached to the table are cooling coils and an electric resistance heater for temperature control over the range -320 to 600° F. Sample and table temperatures are monitored with thermocouples throughout the test. The table can be translated to extract samples from the region of ultraviolet illumination or to locate alternate samples for in situ optical measurements.

The 5-mm-diameter quartz light pipes, also shown in Fig. B-2, are rigidly and concentrically mounted in shorter stainless tubes that are supported in rigidly mounted bearings inside and outside the chamber. The tubes pass through the chamber wall inside flexible stainless steel bellows. This configuration allows the light pipes to be rotated about their centerlines but prevents disturbance of optical alignment during chamber pumpdown or return to ambient pressure. The sample table is mounted on similar supports so that the table can be rotated about an axis lying in the face of the sample and normal to the plane of the light pipes. As a result, through proper manipulation of the light pipes and sample table as indicated in Fig. B-3, the following measurements can be made: (1) spectral bidirectional reflectance for the specular and nonspecular cases, and (2) direct beam transmission measurements for angles of incidence of 45 to 90 deg. All the movements of the light pipes and sample table can be accomplished while the chamber is maintained under high vacuum. Consequently, in situ measurements of sample transmittance and bidirectional reflectance can be performed with the ultraviolet source on or off and under vacuum, selected atmospheres, or ambient pressure conditions.

The radiant source for spectral bidirectional reflectance measurements is a 1,000-W tungsten lamp located in an air-cooled housing at the right of Fig. B-1. The lamp output is focused at the end of one light pipe (at the right in Figs. B-1 and B-2) and interrupted by a 20-cps synchronous motor-driven chopper. The quartz light pipe penetrates the vacuum chamber wall and projects the chopped energy onto the sample. Energy reflected from the sample and striking the end of the second light pipe is collected and transmitted to a collimating lens, then passed through a monochromator. The monochromator is a Bausch and Lomb Grating Monochromator with interchangeable gratings and variable slits, which can be used over the range 0.18 to 3.2 μ. The reciprocal linear dispersions for the gratings of this monochromator are 64 Å per millimeter of exit slit width for the range 0.35 to 0.80 μ; 128 Å/mm for 0.7 to 1.6 μ; and 256 Å/mm for 1.4 to 3.2 μ. Generally, the exit slit width is fixed at 0.2 mm for all wavelengths throughout the region 0.35 to 2.4 μ for measurements taken with this system. The dispersed signal is finally measured by a photodetector. The photodetectors used are a RCA7200 photomultiplier for the range 0.35 to 0.7 μ and a Kodak lead sulphide photoresistor for the range 0.7 to 2.4 μ. The output of the

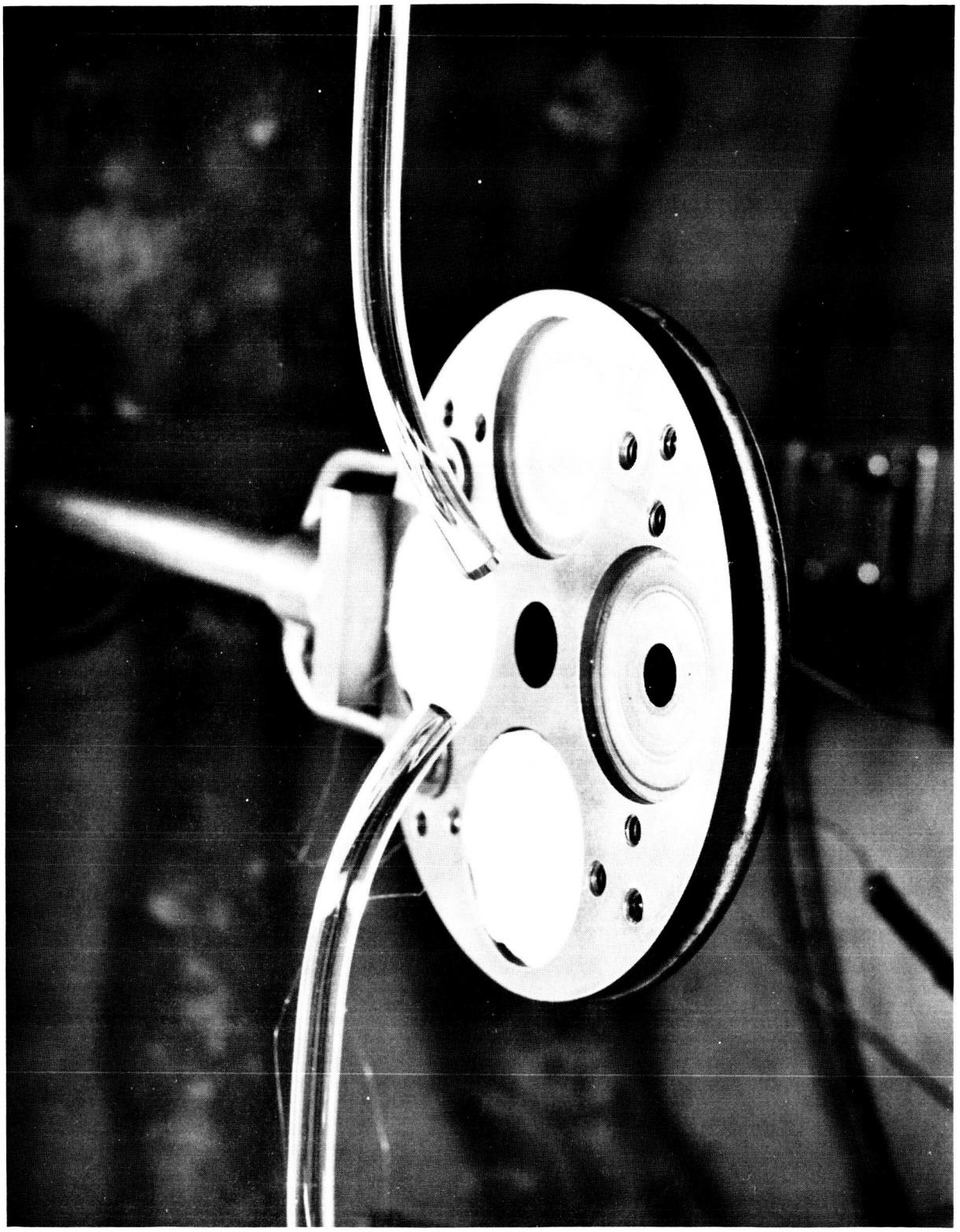

Fig. B-2 Water-Cooled Sample Table and Quartz Light Pipes

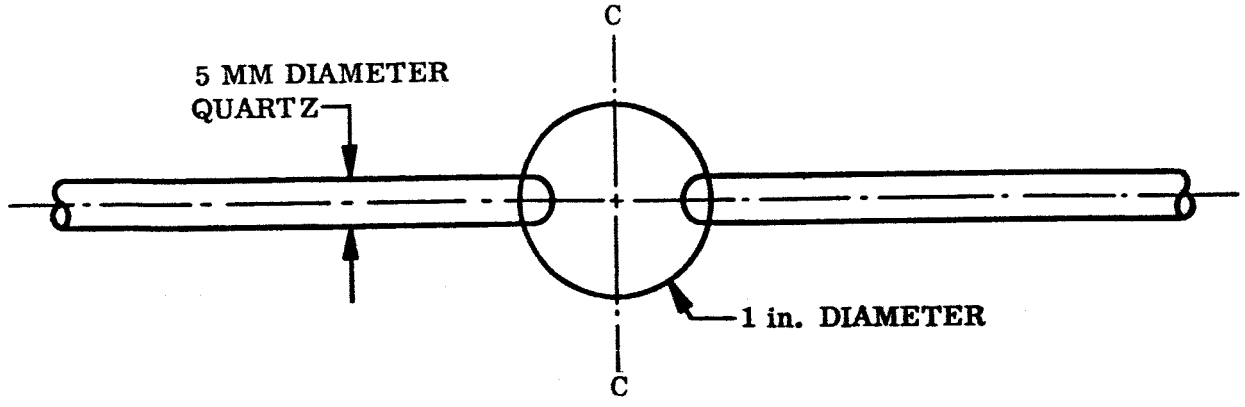

PLAN VIEW

Sample may be repositioned by rotation around axis C for non-specular measurements.

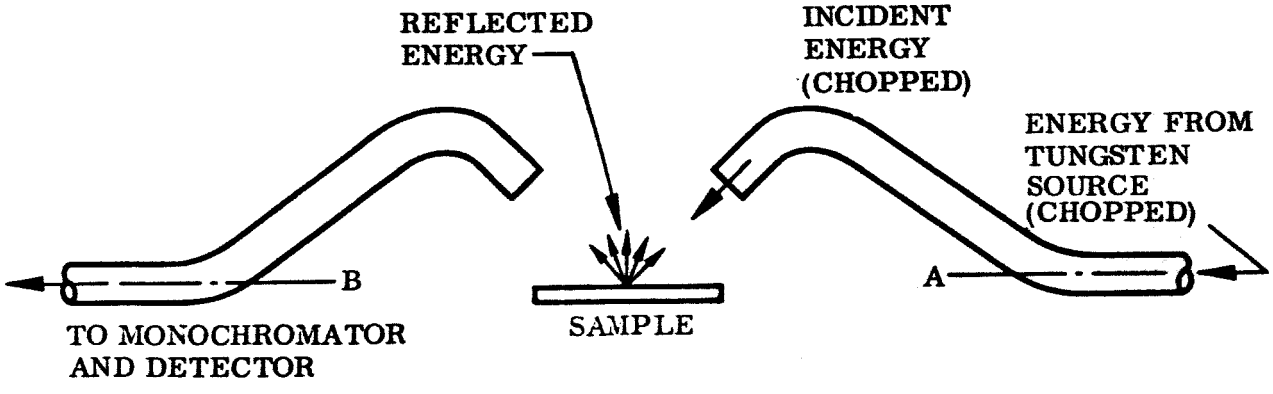

SIDE VIEW

Light pipes are repositioned by rotation around axis A or B for nonspecular or transmission measurements.

Fig. B-3 Schematic of Light-Pipe Geometry in Position for Specular Bidirectional Reflectance Measurement

detector is amplified by a narrow-frequency-band, phase-sensitive amplifier (Princeton Applied Research Lock-In Amplifier Model JB-5) and recorded on a milliampere chart recorder.

Incorporation of the narrow-band amplifier in conjunction with the mechanical light chopper permits measurement of only the reflected energy which originates from the tungsten source. The high-intensity ultraviolet irradiation (damage source), which is predominantly direct current with a significant 120 cycle harmonic, is reflected from the sample and measured by the detector. However, this background, which has no 20-cps component, does not significantly affect the amplifier output signal level.

B.3 PRINCIPLES OF MEASUREMENT

Consider an elementary beam of unidirectional, unpolarized energy, $P(\theta_i, \phi_i)$, incident on a reflecting surface as shown in Fig. B-4. The directional reflectance of the surface, $\rho(\theta_i, \phi_i)$, is equal to the fraction of $P(\theta_i, \phi_i)$ reflected back into the hemispherical space above the surface element. The directional reflectance $\rho(\theta_i, \phi_i)$ can be expressed as the integration of the reflected energy distributed over the hemispherical space above the surface:

$$\rho(\theta_i, \phi_i) = \int_0^{\pi/2} \int_0^{2\pi} r(\theta_i, \phi_i, \theta_r, \phi_r) \sin \theta_r \cos \theta_r \, d\theta_r \, d\phi_r \qquad \text{(B.1)}$$

Equation (B.1) defines the bidirectional reflectance, $r(\theta_i, \phi_i, \theta_r, \phi_r)$, which gives the fraction of the energy incident in direction θ_i, ϕ_i that is reflected in the direction θ_r, ϕ_r through the solid angle $\delta\Omega_r$. In this definition, the bidirectional reflectance of a perfectly Lambertian surface, for which r is constant for all θ_r, ϕ_r is given by

$$\rho(\theta_i, \phi_i) = \pi r(\theta_i, \phi_i) \qquad \text{(B.2)}$$

The bidirectional reflectance of a perfectly specular surface, for which $r = 0$ for $\theta_r \neq \theta_i$, $\phi_r \neq \phi_i + 180$ deg, is given by

$$\rho(\theta_i, \phi_i) = r(\theta_i, \phi_i, \theta_r = \theta_i, \phi_r = \phi_i + 180 \text{ deg}) \qquad \text{(B.3)}$$

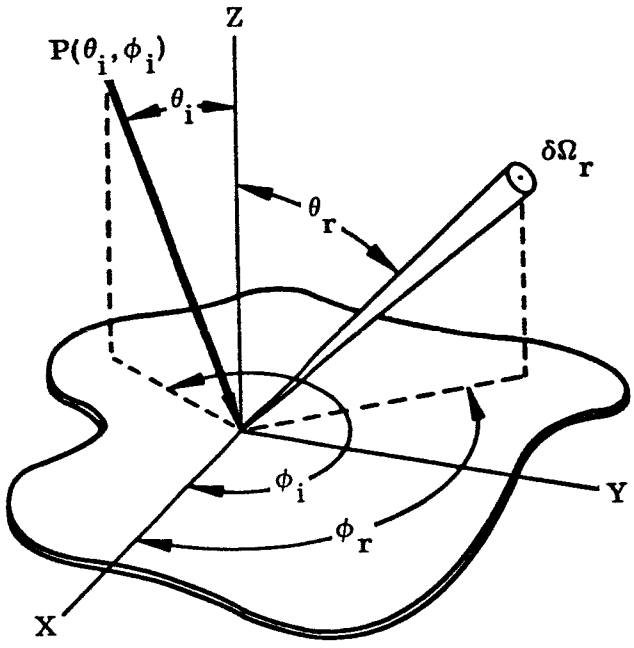

Fig. B-4 Spatial Coordinates for Incident and Reflected Elementary Beams

In both cases, at least one component of bidirectional reflectance is related to the directional reflectance by a constant factor. It is evident that for a real, opaque surface which has a specular component of reflectance that is a small fraction of the directional reflectance, the bidirectional reflectance is still related to the directional reflectance by a constant factor. If radiation damage to a material changes the magnitude but not the directional distribution of reflected energy, then the bidirectional reflectance will continue to be related to the directional reflectance by the same constant factor. This is the basis for use of the bidirectional reflectance measurement technique for in situ measurements of ultraviolet damage to material optical properties.

A schematic of the light pipe and sample configuration is shown in Fig. B-3 with representative dimensions. In the absence of a focusing lens, the energy incident on the sample diverges from the source light pipe sufficiently to strike nearly all of the 1-in. -diameter sample. Because of the index of refraction for quartz, the receiver light pipe collects and transmits energy reflected from a large part of the sample surface. The patterns of Fig. B-5 show the approximate portions of the sample

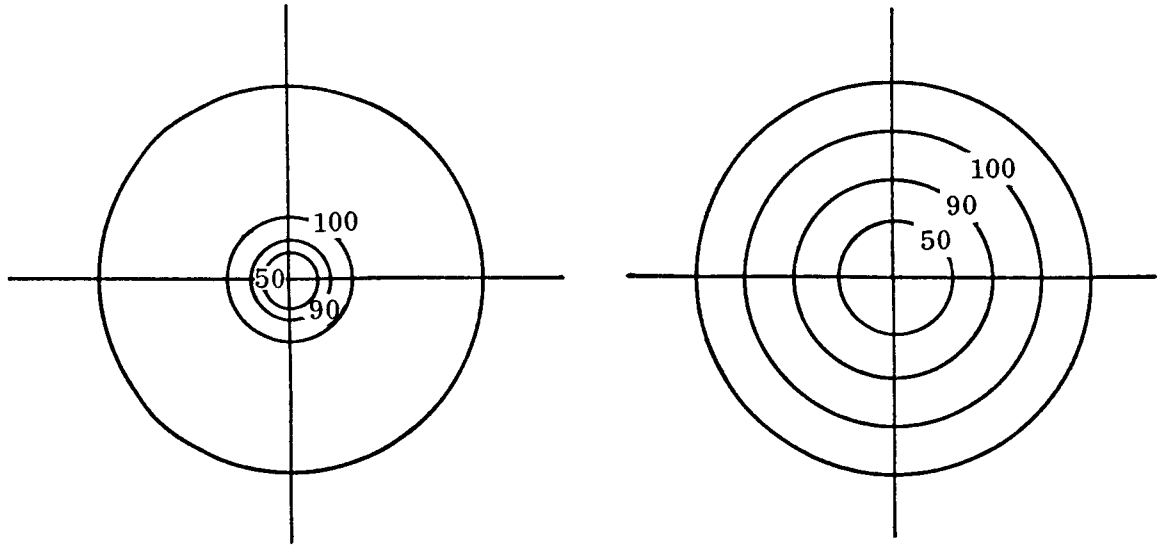

(a) Energy Reflected From Specular Surface

(b) Energy Reflected From Near-Diffuse Surface

Fig. B-5 Reflection Intensity Patterns for 1-in.-Diameter Sample. Numbers represent percentage of total detected energy reflected from area within circle

surface from which the detected energy is reflected for near-specular and near-diffuse surfaces. The patterns are circular because they were obtained using a series of circular masks. Measurements using different mask configurations have shown that the profile lines on the sample surface of equally detected signal strength would be nearly circular. It is evident from Fig. B-5 that the detected signal is reflected from an area comparable in size to the distance between the light pipes and the sample. Such a geometry does not allow a true measurement of bidirectional reflectance, which requires that both the incident and detected energies be confined to small, precisely defined solid angles as viewed from the sample.

B.4 MEASUREMENT PROCEDURE

The spectral bidirectional reflectance is determined by detecting the spectral energy reflected from the sample and collected by the receiver pipe, $E(\lambda)$, with the light

It was reported in the Eight-Month Progress Report on Solar-Induced Damage to the Optical Properties of ZnO-type Pigments that considerable difficulty was encountered in determining the sample temperature during ultraviolet irradiation. Indirect temperature measurement procedures were developed because thermocouples embedded near the irradiated sample surface were directly irradiated and consequently heated to temperatures considerably higher than the sample temperature. Subsequent to the eight-month progress report, satisfactory temperature determination was achieved by using a thermocouple embedded near the sample surface opposite the irradiated surface. At this depth below the top surface, direct irradiation of the thermocouple junction was insignificant. The thermal conductivity of the zinc oxide is large enough to limit temperature differences between front and back sample surfaces to about 20° F during irradiation.

B.5 MEASUREMENT UNCERTAINTIES

For this measurement technique, two types of uncertainties are of primary interest. The first concerns the relationship between the optical properties measured by this apparatus and the optical properties of engineering importance – directional reflectance or transmittance. This question is considered in subsection B.7. The second relates to measurement reproducibility and precision. If the approximate bidirectional reflectance measured can be quantitatively related to the normal reflectance, then the reproducibility of the data is dependent on the repeatability of the optical system. The factors which affect repeatability are discussed here, and the results of an experimental uncertainty investigation are reported.

Alteration of the optical alignment which results in significant errors can occur in several ways. The measurement technique requires the frequent translation of the sample table and rotation of the source light pipe. Mechanical stops are provided to ensure that these components are held in proper position. The manual adjustment of the monochromator grating must be accomplished without stops and hence operator care is the only assurance that grating positions will be repeated. Likewise, the detectors must be interchanged frequently; here stops are also provided. These effects are treated in the following experimental uncertainty evaluation.

The most serious effect on optical alignment was found to be the danger of lateral light pipe movement resulting from the changing differential pressure forces that occur during both evacuation of the chamber and readmission of air to the chamber. This effect has been minimized by employing rigid light pipe supports and has been checked by monitoring the reference energy signal $E_o(\lambda)$ during large changes in chamber pressure. The most effective insurance against this movement has been to start all measurement sequences when the chamber has been roughed down to a pressure below 1,000 μ, by which time all movement due to pressure forces will have occurred. Likewise, all tests are terminated following irradiation and recovery measurements when the chamber has been repressurized to about 1000 μ. It has been verified that at this pressure the partial pressure of oxygen is sufficient to provide the equivalent effects of ambient pressure oxygen on the materials investigated to date.

The repeatibility of the optical source, detector, and amplifier is maximized by using a voltage-regulated power supply. In addition, long-term changes in the tungsten source output, light pipe transmittance, and detector response are accounted for by measuring the reference spectral energy $E_o(\lambda)$ as part of each reflectance run. Because the system is not double-beam, short-term changes cannot be accounted for.

For the wavelength region measured to date, fixed entrance and exit monochromator slits were used. Hence, slit width variations, which are a source of nonrepeatibility, are avoided.

Because of the number of factors that influence repeatability, an experimental uncertainty evaluation is preferable to a theoretical uncertainty analysis. Consequently, such an experimental investigation was performed to evaluate the cumulative uncertainties due to all the factors described. A series of 30 reflected and reference energy measurements was performed at two representative wavelengths over a period of one day. Between measurements, all movable optical components were moved and reset. Periodically, the instrumentation and tungsten source were turned off, cooled, and turned back on to thermally perturb the system. The results are presented in Fig. B-6, where the number of readings taken is related to their percentage deviation from the average of all readings. It can be seen that the repeatability of the system due to

Using the proportionality factors determined by equating the initial spectra, all succeeding bidirectional spectra of a material are presented as in situ measurements of the normal reflectance as it changes due to environmental degradation or recovery. The succeeding spectral normal reflectance values $\rho_{BDR}(\lambda)$ inferred from the ratio of reflected to reference energies are given by the expression

$$\rho_{BDR}(\lambda) = \frac{E(\lambda)}{E_o(\lambda)} \left[\rho_N(\lambda_n) \frac{E_o(\lambda_n)}{E(\lambda_n)} \right]_i \qquad \text{(B.4)}$$

where $\rho_N(\lambda)$ is the spectral normal reflectance determined by the Cary spectrophotometer with integrating sphere; $E(\lambda)$ is the spectral reflected energy; $E_o(\lambda)$ is the spectral reference energy; i denotes values obtained prior to environmental exposure of the sample; and n denotes the wavelength(s) at which the bidirectional and normal reflectances are equated to obtain the proportionality factor(s).

In the normal test procedure, a series of bidirectional reflectance spectra are measured,beginning prior to chamber pumpdown. The series includes several spectra taken before and during irradiation and following irradiation before and after the chamber is reopened to the atmosphere. This procedure provides valuable information on the rate of radiation damage and on the recovery from damage in vacuum and air or other atmospheres. The measurement of each bidirectional reflectance spectrum, including the associated reference spectrum, requires approximately half an hour, depending on the wavelength interval required between spectral measurements for adequate definition of the spectral bidirectional reflectance. This is a long time relative to the rate of recovery from damage for some materials when oxygen is readmitted to the chamber. To observe the kinetics of damage and recovery, the bidirectional reflectance is monitored continuously at one wavelength during important events such as the beginning or end of irradiation or the admission of air to the chamber following irradiation. This procedure does not provide a complete description, but valuable information is obtained if the wavelength to be monitored can be selected with some knowledge of the material under test.

pipes in the positions shown in Figs. B-2 and B-3. Then the source pipe is rotated about its axis so as to view the receiver pipe directly with the sample table withdrawn. The spectral energy $E_o(\lambda)$ detected in the latter alignment is termed the reference energy. The reference energy is measured each time a bidirectional spectrum is measured in order to account for any changes in tungsten lamp output, detector sensitivity, or transmittance of the optical components. The ratio of the reflected spectral energy to the reference spectral energy, $E(\lambda)/E_o(\lambda)$, is proportional to the spectral bidirectional reflectance.

The absolute value of this ratio has no significance because in the detection of both the reflected and the reference energy, no attempt is made to evaluate the losses through the optical system. However, these losses are a constant fraction of the detected signals, and therefore the ratio of the reflected and reference signals will be proportional to the spectral bidirectional reflectance. This ratio, herein termed the spectral bidirectional reflectance, is in turn related to the spectral normal reflectance by a proportionality factor. This factor is established by normalizing the initial spectral bidirectional reflectance so that it equals the initial spectral normal reflectance of the sample as measured on a Cary Model 14 spectrophotometer with an integrating sphere attachment. The in situ bidirectional reflectance data are presented in this way even though the bidirectional reflectance is generally not equal to the directional reflectance for a real surface. This form of presentation depends on the validity of the assumption that the ratio of reflected energy to reference energy will continue to be proportional to the directional reflectance of a material as it is exposed to vacuum-ultraviolet irradiation and to postirradiation recovery effects.

In normalizing the initial bidirectional reflectance so that it equals the initial normal reflectance, it is not necessary to use a different proportionality factor for each wavelength at which measurements are made, but it has been found that one proportionality factor is required for the wavelength region in which the photomultiplier detector is used and another (usually slightly different) is required for the wavelength region in which the photoresistor detector is used. The need for two factors is apparently due to the differences in variation of photosensitivity over the two detector surfaces.

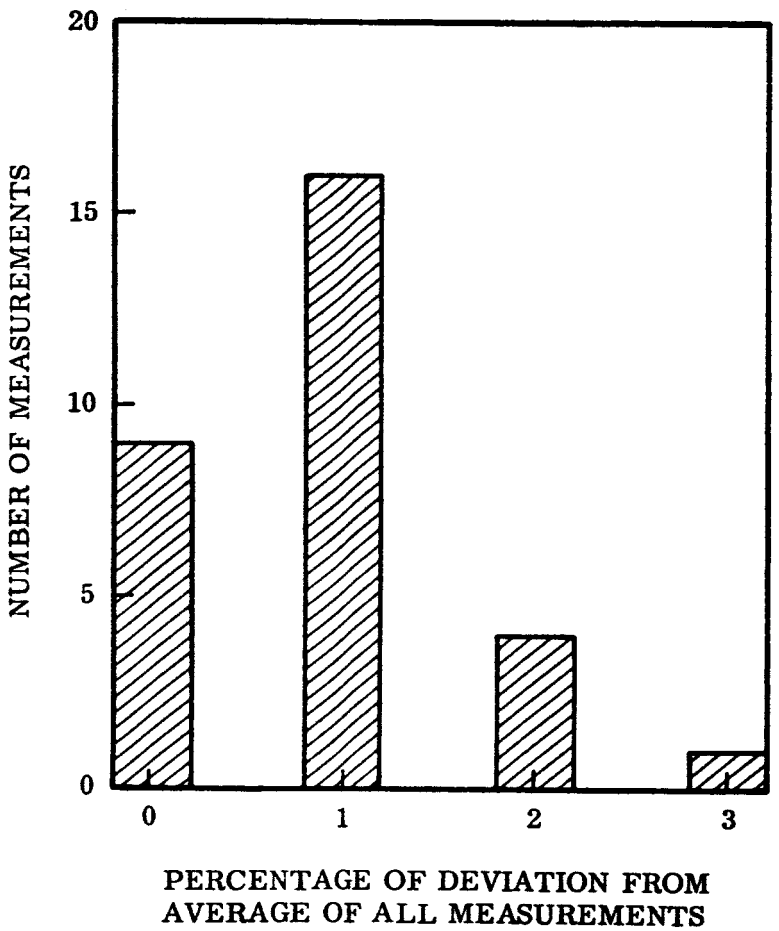

Fig. B-6 Repeatability of Bidirectional Reflectance Measurements Indicated by Distribution of 30 Measurements

random errors is approximately ±2%. The only significant source of error attributable to the setting of movable components was that caused by the setting of the monochromator grating. If reasonable care is not exercised, variations in monochromator setting can cause an increase of random error to approximately ±4%.

A potential cuase of serious systematic error is the influence of the ultraviolet source on the detector output. The narrow-band amplifier effectively eliminates the direct effect of the component of detected energy which originates from the high-intensity ultraviolet source and is reflected into the receiver light pipe from the sample; i.e., all but the signal resulting from the reflectance source is filtered and eliminated. Of course, the detector itself actually sees both the energy from the reflectance source and that from the damaging ultraviolet source. The reflected energy of the ultraviolet source is so intense relative to the 20 cps signal from the reflectance source that it significantly shifts the operating point on the photomultiplier response curve. Generally, this shift is large enough to result in a change in photomultiplier amplification, and hence an apparent change in sample reflectance. This apparent change can be reliably accounted for over the major portion of the visible wavelength and does not appear in the infrared wavelength regions. However, at wavelengths coincident with high-intensity mercury emission lines, the data taken with the ultraviolet source on have been found to be generally unreliable and therefore are not recorded.

B.6 EXPERIMENTAL RESULTS

Bidirectional reflectance spectra are shown for a specular surface in Fig. B-7 and a near-diffuse surface in Fig. B-8. In both cases, only two normalizing constants were used to superimpose the bidirectional spectrum on the normal reflectance spectrum: one for the 0.35 to 0.70 μ region and one for the 0.70 to 2.0 μ region. Surfaces of intermediate directional properties such as a glossy white paint which scatters most of the reflected energy diffusely but has a significant specular component due to front surface reflection from the binder have been measured with equal success. For these surfaces, better results were obtained by rotating the receiver light pipe significantly away from the major specular component. At the specular angle during ultraviolet irradiation the nondegrading front surface specular reflectance is sometimes large

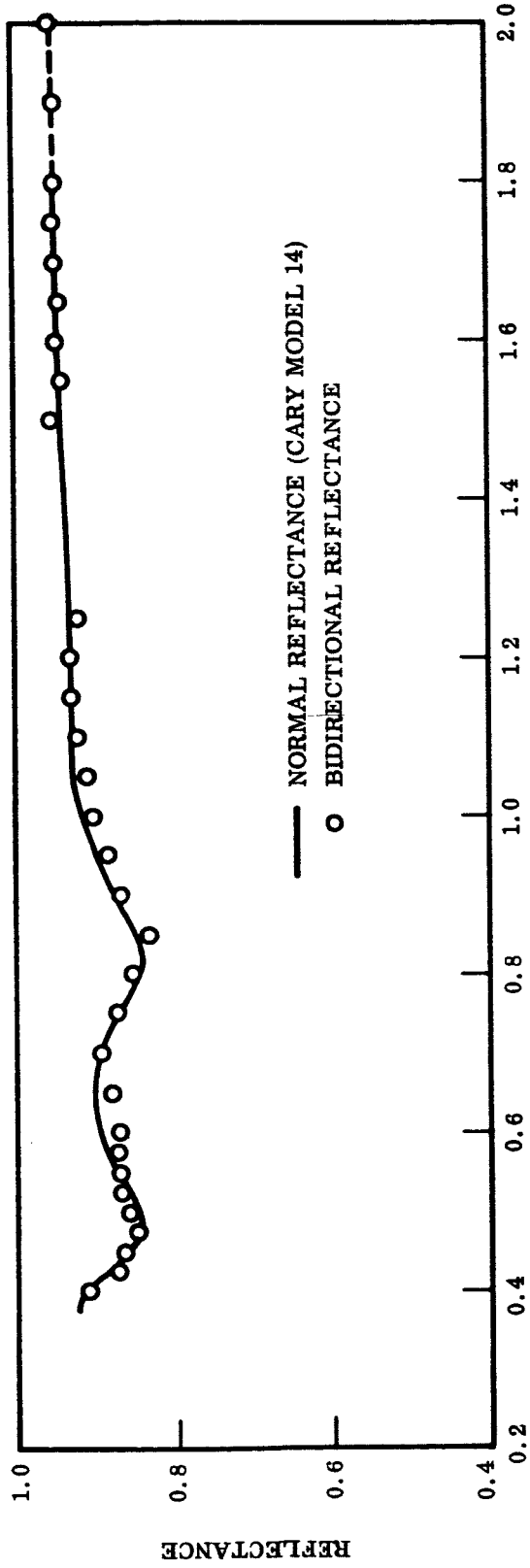

Fig. B-7 Representative Specular Surface – Bidirectional Reflectance Normalized to Directional Reflectance of Vapor-Deposited Aluminum With Thin SiO Overcoat

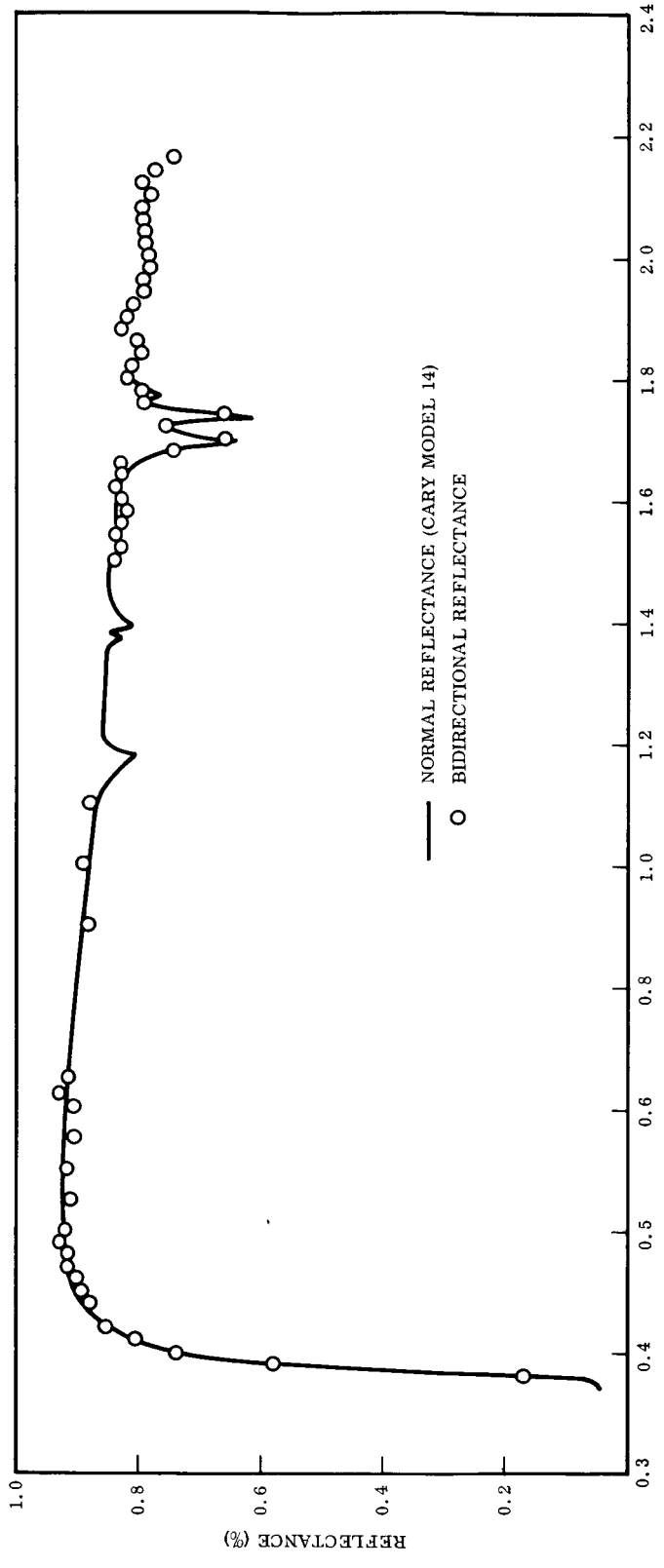

Fig. B-8 Representative Near-Diffuse Surface – Bidirectional Reflectance Normalized to Directional Reflectance of ZnO-Silicone Thermal Control Coating

enough to mask the degradation of the directional reflectance, particularly near the absorption band edge of metallic oxide pigments. This can occur even if the specular component is a small percentage of the total reflectance. At an off-specular angle, good correlation between the changes in directional and bidirectional reflectance due to ultraviolet degradation has been achieved.

B.7 DISCUSSION

The use of in situ bidirectional reflectance measurements to infer changes in directional reflectance due to radiation-induced optical degradation assumes that the directional distribution of reflected energy does not change significantly. If this is true, changes in the bidirectional reflectance of opaque samples are due to changes in total absorption and the measurement technique is valid. Potential errors arising from this assumption can be circumvented by using an integrating sphere located in the vacuum chamber to perform in situ reflectance measurements. This is difficult, however, because (1) the standard highly reflective, diffuse integrating sphere coatings are not suited for use in high vacuum due to their high water content, and (2) the sphere cannot be exposed to the damaging radiation because the reflectance of the coating usually degrades under vacuum-ultraviolet irradiation. This problem can be avoided by locating the integrating sphere adjacent to the sample irradiation position. Reflectance measurements can then be performed by translating the sample out of the damaging irradiation beam and into a measurement position while vacuum is maintained. This procedure raises the question of whether significant recovery of the directional reflectance has occurred between the cessation of irradiation and the directional reflectance measurement. This is a possibility at vacuum pressures compatible with the maintenance of an integrating sphere coating, particularly at elevated sample temperatures. Because the bidirectional reflectance apparatus was constructed for basic material degradation investigations in which the occurrence of such a recovery would be of considerable importance, a major design goal was the capability of measuring reflectance at and immediately following termination of irradiation. Sufficient data have not yet been obtained to ascertain whether such recovery in vacuum could be sufficient to significantly affect engineering test data taken in an integrating sphere arrangement on current material systems.

Another consideration which influenced the selection of a bidirectional reflectance technique is the ease of adaptability of the apparatus to in situ reflectance measurements during multiple environment simulation, such as combined high-energy proton or electron and ultraviolet irradiation. An apparatus with this capability is presently under construction.

The critical consideration in determining the validity of the bidirectional reflectance technique is whether a change in bidirectional reflectance of an opaque surface can with assurance be attributed to a change in total absorption, rather than simply resulting from a change in the directional distribution of the reflected energy. All the surfaces investigated to date are aggregates of particles of submicron size with and without binders; such samples reflect radiation by the process of back-scattering. These surfaces are near-diffuse with a small specular reflectance component. For all but highly grazing angles it has been found that the bidirectional spectral reflectance is directly proportional to the near-normal spectral reflectance over the range 0.35 to 2.4 μ. This proportionality will be maintained during and after irradiation only if the damage does not affect the directional distribution of reflected energy.

Consider, first, the scattering from a single spherical particle. The amount of energy of a given wavelength scattered in a given direction is controlled by the particle size, the real index of refraction, and the extinction coefficient of the material. The particle geometry can be assumed to be unaffected by radiation; a very large number of atomic displacements would be required to produce a measurable change. The real index of refraction is controlled by the largest energy gap in the material band structure. Although this gap is not expected to change under ultraviolet irradiation, scattering calculations were performed for the maximum range of real index changes considered possible under irradiation. The resulting effect on the scattering pattern was insignificant.

The extinction coefficient, on the other hand, is expected to vary under irradiation. Calculations of maximum anticipated changes in extinction coefficient have been performed for selected pigments. It was found that changes in the scattering pattern caused by changes in extinction coefficient are second order compared with the changes

in energy absorbed. Thus, for a single particle it can be shown that changes in directional distribution, if any, are small compared with changes in absorption produced by ultraviolet irradiation.

Because of the complexity of multiple particle scattering, no analysis has been found which provides an explicit answer to the question for aggregates of particles. However, it appears unreasonable to expect the directional distribution of reflected energy to change under irradiation, if the particle spatial distribution is unaltered and the scattering pattern from each particle follows the behavior described above. This extrapolation to the multiple-particle case is substantiated by the experimental data obtained on sintered zinc oxide in the bidirectional reflectance apparatus. The post-test near-normal reflectance determined with a spectrophotometer and associated integrating sphere has repeatedly been found to agree with the final bidirectional reflectance. Either the directional distribution of reflected energy did not change significantly compared with absorption changes under irradiation or the changes had exactly opposing effects on the measurements. The latter alternative seems most implausible.

A number of improvements of the apparatus are presently being considered. The existing optical system is limited to the wavelength region 0.35 to 2.4 μ by the use of a tungsten source and quartz light pipes. This region can be extended further into the infrared by employing light pipes or fiber optics of greater infrared transmittance. Candidate light pipes and infrared fiber optics are becoming generally available. To extend the region further into the ultraviolet would probably require the use of one of a variety of mercury arc lamps. These lamps do not have the steady output characteristics of a tungsten lamp, so difficulties in repeatability would be incurred if a single beam optical system were used. This presents the desirability of modifying the optics to incorporate a double-beam system in conjunction with a recording spectrophotometer. Such a system would provide continuous referencing to account for short-term variations in the system performance. It would provide more rapid

spectral measurements and consequently more detailed information on the kinetics of radiation damage and subsequent recovery in air. Finally, it would provide continuous spectral data rather than the discrete wavelength data provided by the present apparatus. This would enable the investigator to observe the radiation effects on materials through analysis of fine spectral structure.

Appendix C
STATIC ULTRAVIOLET EXPOSURE APPARATUS

The static ultraviolet exposure chamber is shown in Fig. C-1. The test chamber is a water-cooled stainless steel bell jar 14 in. high and 14 in. in diameter. The 1-in. diameter samples are mounted on a water-cooled, semi-cylinder copper sample holder concentric with the ultraviolet source and at a distance of 3.9 in. which results in nominal irradiances of 10 suns of ultraviolet energy. A flux density of 1 sun of ultraviolet energy is defined as the flux density of extraterrestrial radiation at 1 AU from the sun, in the wavelength interval from 2000 to 4000 Å. At these flux densities the sample temperatures were maintained between 100 and 125° F for all ultraviolet tests in this chamber. Thermal contact conductance between the sample and the water-cooled copper sample holder was controlled with individual mounting frames which pressed the back face of the sample against the copper. Vacuums are established prior to initiation of ultraviolet exposure with cryogenic sorption roughing pumps and an electronic high vacuum pump to avoid potential oil contamination problems. The chamber pressure is typically 2×10^{-7} Torr in the last portion of an exposure period and before the lamp is started. At the beginning of the exposure period the pressure typically rises to 1×10^{-5} Torr, because of the relatively high "out gassing" of zinc oxide under irradiation.

The source of ultraviolet energy is a 1-kW A-H6 (PEK Labs Type C) high-pressure mercury-argon capillary arc lamp. Approximately 35% of the lamp's radiant output is in the interval from 2000 to 4000 Å. The total output of the lamp is in the interval 2000 to 26,000 Å. The lamp is water-cooled and has a quartz water jacket and velocity tube. This assembly is lowered into a quartz envelope extended into the exposure chamber from the top. The assembly can be withdrawn to change lamps without disturbing the established vacuum. Unless a lamp ruptures, it is run for 100 hr and then replaced. Each test is begun with a new lamp. This procedure is followed because

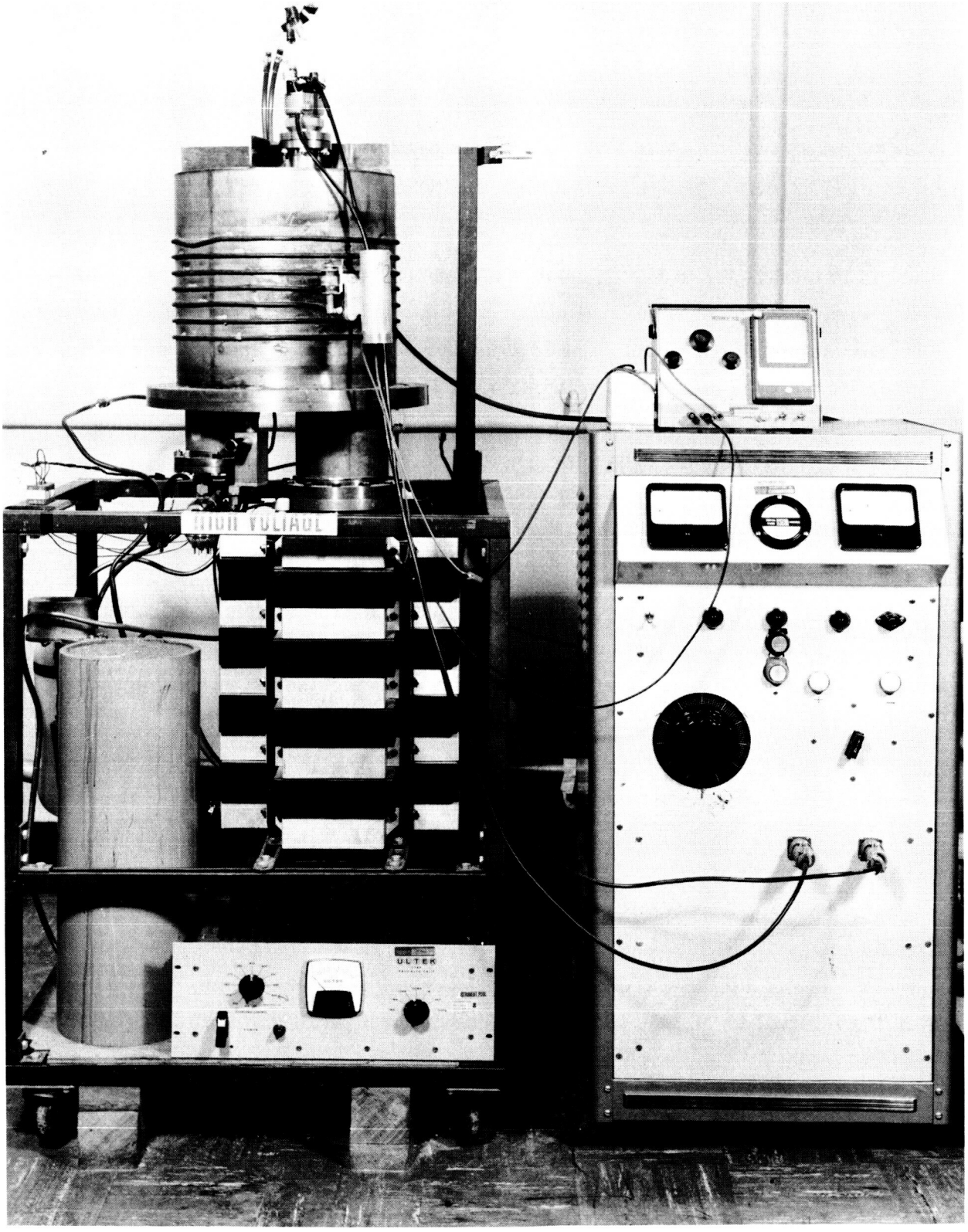

Fig. C-1 Ultraviolet Radiation – High Vacuum Exposure Apparatus

the A-H6 output decreases with time more in the 2000- to 3000-A interval than in the 3000- to 4000-Å interval. Therefore, for materials which are degraded primarily by energy of wavelengths less than 3000 Å, an old lamp will produce less degradation than a new lamp for the same total ultraviolet exposure, expressed in sun-hours. Some control over this effect is achieved through following this standard replacement procedure.

The ultraviolet intensity is monitored external to the vacuum chamber with a calibrated RCA 935 phototube in conjunction with a Corning 7-54 filter, which transmits only the near ultraviolet output of the lamp. The output of the phototube is automatically measured and recorded for a few minutes each hour with a recording microammeter. The intervening quartz window and 7-54 filter are periodically checked for degradation in spectral transmittance and cleaned or replaced as necessary. When desired, a Corning 0-54 filter is used to compare the intensity in the 2000- to 3000-Å region to that in the 3000- to 4000-Å region as a measure of the relative degradation of lamp output in the shorter wavelength regions.

The effect of ultraviolet radiation on the optical properties is evaluated by measuring the spectral reflectance immediately before and after irradiation with a Cary Model 14 spectrophotometer and integrating sphere in the range 0.3 to 1.8 μ. In some cases a Beckman DK-2 spectrophotometer and integrating sphere were used to extend the infrared measurement range from 1.8 to 2.6 μ. Both instruments effectively measure spectral near-normal reflectance.

Appendix D

TRANSIENT PHOTOCONDUCTIVITY APPARATUS

During the course of this investigation two experimental arrangements were employed for the transient photoconductivity studies. The first system employed a 0.5-μsec light source; the second scheme substituted a chopped (10 cps) light source for the spark source. The chopped light scheme allowed a more accurate determination of the decay time because of instabilities encountered in the base line when using the spark source.

D.1 PULSED LIGHT PHOTOCONDUCTIVITY APPARATUS

The photoconductive response of Li doped ZnO was initially measured by a method first used by Haynes and Hornbeck in 1953.* This experimental procedure was later recommended as a standard by the IRE.** It involves a small sample of the semiconductor with end contacts connected to a constant current source. A flash of light, generated either electronically or with a mechanical chopper, is focused on the sample and the changes in conductivity of the sample are measured as changes in the voltage across the sample. The apparatus is shown in Fig. D-1.

For accurate lifetime measurements, the following experimental parameters are recommended:

- Peak conductivity modulation of about 10%
- The electric field across the sample should not be too large, to avoid sweeping the carriers away and altering their distribution or so small as to let diffusion effects predominate
- Elimination of photovoltaic effects at the end contacts by masking

---

*Haynes, J. R. and Hornbeck, J. A., Phys. Rev., 90, 152–153 (1953)
**IRE Standards, Proc. Inst. Radio Engr., 49, 1293–1299 (1961)

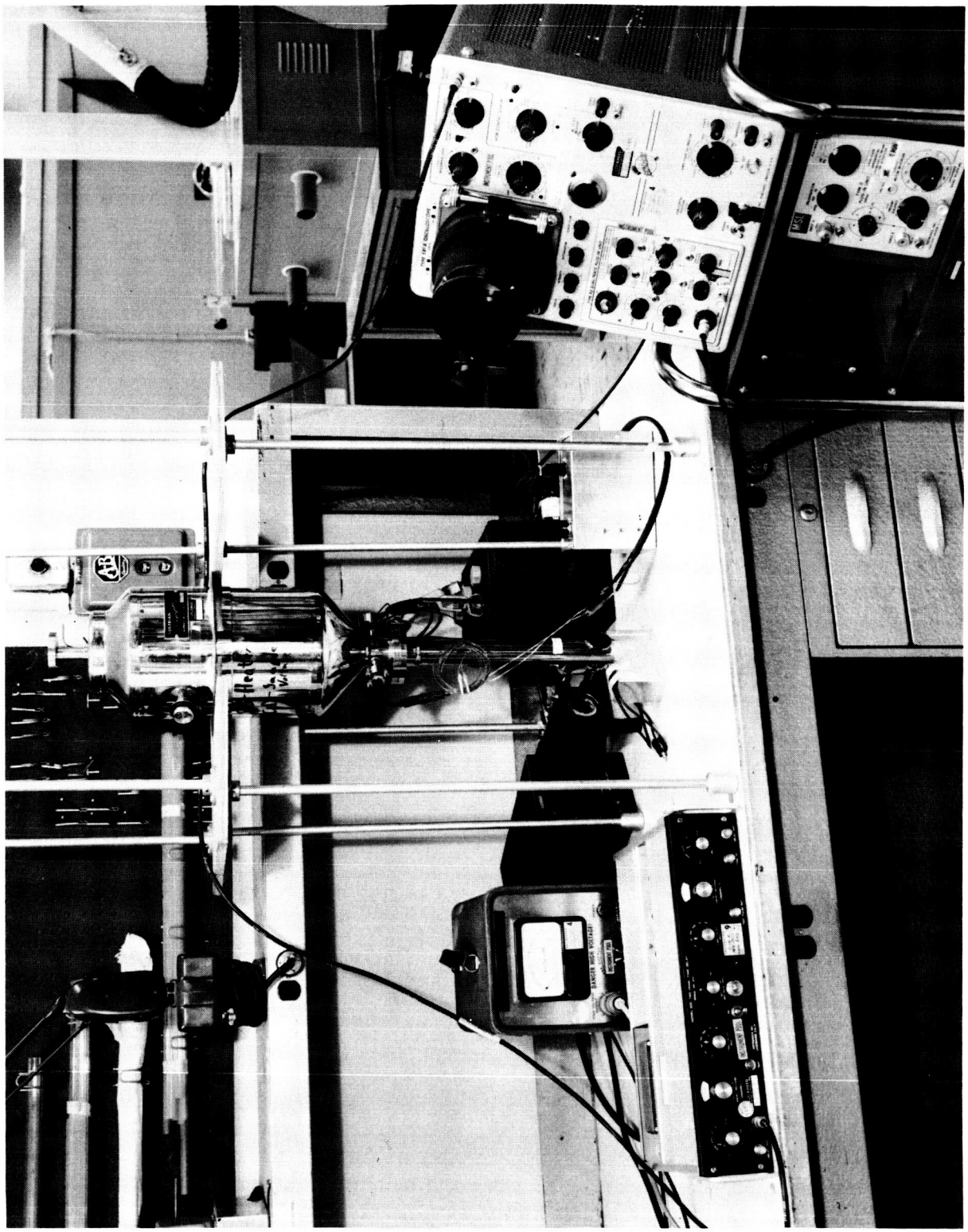

Fig. D-1 Apparatus for Transient Photoconductivity Measurements on ZnO Single Crystals

- Ohmic contacts
- Provision for background illumination to saturate those traps close to the valence band or to optically pump these traps close to the conduction band
- Rapid decay of the light source

The experimental arrangement, as used in ZnO, is illustrated in the block diagram of Fig. D-2. The light source and associated electronics consisted of a high voltage (10 kV) power supply, the Abtronic Point Light Source which was an air discharge spark gap and the Abtronic Time Delay Generator. The light source had a decay time of 0.5 μsec. The purpose of the time delay generator was to delay the light flash for a few microseconds after the time base of a Tektronic 581 oscilloscope had been triggered.

The sample was mounted in a Sulfrian double Dewar, fitted with appropriate windows to allow for the illumination of the sample. As well as being able to cool the sample, it was also possible to heat the sample above room temperature by means of a heater incorporated into the Dewar. The leads from the sample went through a vaccum seal to a cathode follower (for impedance matching) and the output from the cathode follower went to a Tektronic 581 oscilloscope. A 90 V d-c battery was used as the constant current source and was connected across the sample. The light was focused on the sample by using a focusing bellows and a condensing lens. When background illumination was required it was provided by a 6 V d-c tungsten lamp which was positioned to illuminate the sample. Provision was also made for filtering the background illumination.

D.2 CHOPPED LIGHT PHOTOCONDUCTIVITY APPARATUS

The experimental arrangement, as used in ZnO, is illustrated in the block diagram of Fig. D-3. The light source consisted of a 54 W tungsten lamp which was chopped at 10 cycles per second. The sample was mounted in a Sulfrian double Dewar, fitted with appropriate windows to allow for the illumination of the sample. As well as being able to cool the sample, it was also possible to heat the sample above room temperature by

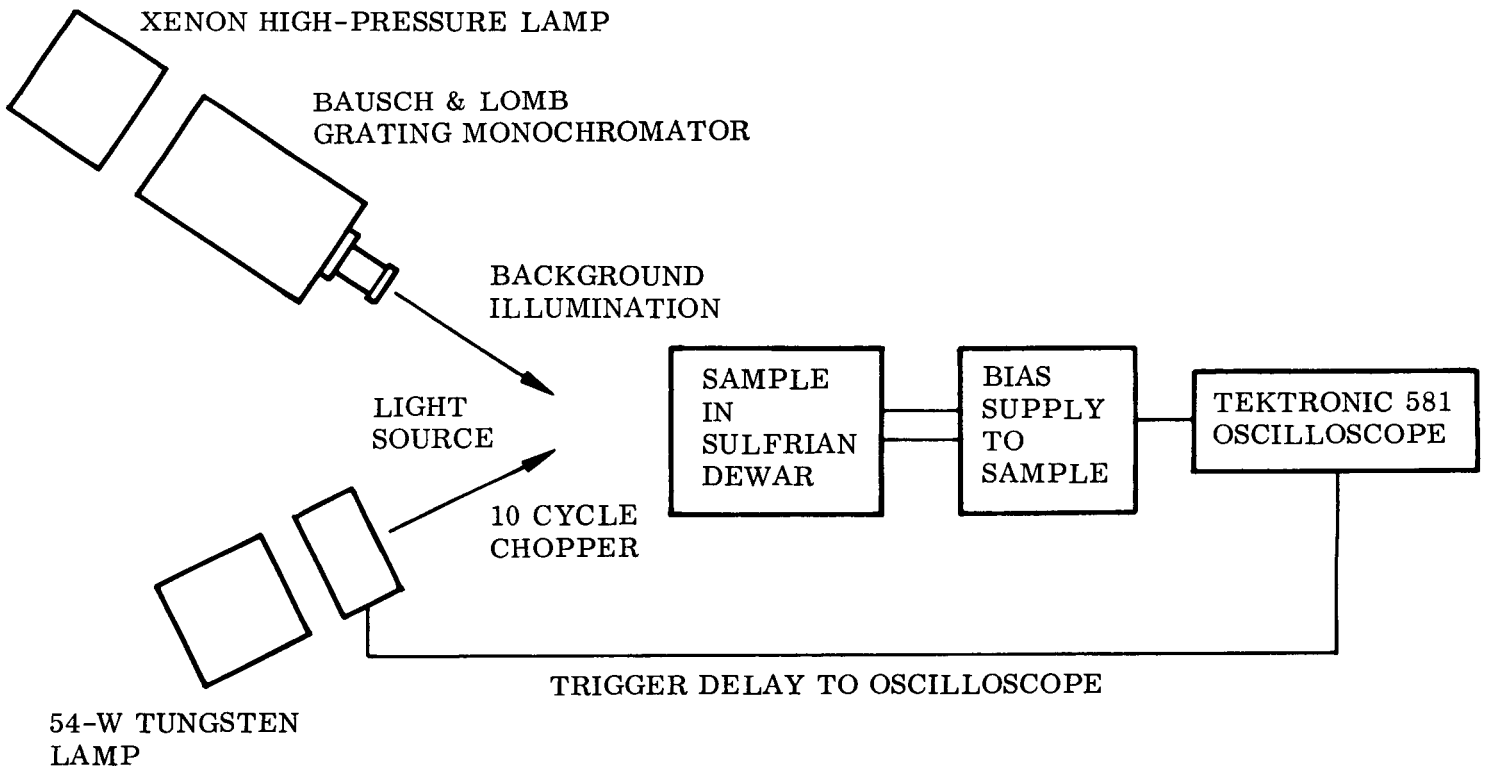

Fig. D-2 Experimental Arrangement for Measuring Photoconductivity

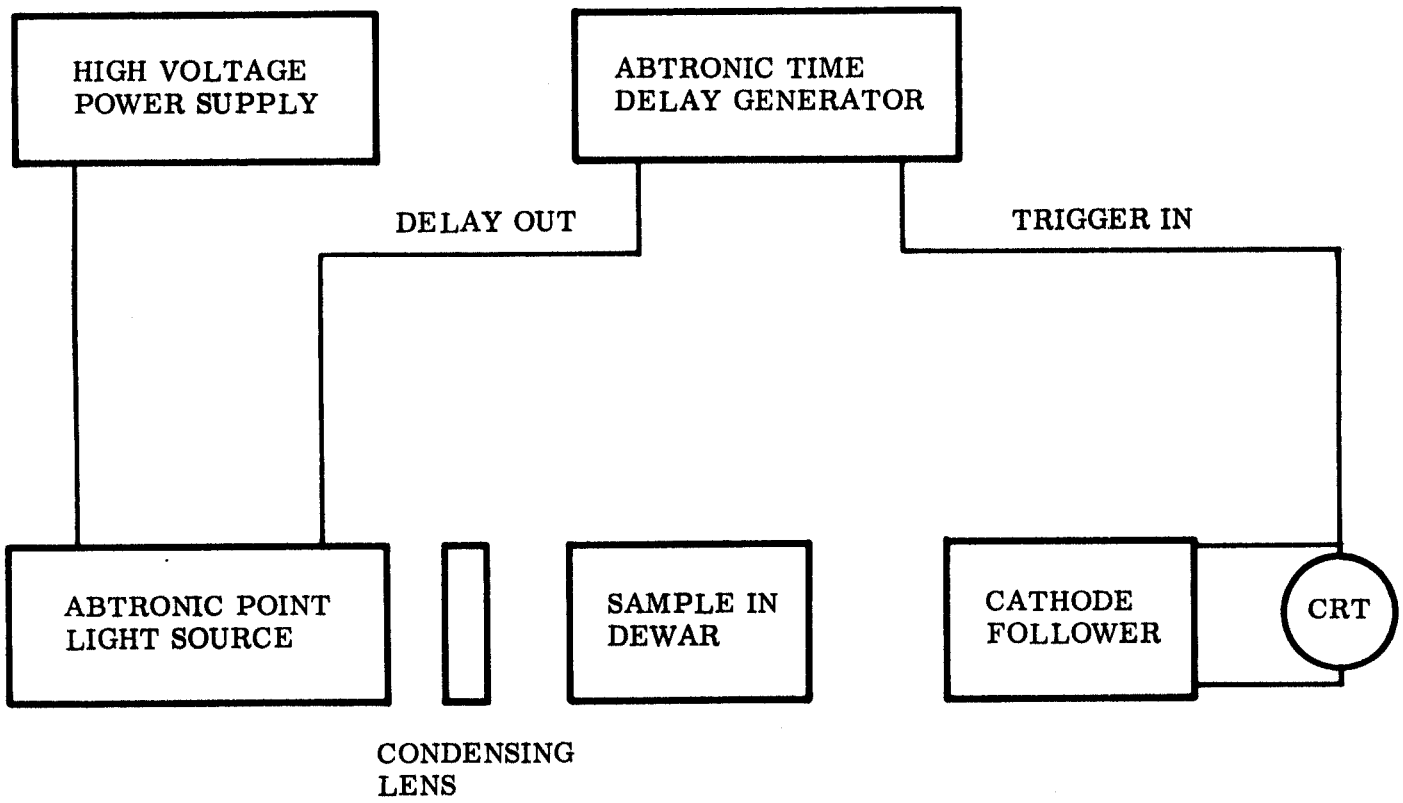

Fig. D-3 Chopped (10 cps) Light Photoconductivity Apparatus

means of a heater incorporated into the Dewar. The leads from the sample went through a vacuum seal to the bias supply which had a 0.1 to 1 MΩ load resistor in series with the sample. The photoconductivity was displayed on the Tektronic 581 oscilloscope by measuring the change in voltage across the load resistor. Background illumination was provided, through a Bausch and Lomb grating monochromator, by a high-pressure xenon lamp.